Design and Operation Optimization of Hybrid Energy Systems for a General Cargo Vessel

Well-to-Wake Emission Analysis and Plant Lifetime Estimation

Arun Datta Beeravelli

Delft University of Technology

TU Delft

Design and Operation Optimization of Hybrid Energy Systems for a General Cargo Vessel

Well-to-Wake Emission Analysis and Plant Lifetime Estimation

by

Arun Datta Beeravelli

Master Thesis

in partial fulfilment of the requirements for the degree of

Master of Science
in Mechanical Engineering

at the Department of Maritime and Transport Technology of Faculty Mechanical Engineering
of Delft University of Technology

to be defended publicly on Monday February 26, 2024 at 10:00 AM.

Student number:	5521777	
M.Sc. track:	Multi-Machine Engineering	
Report number:	2024.MME.8896	
Project duration:	March 2023 – Feb 2024	
Thesis committee:	Dr. Andrea Coraddu,	TU Delft, Supervisor
	Dr. ir. Henk Polinder	TU Delft, Chair
	M.Sc. Foivos Mylonopoulos,	TU Delft, Daily Supervisor

An electronic version of this thesis is available at `http://repository.tudelft.nl/`.

Cover: Image of MV Ankie by Jan Scheurwater

TU Delft

Abstract

The Global Shipping industryis responsible for transporting 90% of global commerce, and is responsible for 3% of global green house gas(GHG) emissions. Addressing this, the International Maritime Organization (IMO) aims to reduce GHG emissions from international shipping by 40% by 2030 and achieve net zero by 2050. This study explores Low Temperature-Proton Exchange Membrane Fuel Cell (LT-PEMFC) hybrid energy systems as a potential solution to reduce shipping emissions. Emphasizing the operational zero-emission capability of PEMFC fueled by hydrogen, the research scrutinizes the emission intensity from hydrogen production and the impact of component degradation on hybrid system efficiency and hydrogen consumption.

The research pivots around optimizing the design and operation of ship hybrid energy systems to minimize costs while considering well-to-wake (WTW) emissions and component lifetime. It investigates two hybrid configurations: PEMFC/Li-ion battery (LIB) and Diesel Generator (DG)/PEMFC/LIB. Employing a Mixed Integer Linear Programming approach for component modeling, the study conducts a two-stage analysis: design optimization considering various hydrogen sources and plant lifetime estimation focusing on PEMFC and battery degradation.

Initial findings reveal that system design costs do not significantly differ across hydrogen grades. The DG/PEMFC/LIB configuration emerges as cost-effective, reducing CAPEX by 62.8% compared to the PEMFC/LIB setup. Carbon Capture and Storage (CCS) hydrogen grades strike a balance between cost and emission reduction, notably cutting emissions by up to 85% in the PEMFC/LIB configuration at a 27% OPEX increase.

Lifetime estimation highlights the effectiveness of a hierarchical optimization method in mitigating PEMFC voltage loss and extending component lifespan, albeit with increased battery cycling aging. The study underscores the importance of selecting the appropriate hydrogen grade and operational strategies to enhance the sustainability and economic viability of maritime hybrid energy systems, aligning with IMO's emission reduction goals.

Key Words: Proton Exchange Membrane Fuel Cell (PEMFC), Li-ion Battery (LIB), Mixed Integer Linear programming (MILP), Hybrid Energy System, Optimization, Degradation.

Preface

With the completion of this thesis, my journey as a master's student at TU Delft has come to a full circle. Transitioning back to academia after a stint in the industry presented its unique set of challenges, from adapting to a more theoretical approach to learning to managing research projects. Despite these hurdles, the experience was enriching, pushing me to evolve both personally and professionally.

I extend my deepest gratitude to my supervisors, Andrea and Foivos, for their unwavering support and insightful guidance. Andrea, your mentorship was instrumental in navigating the complexities of my project, always helping me to refocus and find clarity in moments of doubt. Foivos, your willingness to engage in brainstorming sessions, even during weekends and holidays, and your meticulous attention to detail in modeling and report proofreading have been invaluable. My sincere thanks also go to Henk, my chair, whose constructive feedback significantly enriched my research.

The support from TU Delft's management, especially in accommodating requests during unforeseen personal circumstances, has been remarkable, and I am truly thankful.

On a personal note, I owe a debt of gratitude to my friends and family, whose support has been my cornerstone. My friends, always just a phone call away, provided solace and encouragement. To my sister, Veena, for her support, humor, and motivation. Most importantly, my heartfelt thanks to my parents, whose faith in me has been unwavering. అమ్మ and నాన్న, your sacrifices and belief in me have shaped who I am today.

This thesis not only signifies the culmination of my academic pursuits at TU Delft but also lays the groundwork for my future endeavors. As I move forward, I carry with me the knowledge gained, the relationships built, and the memories cherished during this pivotal phase of my life.

Arun Datta Beeravelli
Den Haag, February 2024

Summary

The Global Shipping industry is responsible for transporting 90% of global commerce and is responsible for 3% of global green house gas(GHG) emissions. The International Maritime Organization(IMO) has set out to cut annual GHG emissions from international shipping by 40% by 2030 and to reach net zero by 2050. Low Temperature-Proton Exchange Membrane Fuel Cell(LT-PEMFC) hybrid energy systems are being considered as one of the solutions to reduce emissions from shipping.

PEMFC fuelled by hydrogen is operationally a zero-emission solution, but a key issue is the production emission intensity of hydrogen as it can be produced from both fossil and non-fossil sources. Another key factor affecting the decisions of vessel owners is the estimated lifetime of the battery and fuel cell components of the hybrid system, and the increase in the hydrogen consumption due to their degradation. The main research question is as follows:

"How to optimize the design and operation of a ship hybrid energy system to minimize the costs considering the WTW emissions associated with the fuels and what is the lifetime of the installed components?"

This study focuses on two hybrid systems consisting of PEMFC, Li-ion battery(LIB), and Diesel Generator(DG): (i) PEMFC/LIB, and (ii) DG/PEMFC/LIB.

This study is split into two stages: (i) Design optimization and emission analysis across various grades of hydrogen, and (ii) Plant lifetime estimation. For both the stages, a Mixed Integer Linear Programming approach was taken for the component modelling of the hybrid systems and implemented using python and Gurobi optimizer. The PEMFC was modelled using linear equations relating current density, stack power output, and H_2 consumption. The battery power is constrained with the C-rate of the manufacturer, and the Diesel Generator was modelled using a Piece-wise linear (PWL) approximation of the output power and Marine Gas Oil (MGO) consumption.

For the first stage design optimization, 5 different hydrogen sources available in the Netherlands, PEM and Alkaline(ALK) electrolysis, Steam Methane Reforming with Carbon Capture and Storage (SMR+CCS), Auto thermal reforming with Carbon Capture and Storage (ATR+CCS), and the conventional SMR are considered. A single objective cost optimization was set up to analyse the cost and emission trade-offs. The objective consists of component, and storage costs(CAPEX) along with the fuel, and CO_2 costs (OPEX).

The hybrid system configurations obtained in the first stage are used as input for the second stage optimization to estimate the lifetime of the PEMFC and battery. A hierarchical multi-objective operation optimization was set up with the minimization of OPEX of a single trip being assigned the higher priority and the minimization of degradation of the PEMFC assigned the lower priority. For the Lifetime estimation only PEM electrolysis hydrogen has been considered. PEMFC degradation is included in the model by using a stack voltage degradation model and the degradation rates found in literature. The cycling and calendar aging effects of the battery are also modelled but are not part of the optimization. For the consecutive optimization runs have been performed until the end of life of either the PEMFC or battery is reached.

The design results of the first stage optimization do not vary irrespective of the hydrogen grade for both the systems. The CAPEX of DG/PEMFC/LIB hybrid system is 62.8% less expensive than the PEMFC/LIB hybrid system. The CCS hydrogen grades provide a good balance between emission reduction and costs. In the PEMFC/LIB solution they lead to an emission reduction of 85% with a OPEX increase of 27%. In the DG/PEMFC/LIB solution they lead to an emission reduction of 21.85% with an OPEX increase of 17%.

For the lifetime estimation, the hierarchical method leads to a voltage loss reduction of 5.83% for a single trip in the PEMFC/LIB solution. This method has also led to an increase in the cycling aging

of the battery. The PEMFC lifetime has been extended by 2-3 months in the PEMFC/LIB solution and battery lifetime has reduced by 2 months due to the increased cycling aging. The degradation of the PEMFC has also led to hydrogen consumption increase of 16.92% in the single objective optimization and 15.13% in multi-objective method.

In the DG/PEMFC/LIB solution, a 35.73% reduction in voltage loss for a single trip was observed with the hierarchical method. This method has also led to an increase in cycling aging of the battery. The PEMFC lifetime has been extended from 27 to 42 months and the battery lifetime has been reduced by 2 months due to the increased cycling aging. The degradation of the PEMFC and battery causes in increase in H_2 consumption by 10.15% in the multi-objective method.

Contents

List of Figures

List of Tables

Nomenclature

Abbreviations

Abbreviation	Definition
ATR	Auto thermal reforming
BoP	Balance of Plant
CAPEX	Capital expenditures
CCS	Carbon Capture and Storage
DG	Diesel Generator
DOD	Depth of discharge
D&O	Design and Operation
GHG	Green House Gas
ICE	Internal Combustion Engine
IMO	International Maritime Organization
LFP	Lithium Iron Phosphate
LH_2	Liquefied hydrogen
LIB	Lithium Ion Battery
LT-PEMFC	Low Temperature-Polymer Electrolyte Membrane Fuel Cell
MGO	Marine Gas Oil
MILP	Mixed Integer Linear Programming
OPEX	Operational expenditures
SLD	System level design
SMR	Steam Methane Reforming
SOC	State of charge
SOH	State of Health
WTW	Well-to-Wake

1 Introduction

1.1. The need for a sustainable shipping industry

The Global Shipping industry is responsible for transporting 90% of global commerce and is responsible for 3% if global green house gas emissions. If shipping were a country, it would be the 6^{th} largest emitter, even ahead of Germany. While 3% doesn't seem to be large in scale, without significant measures in place this would rise up to 10-13% of global emissions. The International Maritime Organization(IMO) has set out to cut annual greenhouse gas emissions from international shipping by 40% by 2030 and to reach net zero by 2050. Figure 1.1 shows the amount of CO_2 reduction needed for different decarbonization scenarios.

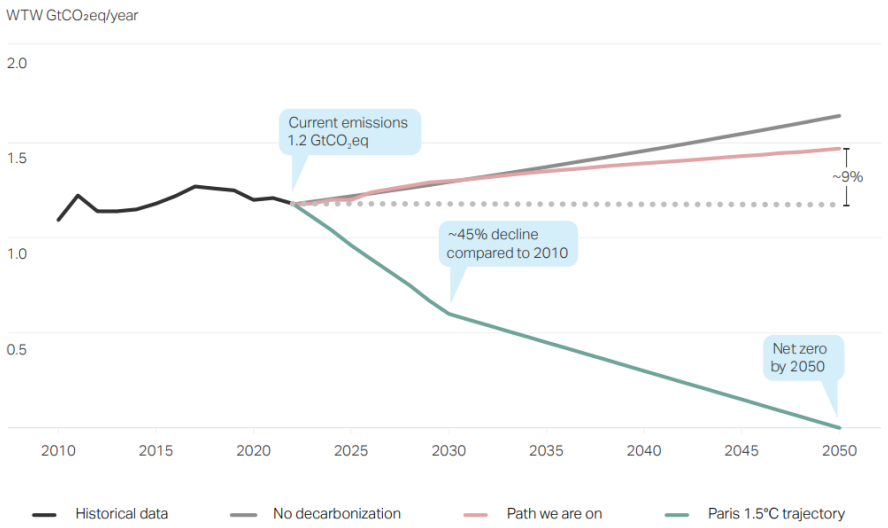

Figure 1.1: Emissions between 2010 and 2050 based on historical data, the path we are on, no decarbonization, and a 1.5°C trajectory based on shipping following the global trajectory presented by the IPCC [1]

In early 2022, the total fleet of seagoing merchant vessels amounted to 102,899 ships of 100 gross tons and above, equivalent to 2,199,107 dwt of capacity. In the 12 months to January 2022, in dwt terms the global commercial fleet grew by 2.95 per cent (table 1.1), an historically moderate growth rate and the second lowest since 2005 (figure 1.2). At the start of 2022, the average age of the global fleet was 21.9 years in terms of number of ships, and 11.5 years in terms of carrying capacity, and in 2022 on both measures the average age continued to increase. Since 2011, the total fleet has aged by 7 per cent, from 20.4 to 21.9 years growing older for all ship types except for bulk carriers, which since 2013 on average have been the youngest vessels (figure 1.2]) [2].

Table 1.1: Global fleet 2021-2022 [2]

World fleet by principal vessel type, 2021-2022 (Thousand dead-weight tons and percentage change)			
Principal types	**2021**	**2022**	**Percentage change 2022 over 2021**
Bulk carriers	913,175 42.75%	946,135 43.02%	3.61%
Oil tankers	619,331 28.99%	629,014 28.60%	1.56%
Container ships	281,825 13.15%	293,398 13.34%	4.11%
Other types of ship:	243,949 11.42%	251,742 11.45%	3.19%
Offshore supply	83,805 3.92%	84,281 3.83%	0.57%
Liquefied Gas carriers	77,458 3.63%	83,770 3.81%	8.15%
Chemical tankers	49,055 2.30%	49,662 2.26%	1.24%
Other/not available	25,443 1.19%	25,690 1.17%	0.97%
Ferries and passenger ships	8,188 0.38%	8,340 0.38%	1.85%
General cargo ships	77,910 3.65%	78,819 3.58%	1.17%
World total	2,136,190	2,199,107	2.95%

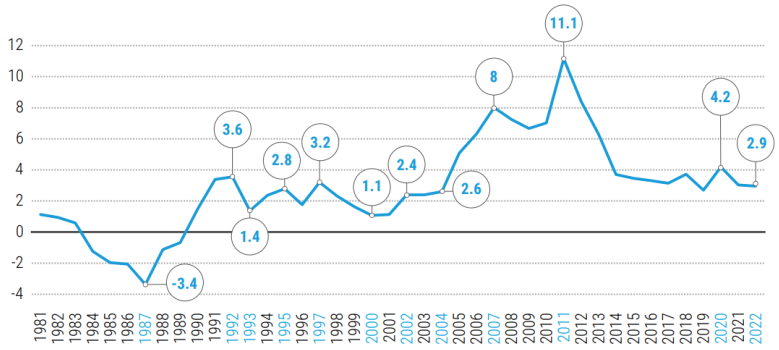

((**a**)) Annual growth rate of world fleet

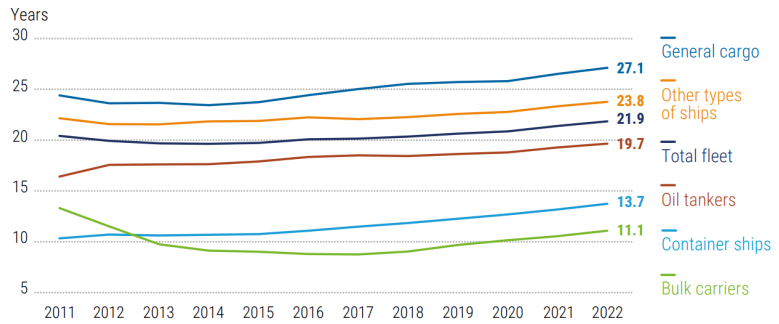

((**b**)) Age distribution of world fleet

Figure 1.2: Age distribution and growth rate of global fleets [2]

The fleet is ageing partly because shipowners and operators, uncertain about future fuel and carbon prices, regulations and technological developments, have delayed investment and are keeping their older vessels in operation [2].

1.2. Fuel Cells for Shipping

Fuel cells, first developed in 1838, are not a new technology but have seen a resurgence of interest in recent years as a key component of renewable energy systems for their ability to convert electricity into hydrogen through electrolysis and vice versa [3]. These electrochemical cells are crucial for the storage, transport, and utilization of renewable electricity [4]. Known for powering hydrogen cars with high efficiency and zero emissions aside from water vapor, fuel cells can also oxidize various fuels, such as hydrocarbons, alcohols, and ammonia, without relying on combustion [5]. This avoids the heat and conversion losses and pollutant formation associated with conventional power generation, offering a cleaner alternative [6]. A simplified fuel cell schematic in figure 1.3 illustrates hydrogen fuel being oxidized at the anode, with the resulting protons passing through a membrane to react with oxygen at the cathode, producing water and electricity through an external circuit to provide useful work [7]

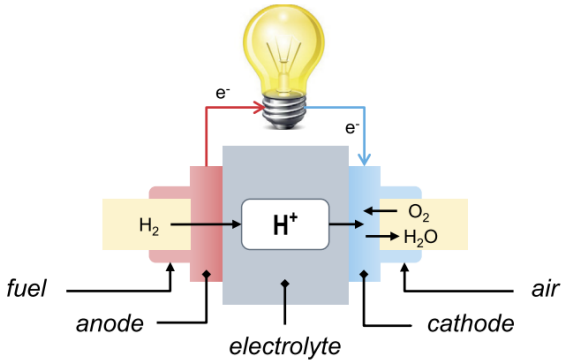

Figure 1.3: Simplified Schematic of the working principle of a fuel cell with a proton conducting electrolyte [7]

Table 1.2: Characteristics of LT-PEMFC, HT-PEMFC and SOFC [8]

	LT-PEMFC	**HT-PEMFC**	**SOFC**
Operating Temperature (°C)	65-85	140-180	500-1000
Electrical Efficiency(%LHV)	40-60	40-50	50-65, up to 90 (CHP)
Fuel Requirements	99.99% H_2	CO <3%	S <20ppm
Gravimetric power density (W/kg)	125-750	25-150	8-80
Volumetric power density (W/L)	50-400	10-100	4-32
Stack lifetime (kh)	5-35	5-20	20-90
System lifetime	$\geq$ 10 years with stack replacement		
Cold start-up time	<10 s	10-60 minutes	>30 minutes
Load transients (0 to 100%)	seconds	<5 minutes	<15 minutes
Current Capital cost ($/kW)	1000-2500	3000-5000	3500-15000
Future capital cost ($/kW)	60-600	150-1500	500-2000
Maritime TRL(2020)	6-7	5-6	4-5
Cooling medium	Liquid	Liquid	Air

The different fuel cell technologies are elaborated on in detail in the appendix B and the most promising technologies identified for maritime applications are Low Temperature-Polymer Electrolyte Membrane

Fuel Cell (LT-PEMFC), High Temperature-Polymer Electrolyte Membrane Fuel Cell (HT-PEMFC), and Solid Oxide Fuel Cell (SOFC) whose characteristics are listed in the table 1.2. Among the three, the most developed fuel cell solution is LT-PEMFC. The main drawback of utilizing LT-PEMFC is the need for high purity hydrogen. HT-PEMFC on the other hand also uses hydrogen, but can cope with lesser quality hydrogen. SOFC's can be fuelled with different types of hydrocarbon fuels, ammonia and also hydrogen. In terms of electrical efficiency LT-PEMFC and SOFC are better compared to HT-PEMFC. SOFC are advantageous if the combined heat and power efficiencies are considered. In terms of power density, LTPEM fuel cells are the most competitive and are also competitive with gas fuelled engines. LT-PEMFC are also better suited to handle load transients, where as SOFC and HT-PEMFC need minutes, and are not flexible in handling load fluctuations. LT-PEMFC are also advantageous with low start-up and shut down times [8].

The figure 1.4 shows the typical operating characteristics of fuel cells which differ from traditional internal combustion engines. Fuel cells typically have a high efficiency at relatively low load, where the electrochemical losses in the stack are limited, while internal combustion engines are usually most efficient close to their operating point [9].

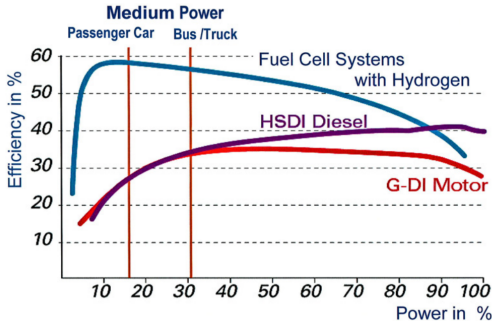

Figure 1.4: Comparison of efficiencies of Fuel cells and Internal combustion engines [9]

Due to the advantages of LT-PEMFC systems compared to the SOFC and HT-PEMFC, the focus of this thesis would be on the adoption of LT-PEMFC systems for reducing emissions from the shipping industry.

1.3. Typical Architecture of PEMFC energy systems for shipping

There are two main possible uses of PEMFC on board of ships: (i) as auxiliary power system or (ii) as propulsion system. Cleary, if PEMFC are used as main propulsion system, the ship will have an electrical propulsion, where an electrical generator (alternator) powers the propellers. Differently, if PEMFC are used as auxiliary power units, the ship can either have an electrical propulsion or a mechanical propulsion, where the shaft of the propulsion Internal Combustion Engine (ICE) is directly connected with the propellers [10].

When PEMFC are used in mobility applications, they are usually coupled wih electrical energy storage systems (EESS) such as batteries into the hybrid power-trains to improve the system response to load changes and to allow the PEMFC to operate in the best of load conditions. This is valid also for shipping applications, and it is particularly the case of PEMFC used for propulsion [11]. Hybrid powertrains generally encompass a main power source (e.g. ICE, PEMFC) and a EESS (e.g. supercapacitors, battery). According to the way the power sources are connects to the EESS, hybrid powertrains can be classified as series, parallel, or series-parallel hybrid [12], [13]. Figure 1.5 reports the simplified schematics of the three hybrid configurations including both ICE and PEMFC. In Figure 1.5 all the electrical power units are connected to a Direct Current (DC) bus, as this type of connection allows an easier and more efficient power distribution between the power units operating in DC and the DC power loads [14], [15], [16]. Indeed, although today ships mainly rely on Alternating Current (AC) grids at fixed frequency, recent studies [14], [15], [16] demonstrated that the latest development in the power electronic technologies and highly stable DC systems could lead to a widespread use of onboard DC grid. As for the

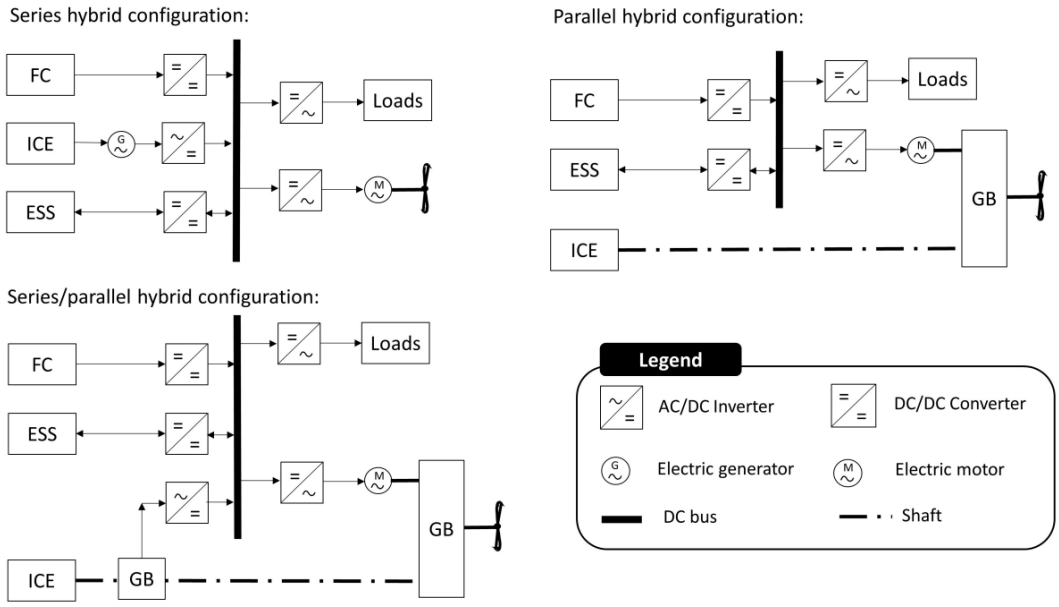

Figure 1.5: Typical configurations of hybrid power-train architectures including both FC and ICE [10]

EESS, Figure 1.5 reports the general case where EESS is recharged by the main power source through a bidirectional power connection with the DC bus. Alternatively, EESS could be directly recharged with onshore electricity when the ship is mooring (i.e. plug-in hybrid) [17]. Although this solution would reduce ICE or PEMFC sizes and fuel consumption [18], it would require additional components to be installed on board, the development of an onshore infrastructure, and it might also imply longer stay at quay for ships at berth to ensure sufficiently long recharging time [19], [20].

The advantages of hybrid energy systems along with emission reduction, reliability and redundancy are the transient load response, adaptation to various operation modes, reduction in fuel consumption and reduced noise and vibrations [21]. These additional energy systems provide a fast system response and the operational capability of the vessel is enhanced. Reduction in fuel consumption, because the engines do not run at part loads also leads to reduction of operational expenditures for vessel owners. As fuel cells and batteries do not have internal moving components as combustion engines, they offer the advantage of reduced noise and vibration [21].

1.4. Research Problem

Two main problems have been identified in the adoption of PEMFC hybrid energy systems for improving the sustainability of the shipping industry, which are described as follows:

(i) Production emissions of hydrogen

LT-PEMFC, powered exclusively by hydrogen, offer a zero-emission solution as they only emit water. However, the environmental impact largely depends on how the hydrogen is produced. Currently, most hydrogen is 'grey,' produced via steam reforming of methane or 'brown/black' from coal. If CO_2 emissions from these processes are captured, the resulting hydrogen is termed 'blue.' In contrast, 'green' hydrogen is produced through electrolysis using renewable energy, and 'pink' hydrogen via nuclear power. As of the end of 2021, 47% of hydrogen production comes from natural gas, 27% from coal, 22% from oil, and only 4% from electrolysis, with less than 1% considered green due 33% of worldwide electricity coming from renewable sources [22].

Therefore, it is important to consider the production emissions of hydrogen during the design stage of the hybrid energy system to provide a holistic view to the vessel owner and aid in decision making.

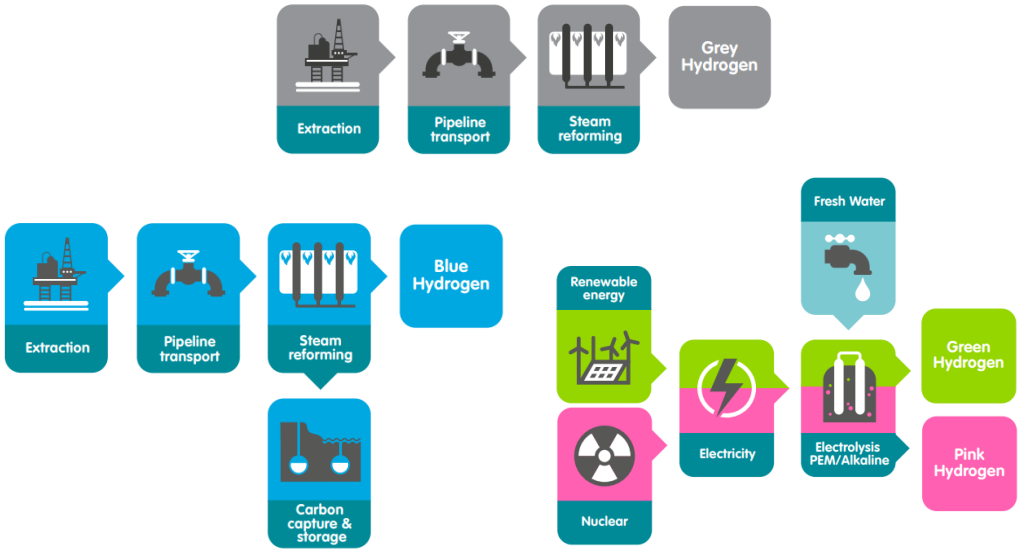

Figure 1.6: Grey, Blue, Pink and Green Hydrogen Production Pathways [22].

(ii) Degradation of PEMFC and battery

Another critical factor influencing vessel owners' decision-making regarding the adoption of PEMFC hybrid energy systems is the anticipated lifetime of the system. This consideration is due to the degradation of the PEMFC and battery systems over time, as well as the increased hydrogen consumption resulting from the reduced efficiency of the PEMFC stack and battery.

1.5. Research Objective and Research Questions

The objective of this thesis is to conduct an in-depth analysis and optimization of two hybrid energy systems in series configuration for a general cargo vessel: (i) PEMFC/LIB, and (ii) DG/PEMFC/LIB where PEMFC refers to (Low-Temperature)Polymer Electrolyte Membrane Fuel Cells, DG denotes Diesel Generators, and LIB stands for Lithium-ion Batteries. This research aims to achieve the following consolidated goals:

1. **Design Optimization and Emissions-Cost Trade-Offs:** To optimize the design of the hybrid energy systems by minimizing total costs while considering the well-to-wake(WTW) emissions from the utilization of various grades of hydrogen. It will include a detailed evaluation of the trade-offs between costs and emissions, offering insights into how different hydrogen grades impact both operational expenses and the environmental footprint of the cargo vessel.

2. **Lifetime Estimation of PEMFC and LIB Components:** To estimate the operational lifetime of the PEMFC and battery components in both hybrid configurations, assessing efficiency and performance degradation over time. This analysis aims to provide comprehensive insights into the long-term operational efficiency and reliability of the hybrid energy systems.

Through these objectives, the thesis intends to contribute to the advancement of sustainable maritime transport by offering a holistic approach to the design and lifecycle management of hybrid energy systems, thereby supporting the industry's transition towards more environmentally friendly and cost-effective operations.

Based on the above objectives the main research question that this thesis would like to answer is:

How to optimize the design and operation of a ship hybrid energy system to minimize the costs considering the WTW emissions associated with the fuels and what is the lifetime of the installed components?

To answer the above main research question, the following sub research questions have been formulated:

- **SRQ-1**: What are the emissions associated with the different types of hydrogen and Marine Fuels?
- **SRQ-2**: What are the different aging modelling methods of PEMFC and Li-ion batteries?
- **SRQ-3**: What are the different mathematical optimization techniques that are currently being utilized in the hybrid energy system design and operation of ships?
- **SRQ-4**: How can the hybrid energy system be modelled for the design and lifetime estimation of PEMFC and LIB components?
- **SRQ-5**: What are the costs and emission trade-offs associated with the PEMFC/LIB hybrid vs DG/PEMFC/LIB hybrid energy system?
- **SRQ-6**: What is the estimated lifetime of the PEMFC and batteries?

1.6. Research Scope and Assumptions

This thesis will research the design and operation optimization of the proposed hybrid energy system configurations for a general cargo vessel. The following points serve as indicators of the research's scope and assumptions:

- The auxiliary loads and sizing of the electric motors/generators will not be included in the optimization problem.
- Weight limitations of the power components would not be considered in this study.
- The weight and volume limitations of H_2 and MGO storage would not be considered in this study.
- Economic uncertainties in fuel, components, electricity, and carbon taxes are not considered.
- The results would be evaluated on the basis of cost and emission trade-off's across both the hybrid system configurations.
- The design results obtained from the first stage design optimization would be fixed for the plant lifetime estimation in the second stage to reduce computational complexity.
- The economic evaluation would neglect the replacement and maintenance costs of the system components.

Key Performance Indicators (KPI's)

To compare the new, optimized layout options with one another and the vessels conventional propulsion system, a number of evaluation criteria must be established. Defining Key performance indicators (KPIs) is a very valuable way of measuring performance and serves as a tool for making decisions. An important aspect of KPIs is that they assist in sorting and limiting the amount of relevant data by making comparisons. KPIs in shipping are often related to costs, emissions, efficiency, delivery time, profits, safety, and more. Three different KPIs will be used to evaluate the new configurations.

- Cost-effectiveness. The hybrid optimum configurations produced from the optimization will be evaluated according to the expenses (investments and operational costs) across the various grades of hydrogen.
- Emission reduction/mitigation. The optimal configurations would be evaluated against the current configuration on-board and the emissions across the various grades of hydrogen would be evaluated.
- Lifetime Estimation. The lifetime of the installed PEMFC and battery components would be evaluated by comparing the results of energy management strategies with and without incorporating the PEMFC degradation.

1.7. Thesis outline

In this section, the structure of the thesis is explained, providing an overview of each chapter and its content.

The chapter 2 provides a literature review of different strategies being employed in reducing emissions from shipping. The different storage media of hydrogen on-board ships, and the emissions and costs of different grades of hydrogen are also explored in this chapter. The working principle of PEMFC along with the main Balance of Plant (BoP) components required is discussed in detail, followed by the cost modelling and degradation prediction methods of PEMFC. Different Li-ion battery chemistries along with the factors affecting their utilization and life-cycle are elaborated on. The final part of the chapter looks into different studies on the design and operation optimization of a hybrid power plant from a mathematical design perspective.

Chapter 4 provides the mathematical modelling approach used to design the hybrid systems is elaborated on. Further on the methodology to calculate the estimated lifetime of the installed PEMFC and battery systems is also described. Chapter 5 presents the results and analysis of the two optimization stages i.e. cost and emission trade-off's and the lifetime of the installed components. The final chapter 6, provides the conclusions of this study.

Table 1.3 provides an overview of all the chapters and specifies the research questions addressed in each chapter, highlighting the alignment between the research questions and chapters.

Table 1.3: Thesis structure

Chapter	Title	Research Questions
1	Introduction	-
2	Literature Review	1,2,3
4	Methodology and Modelling	4
5	Results and discussion	5,6
6	Conclusions	MRQ

2
Literature Review

2.1. Strategies to reduce shipping emissions

The reduction of GHG emissions from maritime transport is a complex issue, which involves various aspects of ship design, construction, operation and disposal. In general, the maritime emission reduction strategies are classified into two macro-categories: (i) operational measures and (ii) technical measures [23], [24], [25], according to whether the measures address (i) the way the ship is operated (e.g. speed, route choice according to weather conditions, etc.) or (ii) the design and technical aspects of the ship (e.g. propulsion systems, hull design, emission abatement systems, fuel type, etc.). Each strategy comes at different costs and technological maturity, and can guarantee different levels of emission reduction. Moreover, it should be noticed that only some of the technical strategies can be applied to existing vessels, i.e. as retrofit measures, while others only apply to existing ships. Differently, all the operational strategies can generally be applied independently to both existing and new built vessels [24]. Table 2.1 reports a summary of the main technical and operational strategies that can be followed for reducing shipping emissions, specifying those that can be applied as retrofit measures to existing vessels [23], [24], [25].

Table 2.1: Main emission reduction measures in shipping (✓= applicable; ✗= not applicable) [23], [24], [25]

Category	Sub-category	Strategy	Retrofit
Technical Strategies	Power and Propulsion	ICE Advanced Turbocharging	✓
		ICE Water Injection	✓
		ICE Air humidification	✓
		ICE hybridization	✓
		Thrust efficiency improvement	✗
		Assisted propulsion with renewable sources	✓
		Alternative power systems	✓
		Alternative fuels	✓
		Onshore Power Supply(OPS)	✓
	Emission Abatement Systems	Scrubber	✓
		Selective Catalytic Reduction (SCR)	✓
	Ship Fluid Dynamics	Hull resistance reduction	✗
		Air Lubrication	✓
		Aft body and forebody optimization	✓
		Ship sizing and weight optimization	✗
Operational Strategies	Voyage Optimization	Speed reduction	✓
		Weather/routing optimization	✓
		Ship speed optimization	✓

	Just-in-time arrival	✓
	Trim, draft, and ballast optimization	✓
Vessel Maintenance	Hull roughness control	✓
	Propellor roughness control	✓
Energy Management	Onboard energy demand reduction	✓
	Fuel quality control	✓

With regards to the technical strategies, a first option is to act on the power and propulsion system. For example, some measures aim to reduce the fuel oil consumption by improving the efficiency of the ICE [26], [27], while others involve the humidification of the inlet air or the water injection to reduce the pollutant emission during combustion [28], [29]. Other measures could be taken to hybridize the ICE with an electric energy storage system(EESS)(e.g. Batteries, super capacitors etc.) to improve the operating conditions of the ICE [26], [27], [30], [13]. Alternatively, some studies [31], [32] propose to assist the propulsion by means of renewable energy sources, particularly solar and wind assisted propulsion, or to substitute ICE systems with low emission power plants(e.g. fuel cells or batteries) [33]. Other papers and initiatives [19], [20], [34] propose the use of OPS to cut the emissions of ships at berth (often referred to as cold ironing). Another sub-category of technical measures is represented by those actions that aim to directly abate the pollutant and/or GHG emissions through the installation of emission abatement technologies on board (e.g. SCR or scrubbers), helping to curb the emission levels under the national and international thresholds [35]. However, the bulkiness and weight of emission abatement systems often hamper their installation onboard [36]. Lastly, other technical strategies involve the improvement of the ship performance in fluid dynamic terms. For example, it could be possible to reduce the fuel consumption and hence emissions from shipping by reducing the hull resistance in the ship design phase, or by installing air lubrication systems that reduce the hull resistance also in existing vessels [27], [30] . Also the way the ship is operated can sensibly help in reducing the fuel oil consumption, and hence emissions. For instance, recent studies are proposing new ship navigation management systems that optimize the route according to the weather and sea conditions [37], [38], or that optimize the ship operation while guaranteeing reduced navigation speed [34]. Lastly, also the control of the hull and propellers roughness to ensure adequate fluid dynamic performance over time, and the energy management onboard (e.g. by limiting the onboard energy demand) could help in reducing shipping emissions [24].

2.2. Hydrogen

In this section, the different storage mechanisms that are suitable to store hydrogen on-board the ship would be looked into, followed by the different production emission intensities of the various grades of hydrogen that are currently available in the market. The final part explores the costs of different grades of low-carbon hydrogen along with the most produced hydrogen type.

2.2.1. Hydrogen Storage

Hydrogen storage systems can be classified into physical storage (compressed gas, cryogenic) and solid materials(physisoprtion, chemical storage) [39]. The gravimetric and volumetric energy densities of hydrogen are used to assess the suitability of the storage media [40]. figure 2.1 compares the volumetric and gravimetric H_2 densities of the most common hydrogen storage methods. Although solid-state hydrogen storage systems have lower volumetric density and theoretical potential, additional system requirements must be met [41]. Further along this section only compressed and liquefied hydrogen storage would be reviewed.

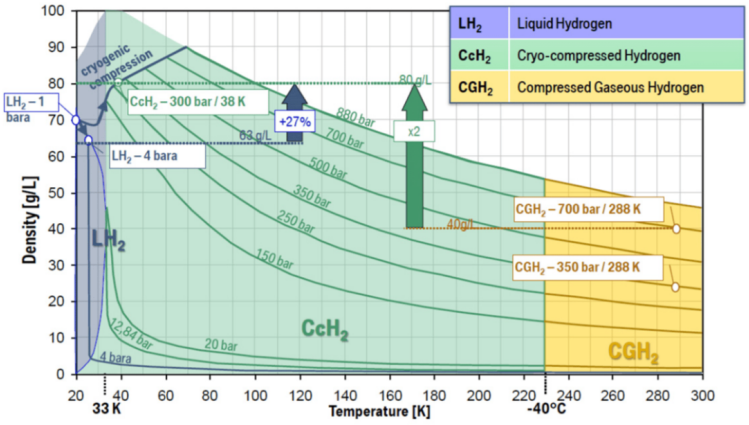

Figure 2.1: Hydrogen density vs pressure and temperature [42], [43]

Compressed Hydrogen

The most mature technology to store hydrogen for mobility applications is CH_2 [44]. Shipping applications make no exception, although in this case the large quantities of hydrogen needed for shipping may be challenging if CH_2 is considered. Indeed, CH_2, is generally characterized by low energy densities, which imply bulky storage on-board. As shown in table 2.2 which reports the main categories of CH_2 cylinders classified according to the materials and storage pressures [44], [45], [46], [47], [48] energy density is particularly low for type-II and type-II cylinders. Nonetheless, Type I and Type II cylinders are also the cheapest ones, and hence are often preferred in maritime applications. Type III and Type IV cylinders, have higher energy densities, mainly related to the materials used for the cylinders liner, but also linked to the higher pressure levels achievable (potentially up to 1000 bar for Type IV cylinders).

Table 2.2: Main characteristics of CH_2 storage cylinders [46], [47], [44], [45], [48], [43]

Type	Materials	Maximum Pressure (bar)	volumetric density (kWH/L)	gravimetric density (kWH/kg)	Cost ($/kg)	Technological Maturity	Composite layers load sharing
I	All-Metal, usually asutenitic steels or aluminium alloys	≤300	0.3-0.5	0.3-0.6	83	++	-
II	Load-bearing metal liner hoop wrapped with resin-impregnated filament	≤700	0.4-0.5	0.5-0.8	86	+	45% load sharing
III	Non-load-bearing metal liner axial and hoop wrapped with resin-impregnated filament	≤700	0.3-0.8	1.1-1.9	700	-	80% load sharing
IV	Non-load bearing non-metal liner axial and hoop wrapped with resin-impregnated filament	≤1000	0.3-0.7	1.4-2.7	600-700	-	100% load sharing

Higher storage pressures also imply higher energy required by the hydrogen compressors of the bunkering stations, and hence higher costs [44]. Indeed, bunkering process and infrastructure have a key role in assessing the technical and economic feasibility of CH2 fuelled ships. In general, the main components of a CH2 bunkering station are: compressors, chiller units, and pressure regulation valves. Chiller

units are needed to keep the hydrogen temperature under the set limits, hence ensuring the right pressure levels and also avoiding material stresses due to high temperature in the CH2 cylinders. A further issue that may arising during CH2 bunkering process is the under-filling of the cylinders [49]. In fact, hydrogen temperature increases also during expansion processes, hence resulting in lower density of the gas and a consequent under-filling of the cylinders. To avoid such issues, the bunkering speed needs to be accurately monitored to keep hydrogen temperatures in the desired range (usually under 85°C) [50]. To avoid the issues linked with the installation and management of such a bunkering infrastructure, some projects [51] proposed the use of swappable CH_2 cylinders that can be loaded/unloaded on/from the ship when needed [52]. Nontheless, such solution may not be convenient for large ships as it would imply long port calls [53].

Liquefied Hydrogen

The storage of hydrogen in liquefied form, i.e. as LH_2, allows to overcome the problems linked to the bulkiness of hydrogen storage systems, as LH_2 itself has a density(at -253°C at 1 bar) of 70.9 kg/m^3, three orders of magnitude higher than hydrogen at atmospheric conditions. Figure 2.2 reports the volumetric and gravimetric energy densities of both CH_2 and LH_2 cryogenic tanks as emerged from the analysis of different commercial products [45], highlighting the convenience of LH_2 over CH_2 in terms of space requirements on board. Nonetheless, the cryogenic storage conditions of LH_2 (at -253°C) required the use of specific materials and of complex safety instrumentation and technologies [47]. Moreover, give the high levels of energy required for hydrogen liquefaction (12kWH for kg of liquefied hydrogen) [54], only a few large plants today produce LH_2, and only recent projects [55] are investigating the possibility of exporting LH_2 by ships. Also for these reasons, time is still needed before LH2 is available on a large scale for use as fuel in shipping. Similarly to what previously seen for CH2, also for LH2 the bunkering system plays a crucial part in assessing the economical and technical viability of a LH2 fuelled ship. Several studies in the literature propose and analyze different configurations for LH2 bunkering stations [56], [57]. For example, in [56] two methods are proposed for the LH2 bunkering for the SF-BREEZE ferry concept. The first option involves the use of a Pressure Building Unit (PBU) to transfer LH2 from the on land LH2 storage system (either stationary or mobile on a truck/ship), while the second option envisages the use of a cryogenic pump. PBU are generally cheaper than cryogenic pumps, although the latter are less energy demanding and allow shorter bunkering times than PBU [58]. As of 2022, only few LH2 bunkering station have been developed [59]. As reported in [60], the lack of infrastructure is indeed one of the most critical bottlenecks in the large scale utilization of LH2 in maritime transportation, and it is hence expected that a transition towards LH2 use in shipping would imply high cost also due to the development or retrofit of the necessary infrastructure.

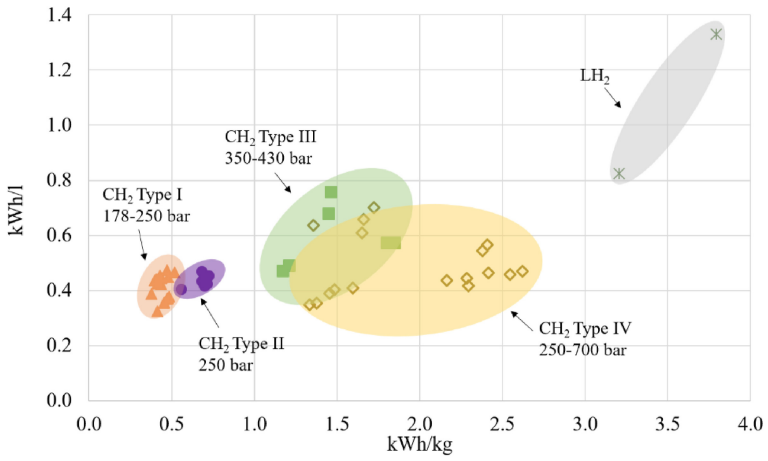

Figure 2.2: Volumetric and gravimetric energy densities of CH_2 cylinders and LH_2 cryogenic tanks [61]

Comparison of the main hydrogen storage media

The other types of hydrogen storage media include metal hydrides, liquid organic hydrogen carriers(LOHC) etc. The different hydrogen storage media are listed in the table 2.4 along with their densities, operating pressures and temperatures, and cost of the storage media [62], [43].

Table 2.3: Comparison of main hydrogen storage media [43], [62]

Storage Technologies	Volumetric Density (kg H_2/m^3)	Gravimetric Density Reversible (wt %)	Operating Pressure (bar)	Operating Temperature (K)	Cost* ($/kg)
Compressed Gas	17-33	3-4.8 (system)	350 and 700	ambient	400-700 *
Cryogenic	35-40	6.5-14 (system)	1	20	200-270*
Cryo-Compressed	30-42	4.7-5.5 (system)	350	20	400
High pressure-solid	40	2 (system)	80	243-298	
Sorbents(H_2)	20-30	5-7 (material)	80	77	
Metal Hydrides (H)	<150	2-6.7 (material)	1-30	ambient-553	>500
Complex Hydrides(H)	<120	4.5-6.7 (material)	1.50	423-573	200-450*
Chemical Hydrides (H)	30	3-5 (system)	1	353-473	160-270**

*cost estimates based on 500,000 units of production. ** Regeneration and processing costs are not included.

2.2.2. Hydrogen Production Emission Intensities

There are multiple methods of production of hydrogen, both from fossil and non-fossil sources. In this section, the production emission intensities of the different types of hydrogen grades are elaborated on. In the report by [63] the Well-to-Gate Production emissions are accounted, and have been used as reference for this study. The exact scope of emissions used in this study are shown in figure 2.3. Scope 1 covers emissions from sources that an organisation owns or controls directly, Scope 2 are emissions that a company causes indirectly and come from where the energy it purchases and uses is produced, and Scope 3 encompasses emissions that are not produced by the company itself and are not the result of activities from assets owned or controlled by them, but by those that its indirectly responsible for up and down its value chain.

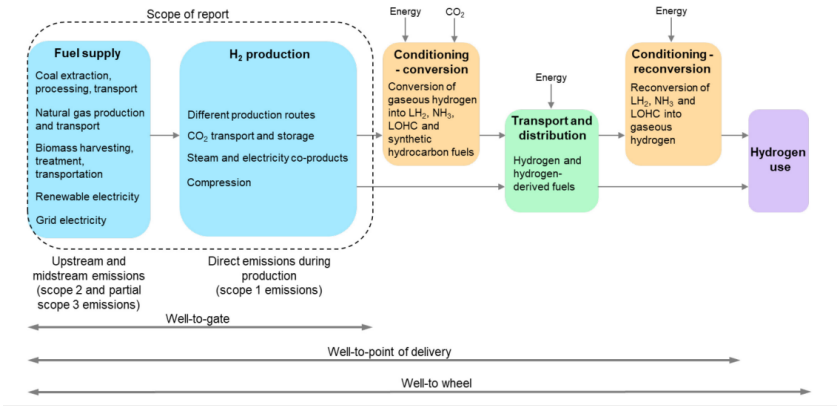

Figure 2.3: Scope and system boundaries for emissions accounting schemes [63]

The emissions according to the different production sources are shown in the figure 2.4. Three primary means of hydrogen are production shown are coal gasification with and without CCS, and the same with Natural Gas Steam Methane Reforming, along with Electrolysis. The production emissions highly depend on the capture rate of CCS for fossil sources and the grid emissions for electrolysis. The production of H_2 using Natural gas without CCS leads to emissions of 11-12 kg CO_2-eq/kgH_2 which is the most common production method of hydrogen currently accounting for 62% of the total. With CCS and SMR the emissions vary between 1.5-6.2 CO_2-eq/kgH_2. Among the fossil sources coal gasification

without CCS leads to highest emissions of up-to 22-26 CO_2-eq/kgH_2, and with CCS the emissions from coal gasification are 2.6-6.6 CO_2-eq/kgH_2 [63].

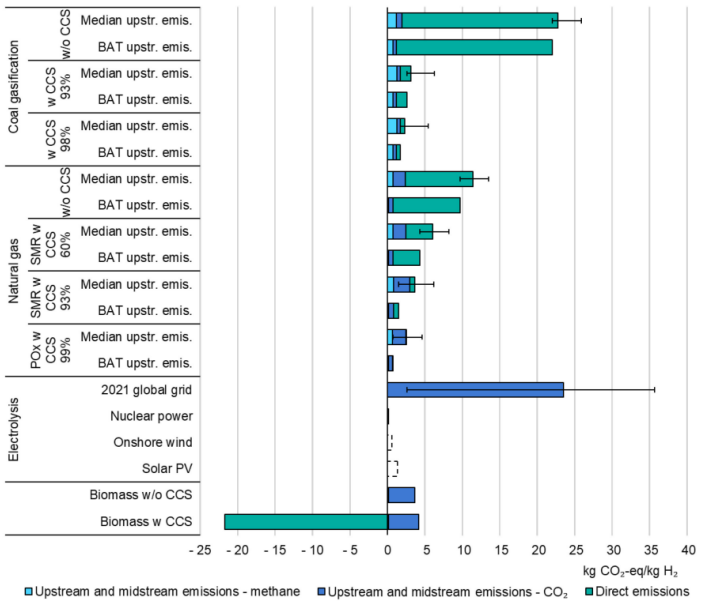

Figure 2.4: Comparison of the emissions intensity of different hydrogen production routes, 2021 [63]

BAT=best available technology, CCS= carbon capture and storage

The electricity source used also highly matters in the amount of emissions from electrolytic production of hydrogen. Using the current average global CO2 intensity of 460 g CO_2-eq/kWh results in an emissions intensity for hydrogen of 24 kg CO_2-eq/kgH_2, similar to the emissions for hydrogen from unabated coal, but can be as low as 0.5 kg CO_2-eq/kgH_2 in a country such as Sweden, which has one of the lowest emission factors for grid electricity production in the world today.

2.2.3. Costs of Hydrogen in the Netherlands

The S&P Global Platts hydrogen assessments tracks the regional price differences and month-on-month changes of hydrogen across the world for different low-carbon hydrogen production methods [64]. The global hydrogen prices as of November 2023 are shown in figure 2.5:

For the Netherlands this index tracks hydrogen produced from four different methods, namely SMR+CCS, ATR+CCS, PEM and ALK electrolysis. The price of SMR without CCS is also added for reference in this study in the following table 2.4, and the prices as of November 2023 for are as follows:

Table 2.4: Hydrogen prices in the Netherlands as of November 2023. [64], [65], [66], [63]

Hydrogen Production Method	Cost $/kgH2	kg CO2-eq/kgH2
SMR + CCS	3.82	2.5
SMR	2	12
ATR + CCS	3.77	3
PEM Electrolysis	8.4	0
ALK Electrolysis	7.19	0

costs of hydrogen with CCS are inclusive of carbon costs.

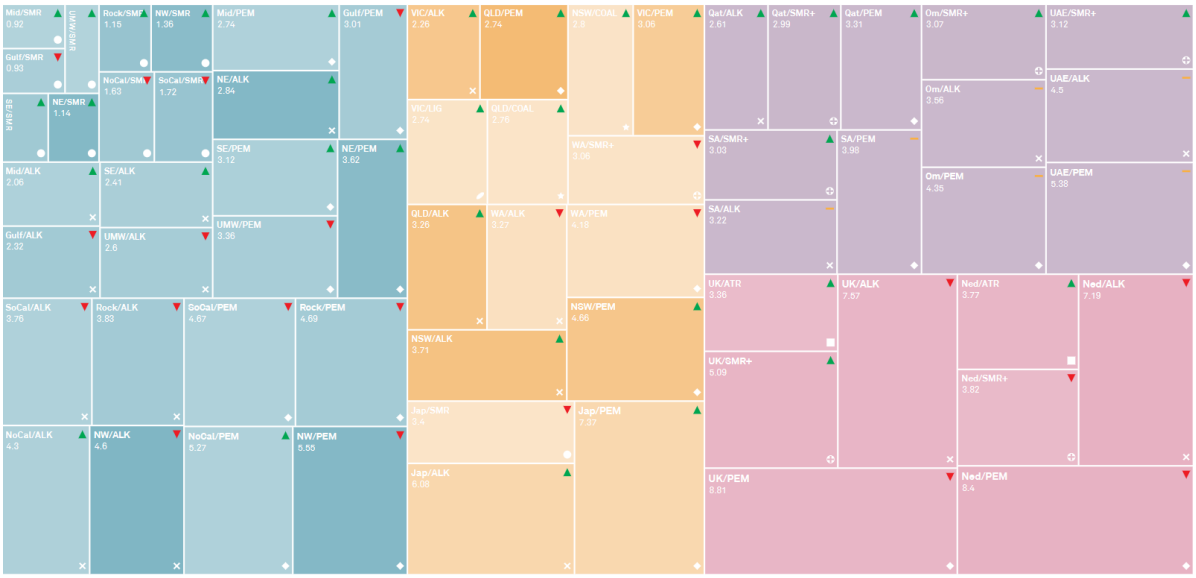

Figure 2.5: S&P Global hydrogen price assessments [64]

2.3. Well-to-Wake emission factors for Marine Fuels

Comer and Osipova have published the Well-to-Wake emission factors for various marine fossil fuels that are currently being used in the shipping industry across a range of ICE [67]. These fuels include Heavy fuel oil(HFO), very-low sulphur fuel oil(VLSFO), Marine gas oil (MGO), and liquefied natural gas(LNG) [67].

The climate pollutants that have been considered in this study, and their associated 100 and 20 year Global warming potentials (GWP) have been shown in table 2.5:

Table 2.5: Global warming potentials of climate pollutants

Pollutant	100-year	20-year
CO_2	1	2
CH_4	29.8	82.5
N_2O	273	273
BC	900	3200

A ship's CO_2e_{WTW} can be calculated based on the mass of the fuel that the ship consumed and a well-to-wake carbon dioxide equivalent factor (CEF_{WTW}) for that fuel, as shown in equation.

$$CO_2e_{WTW} = FC \times CEF_{WTW} \tag{2.1}$$

where:

- CO_2e_{WTW} = well-to-wake emission emissions in gCO_2e
- FC = fuel consumption in g
- CEF_{WTW} = well-to-wake carbon dioxide equivalent factor for that fuel in gCO_2/g fuel.

The carbon dioxide equivalent factors CEF_{WTW} are shown in the figure 2.6.

Fuel type	Engine type	Well-to-wake (g/g fuel)					
		EF_{WTW}				CEF_{WTW}	
		CO_2	CH_4	N_2O	BC	CO_2e100	CO_2e20
HFO	SSD	3.545	0.00404	0.00018	0.00020	3.892	4.559
	MSD	3.545	0.00404	0.00017	0.00050	4.159	5.516
VLSFO	SSD	3.734	0.00453	0.00019	0.00020	4.098	4.792
	MSD	3.734	0.00453	0.00018	0.00050	4.366	5.749
MGO	SSD	3.782	0.00466	0.00019	0.00005	4.016	4.372
	MSD	3.782	0.00466	0.00018	0.00027	4.211	5.073
LNG	LNG-Otto-MS	3.280	0.05336	0.00014	0.00003	4.930	7.801
	LNG-Otto-MS + crankcase	3.280	0.05977	0.00014	0.00003	5.121	8.330
	LNG-Otto-SS	3.280	0.03499	0.00014	0.00003	4.385	6.288
	LNG-Otto-SS + crankcase	3.280	0.04175	0.00014	0.00003	4.586	6.845
	LNG-Diesel	3.280	0.01958	0.00023	0.00002	3.940	5.008
	LBSI	3.280	0.04438	0.00014	0.00003	4.663	7.060
	LBSI + crankcase	3.280	0.05079	0.00014	0.00003	4.854	7.589
	Steam Turbine	3.280	0.01824	0.00008	0.00002	3.859	4.856

Figure 2.6: Well-to-Wake emission factors for each pollutant (EF_{WTW}) and associated carbon dioxide equivalent factors (CEF_{WTW}) [67]

2.4. LT-PEMFC

Starting from a brief overview on the working principle of PEMFC, this section describes the main characteristics of PEMFC that may be relevant for marine applications. A particular focus will be given in section 2.4.2 towards PEMFC degradation.

2.4.1. PEMFC working principle

Figure 2.7 shows a simplified schematic of the PEMFC working principle, representing the operation of a single cell. Hydrogen enters the FC at the anode side, while oxygen enters the cell at the cathode side. Anode and cathode are separated by a polymer electrolyte (i.e. the proton exchange membrane), usually Nafion®[68], that allows only protons (H+) to pass through. At the anode side hydrogen is ionized thanks to a platinum-based catalyst.At this point, the protons migrate through the polymer electrolyte membrane towards the cathode, while the electrons, blocked by the membrane, pass through a wire connection to an electrical load (e.g. a DC motor or an electric accumulator) and eventually reach the cathode. The cathode, supplied with (atmospheric) oxygen, receives the hydrogen protons through the electrolyte and the electrons through the electrical circuit, and thanks to a platinum-based catalyst a chemical reaction that produces pure water is triggered.

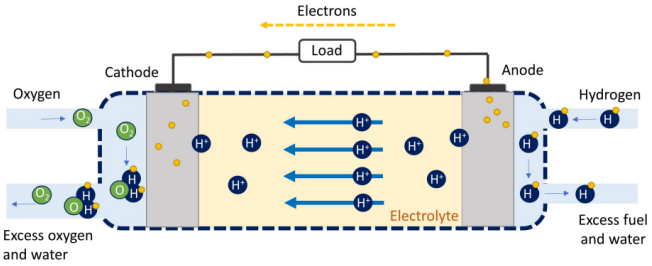

Figure 2.7: PEMFC working principle

PEMFC are modular power units, in which single cells can be grouped together to make a module. Several modules together make up a PEMFC stack, which can eventually be coupled with other stacks to meet the power and voltage required by the specific applications. While recent projects aim to reach MW-scale power plants, it is important to analyze the reason behind such power limitation. Firstly,

MW-scale PEMFC would imply larger hydrogen consumption and hence bulkier and heavier storage systems. Secondly, MW-scale PEMFC plants would also entail a larger and more complex BoP, i.e. the set of auxiliary components needed to run the system. For PEMFC systems, the BoP can be generally divided into three main subsystems:(i) fuel processing and fuel/air supply lines, (ii) cooling circuit, (iii) power conditioning, control and monitoring. Figure 2.8 shows a simplified schematic of the typical structure of a liquid cooled PEMFCs BoP. The fuel processing and fuel/air supply lines subsystem ensures the appropriate conditions of fuel and air at the PEMFC inlet. In addition to the basic components shown in Figure 2.8, the fuel processing line could also encompass a reformer to obtain hydrogen from hydrogen carriers, hydrogen evaporator if LH_2 is considered, hydrogen humidifier to ensure the correct hydrogen humidity at the PEMFC inlet, a condensate collector to remove liquid water from the circuit, and a hydrogen re-circulation pump. As for the air processing line, in addition to the air filter, blower, humidifier, and water separator shown in Figure 2.8, it is important to notice that for maritime PEMFC application it may be necessary to remove sodium chloride vapor from the inlet air in order to prevent the degradation of the PEMFCs membrane due to the exposure to sea-air conditions [69], [53]. The role of the cooling circuit is to keep the operating temperature of the PEMFCs stack in the range of 65-70°C [70]. Liquid cooling system is often preferred for PEMFC in mobility applications, thanks to its large cooling capability and good efficiency [140]. Demineralized water or mixtures of demineralized water and ethylene glycol are typically used as refrigerants [71]. Other types of cooling may be edge cooling, air cooling, and phase change cooling [72]. As shown in Figure 2.8, the cooling circuit subsystem typically encompasses a re-circulation pump, a refrigerant reservoir, and a heat exchanger. In addition, a deionizer might be included in the system to keep the refrigerants conductivity in the desired range, avoiding PEMFC short circuits. Lastly, all the instrumentation and components necessary for acquiring data and monitoring the system operation are part of the power conditioning, control, and monitoring system. Example of components included in the power conditioning, control, and monitoring system are: safety valves, pressure transducers, temperature transducers, power inverter/converter, remote control system. Table 2.6 reports a summary of the main components of a PEMFCs BoP and their role in a PEMFC system.

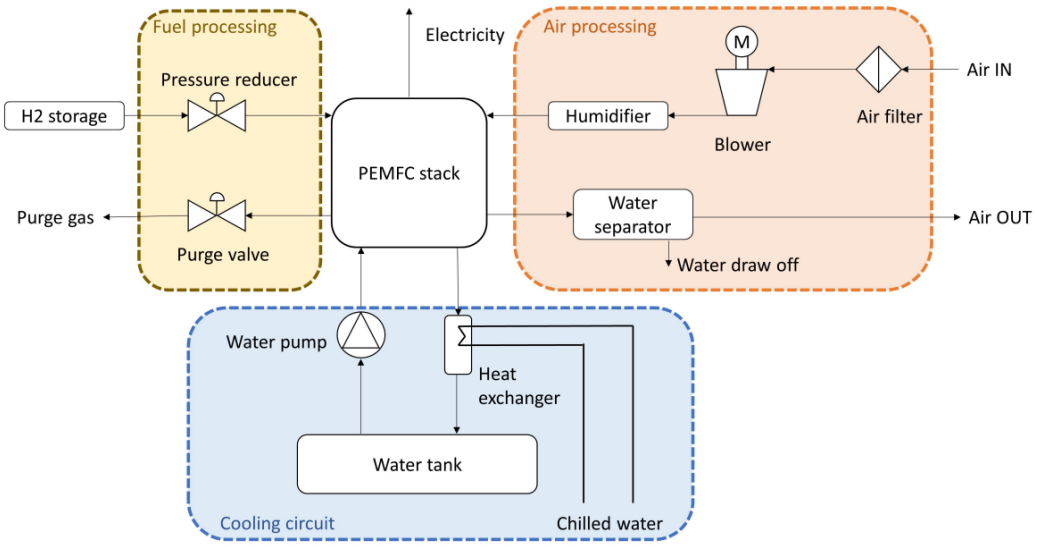

Figure 2.8: Simplified schematic of a PEMFC BoP, divided into three main subsystems. The power conditioning, control, and monitoring system is not represented here for the sake of image clarity [71], [10]

Table 2.6: Main components of each subsystem of the BoP of a PEMFC system [71], [73], [74], [75], [10].

BoP System	BoP Component	Role	Typical Requirements and additional remarks
Fuel processing and fuel/air supply lines	Fuel reformer + purification units	When hydrogen is not stored in its pure form, chemical and/or physical reactions are triggered in the fuel reformer, which convert fuel(eg. LOHC, NH3, and NG) into pure hydrogen for feeding PEMFC. reformers are usually followed by a purifier that guarantees the absence of pollutants in the Hydrogen fuel that may poison the PEMFC stack (eg. CO and NH3)	ISO 14687 and SAE J2719 limits: Max CO: 0.2 ppm. Max NH3: 0.1 ppm
	Hydrogen Evaporator	When hydrogen is stored in liquid form, the evaporator is needed to obtain gaseous hydrogen at the PEMFC inlet.	-
	Hydrogen pressure reducers	Guarantee the right pressure of hydrogen fuel entering the fuel cells	Hydrogen pressure at PEMFC inlet: 3-6 bar.
	Hydrogen humidifier	Guarantees the right level of humidity in the hydrogen fuel to maintain good performances of the polymer electrolyte membrane.	-
	Condensate collector	Prevents residual water in liquid form in hydrogen inlet stream that enters the PEMFC stacks	-
	Hydrogen recirculation pump	Allows the recirculation of residual hydrogen in the system.	-
	Sodium chloride removal pretreatment	Prevents the degradation of the membrane due to exposure to sea-air conditions. It is usually implemented in marine PEMFC applications	-
	Inlet air blower	Pressurizes the atmospheric air that enters the stack, maintains a sufficient air flow to the stack and potentially allows the reduction of stack sizes by increasing the inlet-air density.	-
	Inlet air filter	Prevents pollutant in the inlet air stream to enter the PEMFC.	-
	Inlet air humidifier	Guarantees the right level of humidity in the inlet air to maintain good performances of the polymer electrolyte membrane.	-
	Inlet air condensate collector	Prevents residual liquid water in air inlet stream from entering the PEMFC stacks.	-
	Outlet air condenser and condensate collector	Partially recovers steam residuals in the air outlet stream to reuse in the humidifiers.	-

Cooling circuit (liquid cooling case)	Refrigerant circulating pump	Guarantees a sufficient refrigerant flow rate to the stack to keep the stack temperature in the desired range.	PEMFC desired temperature range: 50-70°C Typical coolant pressure range at the PEMFC inlet: 1.5-2 bar.
	Refrigerant reservoir	In case of liquid cooling refrigerant, ensures that the coolant flow rate remains in the recommended range.	Coolant flow rate dependent on FC stack characteristics and cooling circuit geometry
	Heat exchanger	Dissipate the waste heat of the stack to the surrounding environment or to the heat recovery system.	-
	Deionizer	Usually connected to a conductivity meter, allows to keep the refrigerant conductivity under the set limits to prevent the short circuit of the stack.	Electrical conductivity usually limited to values $<100\mu$s/cm.
Power conditioning, control and monitoring	Safety valves	Ensure the system operation under safe conditions	Usually required to comply with ATEX directives.
	Measuring Instrumentation	Ensures the correct monitoring of the system and the data acquisition needed by the control system. Common instrumentation includes pressure transducers, temperature transducers, flow meters.	-
	Control System	Ensures the correct operation of the stack to guarantee the compliance with safety regulations and power demands of the load. The control system also provides for emergency shutdown procedures	-
	Power inverters/ converters	Ensures the correct connection of the PEMFC with the electric load.	

2.4.2. PEMFC degradation

A major drawback of PEMFC systems is their performance degradation over time, which generally results in a voltage drop that prevents the PEMFC to work properly. In the literature, the following main sources of PEMFC degradation are identified: operation at low or high current, galvanostatic decay, load cycling, and start/stop phases [76]. More in detail, PEMFC operation at low current might result in high cathode voltage, electrodes oxidation, and change in the polymer decomposition mechanism [77], [78]. Differently, when PEMFC are subject to high current, they may incur increased membrane temperature and possibly overcurrent that cause local hot spots if the cooling capabilities are exceeded. Additionally, high current operation may also results in fuel starvation [79], [80], [81]. Also when operating at constant current, the PEMFC is subject to degradation, mainly due to the galvanostatic decay. Nonetheless, galvanostatic decay is often neglected as it is the the degradation cause with the lowest impact on the overall PEMFC degradation rate [82]. As for load cycling, it is considered the first cause of electrode oxidation, platinum dissolution and corrosion of carbon support, as it increases the cathode potential hand hence accelerates its dissolution [83], [84]. Start/stop phases, instead, results in a non-uniform distribution of the reactant gas due to the decrease of the active surface area caused by the carbon oxidation of the anode [84], [85]. All these causes generally concur in determining the overall degradation of the cell, although load cycling and frequent start/stop phases are generally the greatest causes of degradation [76].

PEMFC stack ageing is usually modeled through three approaches: impedance estimation (based on electrochemical impedance spectrometry), remaining useful life estimation, and a stack voltage degra-

dation model. Stack voltage degradation model are often used to limit the computational effort required in solving complex energy system models, although such modelling approach is less accurate with respect to other degradation models and strongly depends on experimental data [86].

2.4.3. PEMFC costs

Kampker, Heimes, Kehrer, *et al.* developed a cost calculation model for Polymer Electrolyte Membrane (PEM) fuel cell systems based on the method of Process Based Cost Modeling (PBCM) [87]. The modelled system consists of the single cell components Bipolar plate (BPP) and Membrane electrode assembly (MEA), the stack components, and the Balance of Plant (BoP) (Figure 2.9).

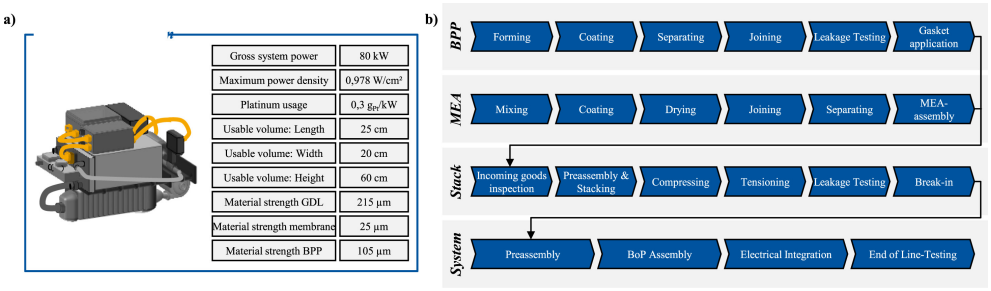

Figure 2.9: (a) Defined Product specification; (b) defined process chain to produce fuel cell systems [87]

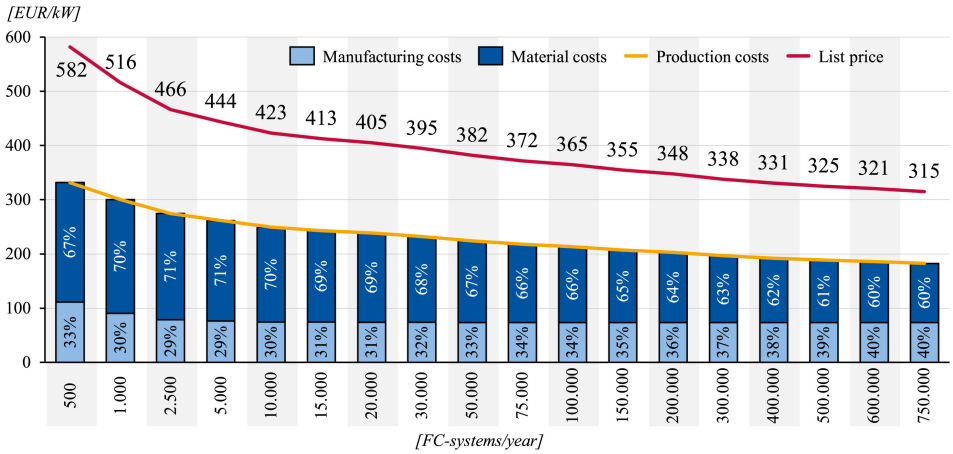

Figure 2.10: Costs of fuel cell systems depending on the annual number of units produced [87]

The resulting costs from the modelling approach are shown in the figure 2.10. The production and list prices have been modelled from annual production volumes of 500 to 750,000 fuel cell systems in 18 steps. For each production volume, the relative distribution of manufacturing and material costs to the production costs is shown. For the defined scenario, it is noticeable that the target price of the product from 30,000 fuel cell systems produced per year is 395 €/kW. this output is equal to the value announced by Toyota in 2020 [88]. The manufacturing costs account for an average of two thirds of the target price. In addition, material costs always account for the largest share of the costs compared to manufacturing costs. Their relative share varies between 60% and 71%. The cost modelling also shows a sharp decline in absolute production costs between production volumes of 500 and 2,500 systems per year [87].

2.5. Energy storage in Batteries

This section provides an overview of the battery(Li-ion) energy storage systems that are applicable for hybridization of PEMFC systems as mentioned in section 1.3. Batteries are storage systems for

electrical energy, which is stored as chemical energy. They can convert this energy back into electrical energy as needed. There are two main types of batteries: primary and secondary. Primary batteries are disposable once they are discharged, while secondary batteries can be recharged and discharged.

There are multiple different types of commercially available battery technologies that are available in the market such as Lithium-Ion, Lead-Acid, Nickel-Cadmium, Rechargeable Nickel, and High-temperature Sodium [89].

2.5.1. Lithium-Ion Batteries

Li-ion batteries are the most prominent batteries that is currently being utilized across the world in various applications ranging from smartphone batteries to electric vehicles.

The term 'specific energy' and 'energy density' are often interchanged with each other. However, the first refers to the amount of energy contained per unit mass, while the second refers to the amount of energy contained per unit volume. The higher specific energy is, the lighter the battery is per energy content. A similar situation occurs regarding energy density. The higher the energy density is, the more compact the battery is per energy stored. The figure 2.11 shows the different types of lithium batteries with respect to specific energy and energy density. The batteries with high specific energy and energy densities are favourable. Another important factor to be considered is that the theoretical energy density and the actual density of the manufactured lithium-ion batteries is many fold lower (shown for a LFP battery).

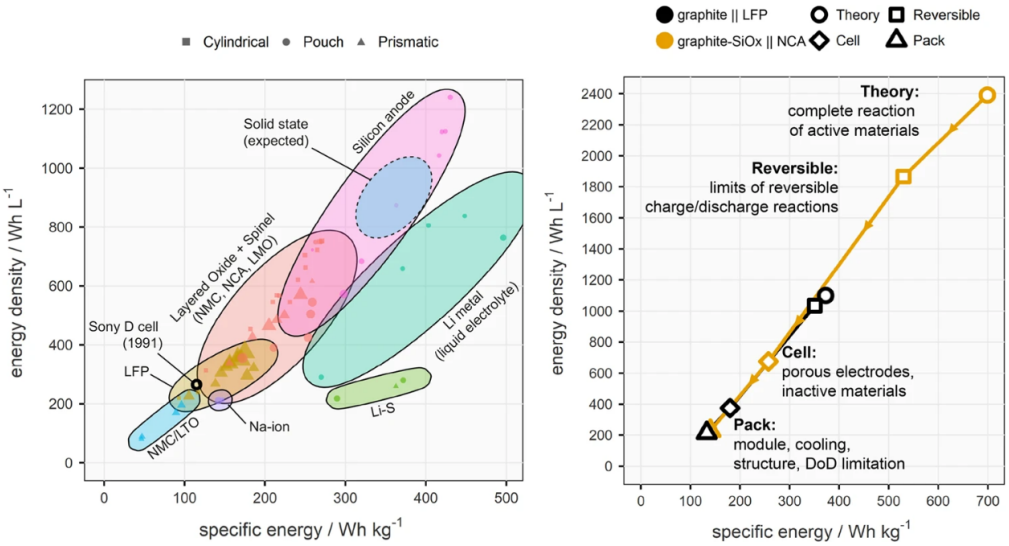

Figure 2.11: Visual representation of the range of energy content of different battery technologies at the cell level and energy losses between theory and system level. [90]

The lithium batteries available all use carbon or graphite based anodes and differ from each other by the cathode chemistry. They are listed as below [89]:

- Nickel Manganese Cobalt Oxide (NMC): $LiNi_{1-x-y}Mn_xCo_yO_2$
- Lithium Iron Phosphate (LFP): $LiFePO_4$
- Nickel Cobalt Aluminium Oxide (NCA): $LiNiCoAlO_2$
- Lithium Cobalt Oxide (LCO): $LiCoO_2$
- Lithium Manganese Oxide Spinel (LMO): $LiMn_2O_4$

The are also advances in the anode chemistry currently being researched such as graphene, titanate and silicon. Batteries that use titanate in the anode of the battery are referred to as Lithium Titanate Oxide (LTO) batteries. The cathode can be other typical chemistries such as LMO or NMC. The use

of titanate will typically increase the power level of the battery as well as greatly increase the cycle life. This battery has actually been available for some time now and is used in applications requiring high power and high cycle life (for instance hybrid cars and buses) [89].

2.5.2. Factors affecting the life-cycle and utilization of batteries

This subsection provides a brief overview of key concepts regarding battery systems. These are important concepts that need to be considered when integrating batteries into maritime power systems [89]:

C-rate: Power vs Energy

Batteries combine the roles of fuel tank and engine, where their energy capacity (kWh) is like the fuel tank size, and power output (kW) is like the engine size. The C-rate, measured as kW/kWh, indicates how quickly a battery can charge or discharge, reflecting the power it can produce relative to its energy capacity. Higher C-rates allow for faster charging and discharging but can reduce the battery's lifetime. Essentially, a larger battery with a specific C-rate can deliver higher power levels, but operating frequently at high C-rates may shorten its lifespan. [89]. Too high currents will create lithium plating and increase the cell temperature which has a negative effect on the lifetime of the battery. In the below figure 2.12 the effect of charging and discharging at various charge rates is shown [89].

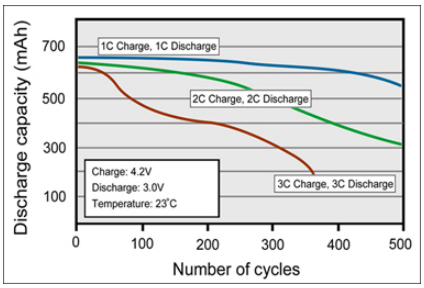

Figure 2.12: Discharge capacity for different charge and discharge C rates

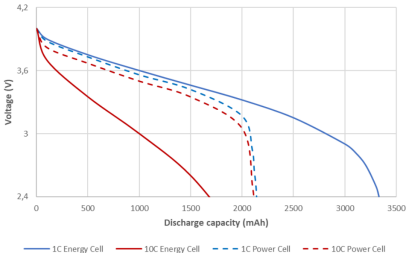

Figure 2.13: Comparison between an energy cell and power cell

Battery cells are designed either for high current handling (power cells) or for high energy storage (energy cells), with a trade-off between current capacity and energy density (Figure 2.13). Energy cells have higher internal resistance and show a more significant decrease in capacity at high discharge rates (C-rates) compared to power cells. Lithium-ion cells, in particular, are more sensitive to fast charging than fast discharging, suggesting that fast charging should be used sparingly to extend battery life [89].

State of charge and Depth of Discharge

State of Charge (SOC) indicates the remaining energy in a battery, similar to a fuel gauge, shown as a percentage of full capacity. Depth of Discharge (DOD) represents the energy used, with 0% DOD indicating a full battery and 100% DOD an empty one. While DOD describes the energy withdrawn, it can be misleading for cycle size since cycles may not reach 100% SOC. Instead, Delta State of Charge (DSOC) or SOC Swing, which measures the range between maximum and minimum SOC during operation, are recommended for clarity. For example, a battery cycling between 75% and 25% SOC has a 50% DSOC. [89].

State of Health

The capacity of the battery decreases over time due to cycling and temperature variations, called degradation of the battery. The initial capacity is called the nominal capacity. The degraded capacity is indicated by the State Of Health (SOH). The SOH is the percentage of the nominal capacity and indicates the amount of energy that can still effectively be used [89].

Thermal runaway

Thermal runaway is the phenomenon in which the lithium-ion cell enters an uncontrollable, self-heating state which can result in ejection of gas, shrapnel and/or particulates, extremely high temperatures, smoke and fire safety risks. Thermal runaway can occur due to an internal short circuit caused by physical damage to the battery or poor battery maintenance. To prevent these risks, batteries need to be stored at their appropriate temperatures with proper ventilation.

Effect of cycle size and SOC

Battery lifetime decreases with larger Delta State of Charge (DSOC) or cycle sizes, but using a larger battery can extend its life, though the impact varies by chemistry and manufacturer. Different lithium-ion batteries (e.g., NMC vs. LTO) show diverse lifespans under the same conditions (Figure 2.14). The specific SOC range affecting cycling also influences lifetime differently; for example, cycling between 100% and 50% SOC may impact lifespan differently than cycling between 50% and 0% SOC, even with the same DSOC (Figure 2.15) [89].

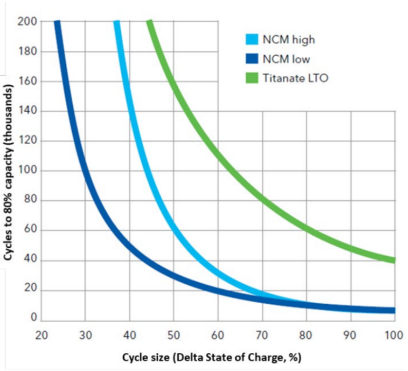

Figure 2.14: Cycles as a function of DSOC for NMC

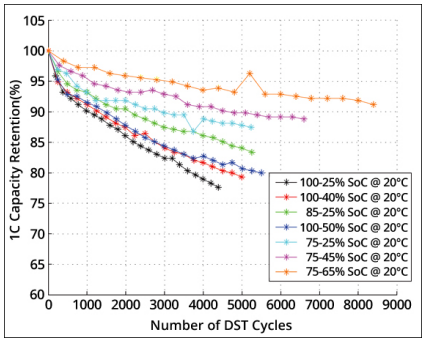

Figure 2.15: Capacity loss as a function of charge and discharge bandwidth [91]

Temperature Effects

An important factor to a long life of the battery system is to keep the cell temperature within the optimal range, usually 20° - 30°C. For low temperatures, the performance of the batteries is reduced resulting in lower efficiency, lower available capacity, higher internal resistance, and reduced allowable power levels (particularly for charging) - even when the elevated internal resistance generates some extra heat. Improper operation at low temperature can lead to significant safety risks. Extended operation of a battery at low temperatures, even within rated specifications, has also been shown to reduce the thermal stability of the battery [89]. Modern lithium-ion batteries are likely to be able to perform well at higher temperatures (for example above 35°C) demonstrating higher efficiency and higher capacity but operation at elevated temperatures will almost always result in reduced lifetime [89].

Calendar aging

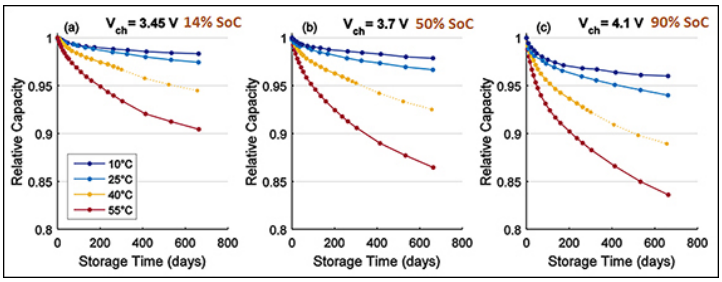

Figure 2.16: Capacity fade by calendar aging with different charge end voltages and temperatures [92]

The figure 2.16 illustrates capacity fade as part of calendar aging over 700 days at different State-of-charge (SoC) levels and temperatures. The largest capacity losses are recorded at high charge voltage, high SoC and elevated temperatures. None of the Li-ion cells were charged to 4.2V/cell to reach full SoC, as done with a mobile phone battery because the capacity losses would be large. Under the right conditions capacity fade in storage can be kept below 10% in 15 years. Calendar ageing and capacity fade are accumulative. Fading is not linear: the highest drop occurs at the beginning and fading slows with time [92].

2.5.3. Overview of lithium battery technologies

Due to the variation in the cathode and anode battery chemistries (figure 2.17), this results in a wide range of properties in lithium batteries. An overview of different lithium technologies is presented in the table 2.7. LCO batteries contain high specific energy but are limited by their low specific power, whereas for LMO batteries are the opposite and are safer than LCO batteries. NMC batteries offer both high capacity and high power, and are the most favoured batteries in the automotive industry. LFP batteries are one of the most safest li-ion batteries due to their high thermal runaway temperatures, but offer low capacity. NCA batteries share similarities with LCO batteries but are lighter and serve as energy cells. LTO batteries offer significantly long life and can be charged and discharged rapidly, but suffer from lower specific energy. LTO batteries can also be operated in a wider temperature range.

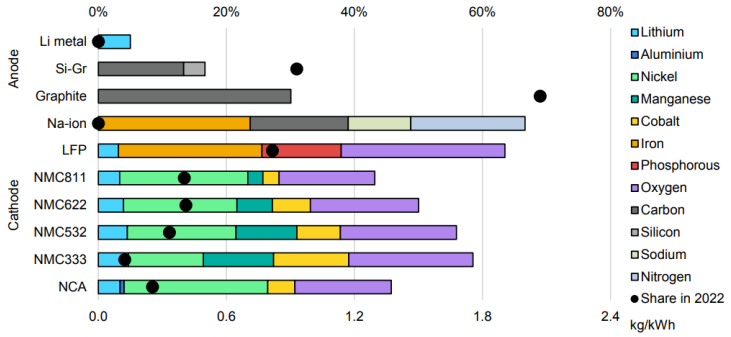

Figure 2.17: Material content of different anodes and cathodes in Li-ion batteries [93]

Table 2.7: Overview of different lithium battery characteristics [94], [95], [96].

	Lithium Cobalt Oxide (LCO)	**Lithium Manganese Oxide (LMO)**	**Lithium Nickel Manganese Cobalt Oxide (NMC)**	**Lithium Iron Phosphate (LFP)**	**Lithium Nickel Cobalt Aluminum Oxide (NCA)**	**Lithium Titanate (LTO)**
Anode	Graphite	Graphite	Graphite	Graphite	Graphite	$Li_4Ti_5O_{12}$
Cathode	$LiCoO_2$	$LiMn_2O_4$	$LiNi_{1xy}Mn_xCo_yO_2$	$LiFePO_4$	$LiNiCoAlO_2$	NMC or LMO
Nominal voltage (V)	3.60	3.70 (3.80)	3.60 (3.70)	3.20, 3.30	3.60	2.40
Full charge voltage (V)	4.20 V	4.20 V	4.20 V (or higher)	3.65 V	4.20 V	2.85 V
Discharge voltage (V)	3.00 V	3.00 V	3.00 V	2.50 V	3.00 V	1.80 V
Minimal Voltage (V)	2.50 V	2.50 V	2.50 V	2.00 V	2.50 V	1.50 V
Charge rate (C)	0.7C-1C	0.7C-1C	0.7C-1C	1C	1C	1C (5C max)
Discharge rates (C)	1C	1C (10C possible)	1C-2C	1C (25C pulse)	1C	10C possible
Specific Energy (Wh/kg)	150-200	100-150	150-220	90-120	200-260	50-80
Energy Density (Wh/L)	400-640	240-360	150-400	100-300	490-670	170-230
Life cycle at 80% DOD	500-1000	300-700	1000-2000	2000	500	3000-7000
Thermal Runaway (^oC)	150^oC	250^oC	210^oC	270^oC	150^oC	-

2.6. Optimization of hybrid energy systems

Designers need to manage trade-offs in energy density, specific energy, cost, and storage type when planning adoption of alternative fuels and technologies. Moreover, regulations, fuel infrastructure and converter technology will undergo a transformation during a new vessels 25-30 year lifetime. The range of suitable technologies for a given vessel, and their economics, depend on key decisions made in the new-build concept design phase. Failure to manage and adapt to these changes risks rendering a vessel economically unfit.

Cost-optimal selection of fuels, machinery and energy efficiency measures for ships involves searching through a large space of alternatives. in order to deal with this complex problem of optimal sizing and selection, various optimization techniques have been used to determine the choice of energy systems and sizing.

In the first part of this section, an introduction to system level design (SLD) of hybrid energy systems in vehicles is presented along with the different control strategies for energy management of hybrid vehicles. In the second part, different state-of-art optimization studies that have been currently implemented in various sectors are analysed.

2.6.1. System level design (SLD) of hybrid power plants

Having more than one source of power, hybrid power-trains give birth to a large design space for the physical system and increase the complexity of the control algorithm. The coupling (dependence) between the parameters of the physical system (e.g., topology) and the parameters of the control algorithm transforms the problem into a multilevel problem (as depicted in Fig 2.18) that, if solved sequentially, is by definition sub-optimal [97]. Therefore, the physical system and the control algorithm should be designed in an integrated manner to obtain an optimal system design [98]. For the plant design and control problem, there are three coordination architectures as shown in fig 2.19.

1. alternating plant and control design, i.e., first, the plant is optimally designed. Using this outcome, the controller is optimally designed. Subsequently, the plant is optimized again, etc. The coordinator alternates between optimizing the plant and optimizing the control until the coupled variables have converged;
2. control design nested within plant design, i.e., every evaluation of a plant requires the full optimization of the controller design;
3. simultaneous plant and controller design (i.e., solving (2) all in one).

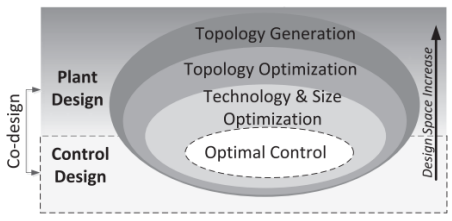

Figure 2.18: Hybrid electric vehicle(HEV) system level design(SLD) and it's multilayers [98]

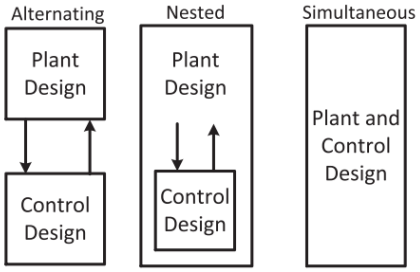

Figure 2.19: Coordination architectures for system level design [98]

Control strategies for energy management

As described in section 2.6.1 the power plant design of a hybrid electric vehicle along with control optimization(energy management) leads to optimal solutions. the control strategies for energy management of hybrid vehicles can be categorized into two, namely rule based and optimization based (figure 2.20) [99]. Rule-based control strategies are fundamental control schemes that depend on mode of

operation. They can be easily implemented with real-time supervisory control to manage the power flow in a hybrid drive train. The rules are determined based on human intelligence, heuristics, or mathematical models and generally without prior knowledge of a drive cycle [99]. In optimization based control strategies, the goal of a controller is to minimize the cost function. The cost function (objective function) for an HEV may include the emission, fuel consumption, and torque depending on the application [99].

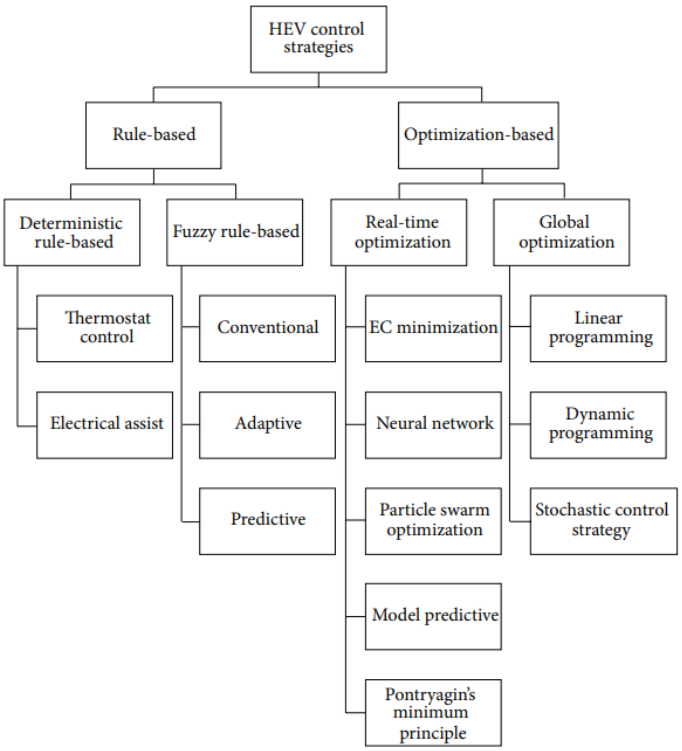

Figure 2.20: Classification of control strategies for energy management in hybrid vehicles [99]

Energy vs Power Management

A suitable control system is a prerequisite for the successful and efficient operations of a hybrid vessel. A basic feature is that the momentary load should be split between the available power sources(ICE, fuel cell, battery) on-board. On a larger timescale, the available energy should be managed properly in order to execute a mission in an energy efficient way. Energy management can be approached from different perspectives. Examples of objectives are to minimize fuel consumption, sustain battery state of charge to maximise the fuel cell or system efficiency.

A control scheme of a hybrid system typically has two management levels: energy management and power management. The energy management system is at the top level to ensure that sufficient energy is provided to execute a given task. It determines the power set-points for the energy suppliers. The task may take minutes (manoeuvring) to several hours (voyages), so the timescale is generally large. For example, a given task for the battery system could be to provide boosting power for sailing at high speeds. The EMS should ensure that the battery is sufficiently charged to do so. Power, being the rate at which energy is delivered, should also be managed at a smaller timescale. The power management system (PMS) controls the current and voltage set-points to prevent that limits are exceeded.

2.6.2. Review of Optimal Sizing Studies

There are lot of uncertainity in the future of maritime ship energy systems. To tackle this problem for ship owners Ritari, Huotari, and Tammi performed a multi-period modelling considering retrofits and alternative fuels [100]. In this study, the choice of energy sources and converters based on future price

forecasts was answered to minimize the total cost of ownership to the owner, even considering factors such as carbon taxes. The decision problem was formulated as a mixed integer linear programming problem (MILP), and was applied for a roll-on roll-off ferry operating in the Baltic sea. It was found that retrofitting existing technologies to adopt alternative fuels was more economical than fuel switching alone, and the use of batteries reduced costs. previous studies considered fixed docking times, and this resulted in less than optimal installation times. The unique contribution of this study was the simultaneous consideration of discrete (installation) and continuous (sizing) design decisions for the lifetime investment planning of the vessel.

Baldi, Brynolf, and Maréchal performed a study to minimize the total cost of ownership of a vessel in the the pathway towards reducing GHG emissions proposed by the international maritime organization. The study was modelled as a MILP problem and was studied for a container ship, cruise ship and a tanker. In this study retrofits were excluded [101]. It was found that the costs to reduce GHG emissions upto 75% were relatively similar to baseline of IMO's proposed targets (50-70% higher), but moving towards full decarbonization resulted in costs of 280-340% higher than the business as usual scenario. In [102], a model for concurrent optimization of machinery system design and emission control installation was developed. Interactions and compatibility issues between controls and between controls and machinery systems have been taken into consideration. Satisfying power demand at all time and complying with emission regulations were modeled as main constraints while the solution was driven by costs.

In the study [103] by Trivyza, Rentizelas, and Theotokatos, economic and environmental factors are combined to guide the design of ship energy systems. It utilizes a simulation model to predict the performance of energy systems over the ship's lifetime and employs a genetic algorithm, NSGA-II, to solve the multi-objective optimization problem of selecting the optimal configuration. The method's application to an Aframax oil tanker case study demonstrates that adopting technologies such as LNG fuel, dual fuel engines, fuel cells, and carbon capture can enhance sustainability, but the latter comes at a higher cost, highlighting the need for trade-offs in decision-making.

For the sizing optimization of anchor handling tug supply vessel, Zhu, Chen, Wang, *et al.* used NSGA-II (introduced by Deb, Pratap, Agarwal, *et al.*) to search the design space. In this study the optimization was done for a Diesel ICE-Battery hybrid system in which shore power was used to charge the battery. The pareto solutions of NSGA-II are compared against (multi-objective particle swarm optimization) MOPSO[106], the solutions generated by NSGA-II solutions were less distributed [104]. In [104], the outer search space for component sizing uses Multiobjective particle swarm optimization(MOPSO), and in the inner layer of control for energy management uses AECMS(adaptive equivalent consumption minimization strategy). Real time HIL tests were also conducted for this study to test the effectiveness of the optimization. the optimal solution of the proposed methods was also found to be significantly superior to single-level optimizations.

Dolatabadi and Mohammadi-Ivatloo present a risk-based stochastic model for determining the optimal sizing of a hybrid PV/diesel/storage power system for merchant marine vessels. It considers the influence of solar radiation intermittency and utilizes a scenario reduction technique to reduce computational complexity, balancing the expected cost of system sizing with the risk of high costs in worse scenarios using the CVaR methodology [107]. In [108], Wang, Chen, Guo, *et al.* propose a hybrid diesel engine/battery/shore power propulsive system for a polar cruise and a tri-objective optimization considering annual fuel consumption, lifecycle cost and annual pure electric time is carried out. The results show that 0.27% fuel reduction and 37.48% annual pure electric time are gained by sacrificing 7.85% lifecycle cost compared with the conventional diesel electric propulsive system. In [109], Bao, Xu, Zhang, *et al.* use Mixed integer quadratic programming (MIQP), for energy storage system (ESS) sizing and power system scheduling optimization which are simultaneously conducted.

In [110], Prasanthi, Shareef, Asna, *et al.* present a methodology for sizing hybrid energy sources in hybrid electric vehicles (HEVs) that combines ultracapacitors (UC), fuel cells (FC), and battery units (BU). The authors formulate a multi-objective problem considering factors such as initial cost, weight, running cost, and source degradation. They propose an adaptive energy management strategy (AEMS) that considers dynamic-source characteristics and drive cycle power demand, and they enhance the butterfly optimization algorithm (BOA) using the quantum wave concept to effectively explore the search space. Simulation results in Matlab demonstrate that including UC and FC units can reduce battery size

by approximately 40%, and the proposed AEMS outperforms a conventional power-splitting approach, achieving a 16% reduction in system relative cost and a 10% reduction in weight for the BU-UC-FC configuration.

Wang, Shipurkar, Haseltalab, *et al.* developed a nested plant and control design architecture for a PEMFC-ICE-Battery hybrid vessel. In the external plant design optimization layer, NSGA-II multi-objective optimization was used to reduce CAPEX, OPEX and emissions by varying the size of components. In the inner layer MILP was used to design the optimal control strategy to minimize OPEX based on the size of the components generated by the NSGA-II algorithm [111]. This study was further extended by Karagiorgis, Nasiri, and Polinder to include uncertainty of fuel and electricity prices into the model for retrofitting a vessel [112]. For the PEMFC and battery hybridization of a coastal ferry Wu and Bucknall used a similar nested optimization architecture, where in the external layer, MILP was used in minimization of emissions and cost. The component sizes generated in the external layer are passed from the outer layer into the inner layer for the optimization of energy management (power split) to reduce costs, which was done using deterministic dynamic programming (DDP). In this study the degradation effects of the PEMFC and battery are also modelled [17]. In [113], Pivetta, DallArmi, and Taccani considered the performance degradation of PEM fuel cells in the multi-objective optimization problem using MILP. The proposed algorithm resulted in a 65% reduction in fuel cell degradation, but an increase of battery capacity by 136%. In [114], battery degradation effects were considered in the sizing optimization.

In [115], component sizing, energy and power management approaches were proposed by Haseltalab, Biert, Sapra, *et al.* to enable the use of LNG fuelled SOFC's as the main power source on-board. The results indicate a 53% reduction in CO_2 emissions and 21% higher fuel utilization efficiency compared to conventional diesel electric vessels. In [116], Baldi, Wang, Pérez-Fortes, *et al.* present a cogeneration system for off-grid applications that combines solid oxide fuel cells (SOFCs) and proton exchange membrane fuel cells (PEMFCs) with hybrid storage. The system utilizes the complementary characteristics of SOFCs and PEMFCs, while incorporating a hybrid storage system consisting of batteries and supercapacitors. Baldi, Wang, Pérez-Fortes, *et al.* use a mixed integer-linear optimization framework for the sizing of the different components of the system, and for identifying the optimal trade-off between round-trip efficiency and investment cost of the battery-based and hydrogen-based storage systems. In [117], energy, cost and emission savings on ships from the use of SOFC's was investigated. The problem of sizing the system was approached using MILP and solved using OSMOSE framework [118], which was specifically developed for the solution of MILP-based energy integration problems.

Sukumar, Marsadek, Ramasamy, *et al.*, compare different meta-heuristic algorithms for sizing of a battery energy storage system in a micro-grid and found that grey wolf optimizer produces the most optimal solution [119]. In [120], considering system cost and battery lifespan, a multi-objective grey wolf optimizer is used in generating a Pareto front. With the optimal parameters, the offline optimal power splitting results by dynamic programming (DP) under different driving patterns are analyzed. Then, the random forests (RF) method is used to learn control rules from the DP results. Driving pattern recognition (DPR) is implemented by the support vector machine (SVM). The intelligent EMS is composed of RF to guide power distribution and SVM to realize DPR and energy losses are reduced by 0.74%-9.49% in this method.

A brief over view of the different sizing studies reviewed in this literature study is listed in the table 2.8:

Table 2.8: Optimization studies

S.No	Objective function	Method	Application	Reference
1	Minimize Total Cost of Ownership (CO_2 emission costs)	MILP	Roll-on roll-off ferry	[100]
2	Minimization of CAPEX and OPEX (CO_2 emission costs)	MILP	container ship, cruise ship, and tanker	[101]
3	Minimize lifecycle costs and emissions.	NSGA-II	Aframax oil tanker	[103]
4	Minimize fuel consumption, GHG emissions, and life cycle costs	NSGA-II, MOPSO (outer layer-sizing) AECMS (inner layer-energy management)	AHTS	[104]
5	Minimize investment and operational costs	Stochastic MILP (sizing) Monte Carlo simulation (solar radiation)	Merchant vessesl	[107]
6	Minimize lifecycle costs, fuel consumption, and pure electric time	NSGA-II	Mini polar cruise	[108]
7	Minimize operational and investment costs	MIQP	Ferry	[109]
8	Minimization of cost, weight, running cost, and source degradation	BOA, PSO AECMS	HEV	[110]
9	Minimization of CAPEX, OPEX	NSGA-II (Outer layer-sizing) MILP (Inner layer-energy management)	Offshore support vessel	[111]
10	Minimization of CAPEX, OPEX (CO_2 emission costs)	NSGA-II (Outer layer-sizing) MILP (Inner layer-energy management)	offshore support vessel	[112]
11	Minimization of costs and emissions	MILP (outer layer-sizing) DDP (inner layer-energy management)	Coastal ferry	[17]
12	Minimization of costs	MILP	Ferry	[113]
13	Minimization of costs	Convex programming	PHEV-(public bus)	[114]
14	Minimization of CAPEX and OPEX	MILP	Off-grid dwelling cruise ship	[116]
15	Minimize system costs	GWO Dynamic programming (power split) Random forests (learn control rules) SVM (driving pattern recognition)	HEV	[120]

2.7. Challenges and research gaps

The main challenges identifies from the literature with respect to implementing PEMFC hybrid energy systems in shipping are as follows:

- Majority of studies in the design optimization of hybrid energy systems do not consider the Well-to-Wake (WTW) emissions associated with the hydrogen, or only consider green hydrogen for the studies. Similarly with diesel, the WTW emissions are not considered.
- The studies either optimize the design for PEMFC/LIB hybrid configuration or DG/PEMFC/LIB hybrid configuration, but both the systems are not compared in terms of cost and emission trade-off's.
- Limited studies on the impact of degradation of the PEMFC and LIB on the performance, efficiency and increase in fuel consumption of the hybrid power plant.
- There are no studies comparing the lifetime of the installed fuel cell and battery components across the both (i) PEMFC/LIB, and (ii) DG/PEMFC/LIB hybrid systems.
- Limited studies on the Health conscious EMS to limit the PEMFC degradation.

3
System Description

This chapter presents the main characteristics of the case study vessel, the propulsive demand, the selected components, and the proposed hybrid energy system configurations.

3.1. Main characteristics of the vessel chosen as case study

A short sea general cargo vessel ANKIE(figure 3.1) has been chosen for this study. General cargo or multi-purpose vessels are designed for flexibility and carry a huge variety of cargo. The vessel operates between multiple European Ports, and a single power profile has been acquired for the vessel operating between the Netherlands and Finland. The key characteristics of the vessel are listed in the table 3.1. The vessel is powered by a 1.8MW Wartsila 9L20 main diesel engine, which drives a controllable pitch propeller. The Capital expenditure (CAPEX) of the current mechanical propulsion system is estimated to be $540000 with the diesel engines costing $300/kW based on [121], [122] and [104].

Figure 3.1: ANKIE General Cargo Vessel
Image of MV Ankie by Helge Massamann

Table 3.1: Main Characteristics of ANKIE General Cargo Vessel

Parameter	Value
Name	ANKIE
Build year	2007
Engine	Wartsila 9L20, 1.8MW @ 1000RPM
Propeller Type	Controllable Pitch Propeller
Length × Width	89.9 m × 12.5 m
Dead Weight Tonnage (DWT)	3638 T
MGO Tank Capacity	285 m^3
Engine Room Volume	465 m^3
Speed	10.5 knots

Power demand profile of the vessel

The power profile of the vessel is shown in the figure 3.2. The vessel starts travelling on 16-April-2022 in the morning 07:20, and ends its journey on 20-April-2022 at 13:20. The total duration of the trip is 102 hours and the original load profile of the ship has been acquired with a sampling period of 5 minutes. The load profile has been linearly interpolated to a sampling period of 1 minute intervals for better accuracy. Across the entire length of the trip the vessel consumes 19.7 tonnes of Marine Gas Oil(MGO).

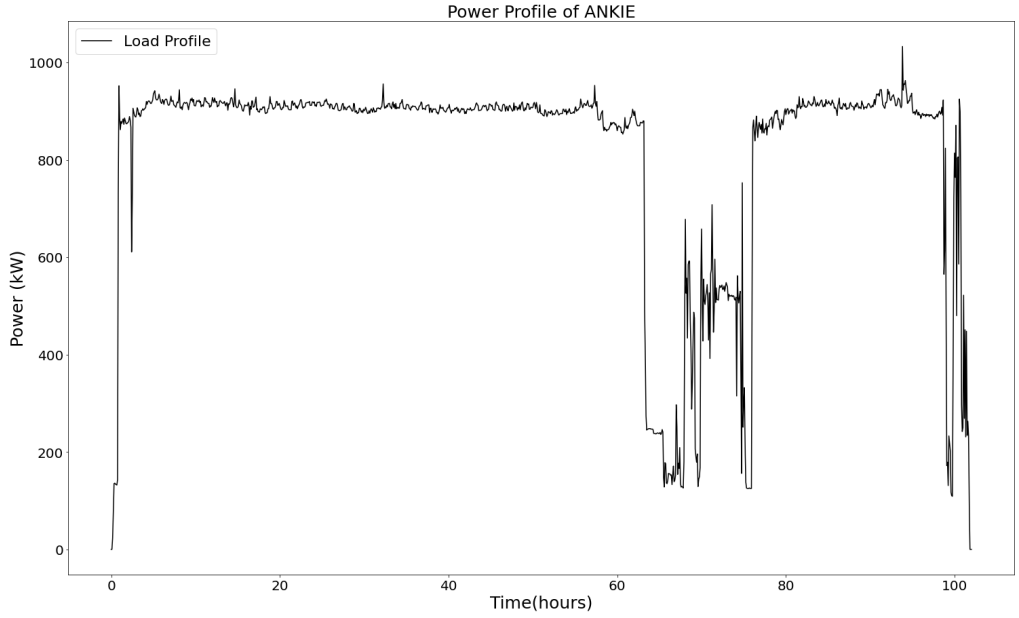

Figure 3.2: Propulsive power demand of the general cargo vessel ANKIE chosen as case study for the PEMFC hybrid energy system

3.2. Proposed energy systems and choice of components

In this study, two types of hybrid energy systems are evaluated: (i) PEMFC/LIB hybrid energy system and (ii) DG/PEMFC/LIB hybrid energy system. Both these systems are of a series hybrid configuration, where all the power outputs of the components are connected to a common DC bus. The installed LIB battery can be charged and discharged and is coupled with a bi-directional DC-DC converter. The

hydrogen is assumed to be stored in liquid form in a cryogenic tanks, with the aim of reducing the volume and weight for the storage system in comparison to other types of hydrogen storage systems. The hydrogen from the cryogenic tank is sent to the evaporator to regasify, and is fed into the PEMFC stacks that are installed, which are coupled with a Boost DC-DC converter. The diesel generator is coupled with a AC/DC converter and the output is fed onto the common bus. The output of the bus is sent to the propulsion motor which is coupled with a propeller.

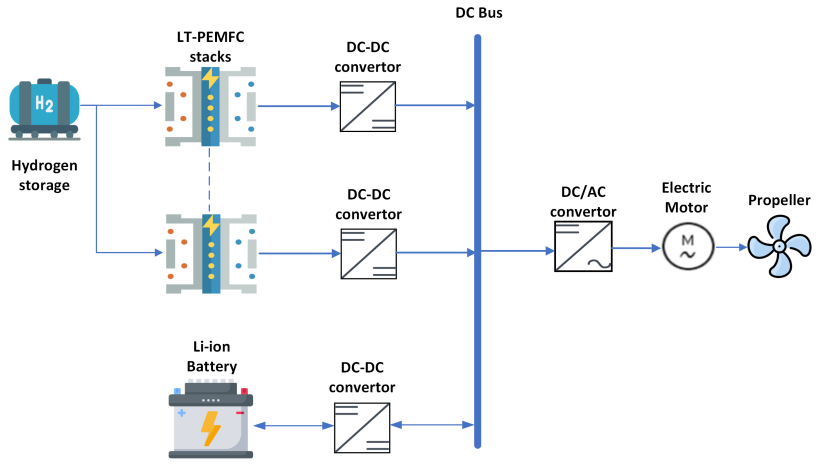

Figure 3.3: PEMFC/LIB hybrid energy system

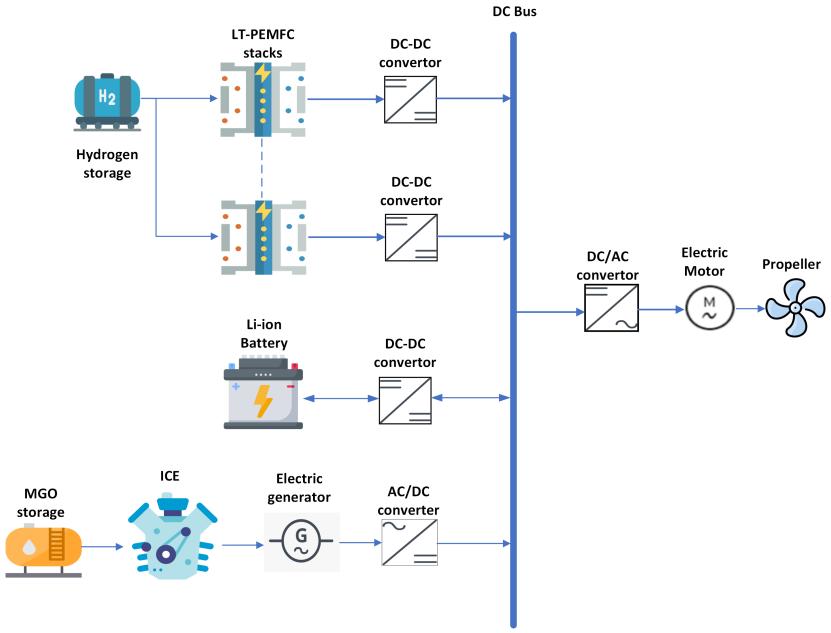

Figure 3.4: DG/PEMFC/LIB hybrid energy system

Li-ion battery

Among the different Li-ion chemistries that are available, NMC and LFP are the most widely used chemistries in shipping. The former have a relatively high energy density, low cost, and are characterized by high flexibility in terms of energy and power performances. The latter are characterized by relatively low energy densities, but are generally highly resilient to temperature fluctuations, have good safety performances, and can reach good levels of power density if the cathode is appropriately

doped. In this study LFP chemistry has been chosen due to it's safety that is required for Maritime applications.

EASy Marine®80Ah LFP Lithium Ion Battery Module(figure 3.5) has been chosen for this study. The following table 3.2 lists the characteristics of the module.

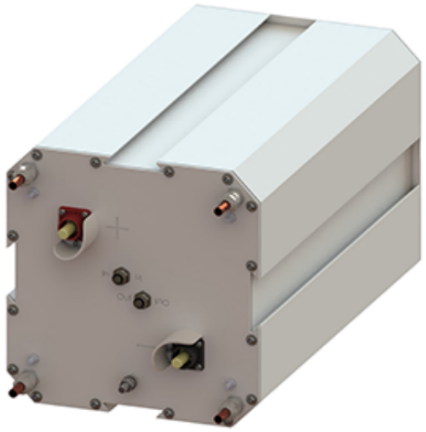

Figure 3.5: EASy Marine®80 Ah LFP Battery Module [123]

Table 3.2: EASy Marine 3.1kWh LFP Battery Module characteristics [123]

Mechanical Characteristics Module	
Width	290 mm
Height	290 mm
Depth (excluding cover)	559 mm
Weight (approx.)	62 kg
Volume	47 ltr.
IP class	IP65
Chemical Characteristics	
Cathode	LFP
Anode	Graphite
Electrical Characteristics	
Nominal capacity @ 1C @ 25 °C	80 Ah
Nominal operating voltage	38.4 V
Recommended charging voltage	42 V
Maximum charging voltage	43.2 V
Recommended cut-off discharge voltage	30 V
Energy	3.1 kWh
Specific energy	50 Wh/kg
Energy density	66 Wh/l
Specific power	
Continuous discharge @ 5C/ 50% SOC	250 W/kg
2s pulse discharge @15 C / 50% SOC	750 W/kg

Power density	
Continuous discharge @ 5C /50% SOC	328 W/l
2s pulse discharge @ 15C / 50% SOC	989 W/l
Operating conditions	
Recommended charging method	Constant current/ constant voltage
Recommended continuous charging current	80 A (1C)
Maximum continuous charging current	240 A (3C)
Discharge current @ 25 °C	
Recommended	80 A (1C)
Maximum continuous	400 A (5C)
Maximum pulse (2s)	1200 A (15C)
Storage and transport conditions	25 to 50% SOC
Maximum temperature range	-20 °C to 50 °C
Recommended temperature range	10 °C to 25 °C
Operating temperature	
Discharge	0 °C to 40 °C
Charge (recommended)	10 °C to 30 °C
Cycle Life @ 20 °C (EoL @ 80% of nominal capacity)	
100 % DoD, 1C	>5000 cycles
80 % DoD, 1C	>6250 cycles

There are other commercially available Li-ion batteries that are currently available in the market from various manufacturers that are suitable for the shipping industry such as Corvus Energy, Zero Emission services, EST float tech etc.

150kW PEMFC stack

LT-PEM fuel cells are the most technologically advanced market ready solutions that are suitable for use in the shipping industry to reduce emissions. In this study zepp.X150 Modules(figure 3.6) have been considered. The specifications are listed in table 3.3, and the typical system efficiency and fuel consumption of zepp.x150 at beginning of life are shown in figure 3.7.

Figure 3.6: zepp.x150 PEMFC module [124]

Table 3.3: zepp.X150 PEMFC specifications [124]

Specifications	
Net Rated power output	150 kWe
Efficiency at max.power	51 % LHV
Efficiency at 50% power	57.5 % LHV
Dimensions	1250 × 700 × 680 mm (L×W×H)
Volume	595 L
Mass	355 kg
Output voltage range	520-750 VDC (integrated DCDC converter output)
LV supply	12/24 VDC (max 500W)
Fuel Type	Hydrogen gas
Fuel Quality	ISO 14687:2019, SAE J2719
Oxidant	Ambient air
Coolant	Glysantin FC G20 RM
Coolant temperature in	75 °C
Ambient operating temperature	-30 °C to 50 °C
IP protection	IP 67
Max operating altitude	2000m

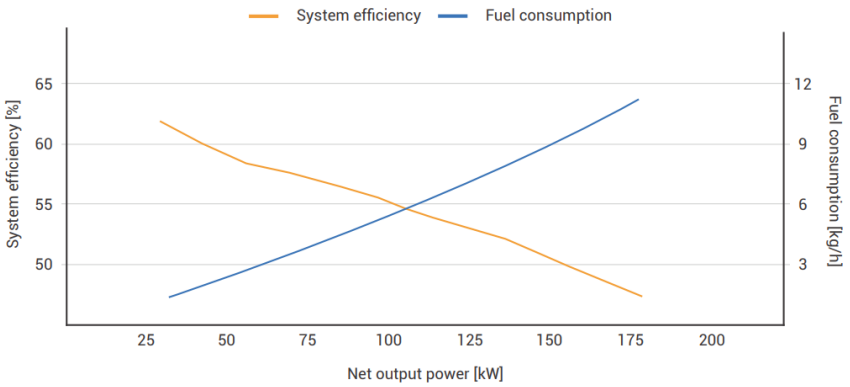

Figure 3.7: typical system efficiency and fuel consumption at beginning of life, 20 °C ambient at sea level, with ±3% tolerance [124]

The other commercially available PEMFC that are suitable for application in shipping are from Nedstack, Ballard, accelera™by cummins, inocel, Proton Motor, PowerCellution, TECO2030, EODev, Corvus Energy, and Helion etc.

800kW Diesel Generator

For the selection of the diesel generator, the current OEM of the installed ICE-Wartsila has been chosen, and using the engine configurator tool on the website, a 50Hz, MGO fuelled, IMO Tier 3 diesel generator has been selected. From the options provided, the smallest Diesel generator has been selected which is the Wartsila 4L20. The following are the specifications of the Wartsila 4L20 Diesel generator.

Table 3.4: Wartsila 4L20 Marine Diesel Generator [125]

Engine Technical Information	
Product Name	Wartsila 4L20
Application Type	Marine auxiliary engine, Marine main engine diesel-electric
Feature	IMO Tier III optimized (SCR)
Number of cylinders	4
Engine speed	1000 RPM
Engine speed mode	constant
cylinder output	200 kW
engine output	800kW
Fuel type	HFO/MDF

The following figures represent the SFOC in (g/kWh) and the output power vs fuel consumption (kg/hr) of the ICE.

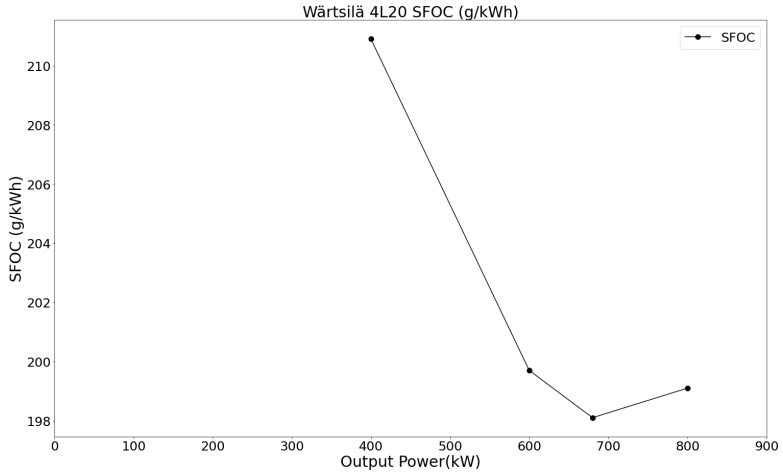

((**a**)) SFOC

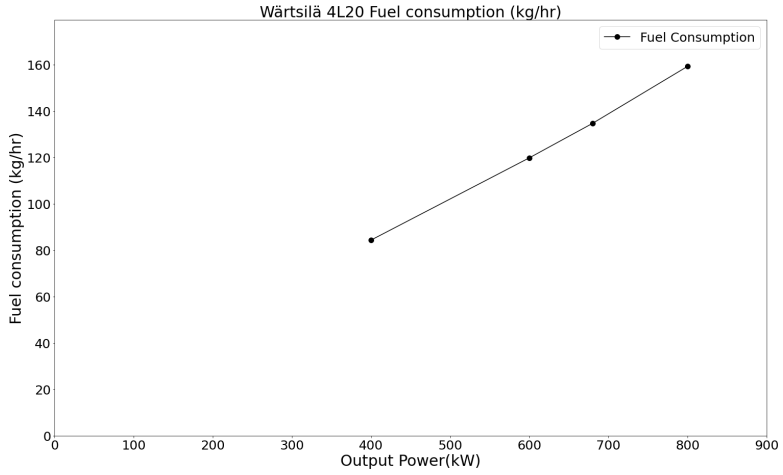

((**b**)) Fuel consumption

Figure 3.8: SFOC(g/kWh) and Fuel consumption (kg/hr) of Wartsila 4L20

4
Methodology and Modelling

This chapter presents the general methodology developed to address the research gaps identified after the literature review on PEMFC based hybrid systems for shipping.

4.1. The Optimization Problem

As widely recognized, the MILP approach is appropriate for the optimization of complex energy system as it allows to reduce the computational effort with respect to other optimization techniques . Therefore, it has been chosen to adopt a MILP approach to develop and solve the optimization problems proposed hereafter. In general, all the optimization problems are hence set as:

Find the optimal value of x*(t) and δ*(t) that maximize or minimize the objective function(s) Z (Equation 4.1) subject to the equality constraints g(t) and inequality constraints h(t) (Equations 4.2 and 4.3), on which the model of the energy system of the considered ship is based. The continuous variables (x) and binary variables (δ) are the decision variables of the optimization problem. In particular, binary variables have been used to decide about on/off status of each energy unit during operation. All the models have been developed in Python programming language and solved with Gurobi Optimizer.

$$Z = f(x^*(t), \delta^*(t)) \tag{4.1}$$

$$g(x^*(t), \delta^*(t)) = 0 \tag{4.2}$$

$$h(x^*(t), \delta^*(t)) \leq 0 \tag{4.3}$$

This thesis draws from the scholarly contributions of Pivetta, DallArmi, and Taccani, serving as a crucial framework for the exploration and analysis presented herein [113], [126], [10].

The methodology has been developed in different optimization phases. Firstly a deterministic design and operation optimization has been run in-order to determine the optimal sizes of the energy conversion and storage units of the energy systems and their optimal operation over a single trip along with the emission analysis across various grades of hydrogen. Afterwards, a further operation optimization has been performed consecutively taking into account the performance degradation of the PEMFC and LIB installed until the end of life of the PEMFC and LIB components is reached.

In the following sub sections, firstly a brief overview is given on the MI(L)P solving procedure of gurobi in 4.1.1 followed by the sets, indices, parameters, and decision variables in 4.1.2. In 4.1.3, 4.1.4 the two methodology phases (i.e. the two optimization problems) are described, with particular reference to the objective function(s) of the problems, the main constraints describing the components operation, and the ones setting the energy system power balances and limits on the volume of the engine room.

4.1.1. Gurobi MI(L)P solving procedure

Gurobi solves Mixed-Integer Linear Programming (MILP) problems using a combination of advanced mathematical algorithms and computational techniques [127]. The solution process typically involves the following key steps and methods:

1. **Preprocessing:** Before diving into the solution process, Gurobi performs a preprocessing phase to simplify the MILP problem. This can involve removing redundant constraints, tightening bounds, and identifying special structures that can be exploited. The aim is to reduce the problem size and complexity, which can significantly improve the efficiency of the solver.

2. **Linear Programming (LP) Relaxation:** The core of solving an MILP problem starts with solving its linear programming (LP) relaxation. This means solving the problem without considering the integer constraints on the variables, which transforms it into a simpler LP problem. Gurobi uses the simplex method or the interior point method for this purpose. The solution to the LP relaxation provides a bound on the objective value of the MILP problem and serves as a starting point for further exploration.

3. **Branch-and-Bound Algorithm:** Gurobi primarily uses the branch-and-bound algorithm to systematically explore the set of possible solutions. This method involves creating a search tree where each node represents a subproblem with a particular set of bounds on the variables. The algorithm explores branches (subproblems) by solving LP relaxations, pruning branches that cannot yield better solutions than the current best solution, and branching further until integer solutions are found or the entire tree is explored. This process is efficient due to the ability to discard large portions of the search space that do not contain optimal solutions.

4. **Cutting Planes:** To enhance the efficiency of the branch-and-bound process, Gurobi may also employ cutting planes. These are additional constraints that are added to the LP relaxation to cut off fractional solutions without removing any feasible integer solutions. By tightening the LP relaxation in this way, Gurobi can often reach integer solutions faster and improve the bounds used for pruning the search tree.

5. **Heuristics:** Gurobi implements various heuristic methods to quickly find good feasible solutions early in the search process. These solutions provide bounds that help to prune the search tree more effectively. Heuristics can be particularly valuable in finding near-optimal solutions to very large or difficult MILP problems where finding the exact optimal solution might be computationally infeasible within a reasonable time frame.

6. **Parallel Computing:** Gurobi is designed to take advantage of modern multi-core processors and distributed computing resources. It can run many parts of the MILP solution process in parallel, including the exploration of different branches of the search tree, which significantly speeds up the computation.

7. **Optimization Techniques:** In addition to these steps, Gurobi employs a range of optimization techniques tailored to specific problem structures, such as presolve reductions, dual simplex optimizations, and advanced basis starts for reoptimization problems. The solver is highly configurable, allowing users to adjust parameters to balance between solution time and solution quality based on their specific needs.

Gurobi's effectiveness in solving MILP problems lies in its sophisticated integration of these algorithms and techniques, along with continuous advancements in optimization research and computational power.

4.1.2. Sets, Indices, Parameters and decision variables

Sets and Indices

Table 4.1: Sets and Indices

Numerical Sets	
$\mathbb{R}_0^+$	Set of all positive real numbers including 0
$\mathbb{Z}_0^+$	Set of all positive integers including 0
$\mathbb{B}$	Set of binary integers(0,1)
Modelling sets	
I	Set of PEMFC stacks
J	Set of Diesel Generators
T	Set of Time Steps (1 min)
Indices	
i	index for the PEMFC stack $i \in I$
j	index for the DG set $j \in J$
t	index for time step $t \in T$

Optimization Parameters

Table 4.2: Optimization Parameters

PEMFC parameters	
C_{FC}	Cost of PEMFC
V_{FC}	specific volume of the PEMFC stack
Δ_{PFC}	Max allowable load change of fuel cell stack
k_{1p}, k_{2p}	coefficients for current density vs load of fuel cell stack
k_{1f}, k_{2f}	coefficients for current density vs H_2 consumption of fuel cell stack
I_{fcmin}	lower limit of current density of a single cell
I_{fcmax}	upper limit of current density of a single cell
k_{fcmin}	lower power limit of fuel cell stack
k_{fcmax}	upper power limit of fuel cell stack
P_{fcmax}	Maximum rated power of the fuel cell stack
F_{start}	additional hydrogen consumed due to start up of PEMFC stack
F_{max}^{fc}	Hydrogen consumption of the PEMFC stack at the maximum rated power
Δv_{load}	Voltage loss due to transient loading
Δv_{stup}	Voltage loss due to start/stops of the fuel cell stack
k_{1dv}, k_{2dv}	coefficients to calculate the voltage loss due to stack operation

$V_{ref,fc}$	Reference cell voltage
k_{1deg}, k_{2deg}	coefficients of equation relating the voltage loss to the coefficient of the power curve k_{1p}
Hydrogen Parameters	
C_{H2}	cost of the different grades of hydrogen per kg
$CO_{2eq}^{H_2}$	emission intensity of the different hydrogen grades
C_S^{LH2}	cost of hydrogen liquid hydrogen storage onboard per kg
C_{LiqH2}	Liquefaction cost of hydrogen
Battery parameters	
C_{batt}	cost of lithium ion battery
η_{batt}	charge and discharge efficiency of battery
V_{batt}	Specific volume of the battery
SOC_{min}	minimum state of charge of battery
SOC_{max}	maximum state of charge of battery
E_{module}	individual module rating
$C_{ratemax}$	Maximum allowable charge and discharge C-rate
Diesel Generator parameters	
C_{DG}	Cost of the diesel generator
k_{ENGmin}	lower operating limit of the ICE
k_{ENGmax}	upper power limit of the ICE
η_{DG}	efficiency of the generator
P_{ENGmax}	Maximum rated power of the ICE
V_{DG}	specific volume of the diesel generator
k_{1dg}tok_{6dg}	coefficients of output power vs MGO consumption
Δ_{ENG}	max allowable increase in load between time steps
Marine Gas Oil (MGO) Parameters	
C_{MGO}	cost of marine gas oil per kg
C_S^{MGO}	cost of storage of marine gas oil
CO_{2eq}^{MGO}	WTW emission intensity of MGO for MSD ICE
Other Parameters	
M	Big M
CO_{2tax}	carbon tax
V_{ENG}	Volume of currently installed power system
C_{ov}	Correction over sizing factor
C_{elec}	Cost of electricity on-shore
$Load_t$	Power demand at time $t \in T$

Decision variables

Table 4.3: Decision variables

PEMFC design variables	
$n_{FC} \in \mathbb{Z}_0^+$	Number of fuel cell stacks required
$x_i^{FC} \in \mathbb{B}$	1 if PEMFC stack $i \in I$ is selected, 0 otherwise
PEMFC operation variables	
$P_{it}^{FC} \in \mathbb{R}_0^+$	power output of PEMFC stack $i \in I$ at time $t \in T$
$I_{it}^{FC} \in \mathbb{R}_0^+$	current density of PEMFC stack $i \in I$ at time $t \in T$
$F_{it}^{FC} \in \mathbb{R}_0^+$	H_2 consumption of PEMFC stack $i \in I$ at time $t \in T$
$\delta_{it}^{stup} \in \mathbb{B}$	1 if PEMFC stack $i \in I$ is started at time $t \in T$, 0 otherwise
$\delta_{it}^{FC} \in \mathbb{B}$	1 if PEMFC stack $i \in I$ at time $t \in T$ is on, 0 if switched off
PEMFC voltage loss variables	
$dV_{it}^{load} \in \mathbb{R}_0^+$	voltage loss of PEMFC stack $i \in I$ at $t \in T$ due to transient loading
$dV_{it}^{stup} \in \mathbb{R}_0^+$	voltage loss of PEMFC stack $i \in I$ due to start/stops at $t \in T$
$dV_{it}^{PFC} \in \mathbb{R}_0^+$	voltage loss of PEMFC stack $i \in I$ due to operating power output at $t \in T$
$dV_{it} \in \mathbb{R}_0^+$	Total voltage loss of PEMFC stack $i \in I$ at $t \in T$
DG design variables	
$n_{DG} \in \mathbb{Z}_0^+$	Number of diesel generators required
$x_j^{DG} \in \mathbb{B}$	1 if DG $j \in J$ is selected, 0 otherwise
DG operation variables	
$P_{jt}^{ENG} \in \mathbb{R}_0^+$	power output of ICE $j \in J$ at time $t \in T$
$P_{jt}^{DG} \in \mathbb{R}_0^+$	power output of DG $j \in J$ at time $t \in T$
$F_{jt}^{DG} \in \mathbb{R}_0^+$	MGO consumption of DG $j \in J$ at time $t \in T$
Battery design variables	
$E_{battmax} \in \mathbb{R}_0^+$	Required battery capacity to be installed
$n_{batt} \in \mathbb{Z}_0^+$	number of battery modules required
Battery operation variables	
$E_t^{batt} \in \mathbb{R}_0^+$	energy content of the battery at time $t \in T$
$P_t^{batt+} \in \mathbb{R}_0^+$	Battery discharge power at time $t \in T$
$P_t^{batt-} \in \mathbb{R}_0^+$	Battery charge power at time $t \in T$

4.1.3. Stage 1: Design optimization and emission analysis across various grades of Hydrogen

The first phase of the optimization is aimed at determining the optimal size of the energy conversion and storage units, along with the emission and cost analysis for the various grades of hydrogen that are available. To design the hybrid energy system configuration, the entire system operation is optimized for a single trip (figure 3.2).

A single objective optimization has been set to define the optimal design and operation of the hybrid propulsion system that allows for the minimization of total costs. Following the general approach outlined in the equations 4.1, 4.2, and 4.3, the total investment and single trip operation cost is set as the main objective.

Objective function

Since there are two different types of hybrid energy systems that are being designed, this subsection is further split into two: (i) PEMFC/LIB hybrid energy system, and (ii) DG/PEMFC/LIB hybrid energy system.

(i) PEMFC/LIB hybrid system

In the equation 4.4, representing the objective of total cost, $E_{battmax}$ represents the required battery capacity, C_{batt} is the cost of batteries per kWH, n_{FC} is the number of installed PEMFC stacks of rated power P_{fcmax} and cost C_{FC}. F_{it}^{FC} is the amount of hydrogen consumed by the i^{th} PEMFC stack at time t, and C_{H2} is the cost of different grades of hydrogen per kg (table 2.4) . The hydrogen consumed is subject to carbon tax according to EU ETS (CO_2tax), and the cost of using liquefied hydrogen is also included in the objective function (C_{liqH2}). The objective function also consists of the costs of liquefied hydrogen storage (C_S^{LH2}) which is part of the CAPEX. The final part of the objective function is the cost (C_{elec}) of shore charging the installed battery.

$$\underset{\mathrm{n}_{fc},\mathrm{n}_{batt},\mathrm{P}_{it}^{FC},\mathrm{P}_{t}^{batt\pm}}{\text{Minimize}} \quad \mathrm{J}(\mathrm{n}_{fc},\mathrm{n}_{batt},\mathrm{P}_{it}^{FC},\mathrm{P}_{t}^{batt\pm}) = E_{battmax}\cdot C_{batt} + n_{FC}\cdot P_{fcmax}\cdot C_{FC}$$
$$+\sum_{i\in I}\sum_{t\in T} F_{it}^{FC}\cdot C_S^{LH2} + \sum_{i\in I}\sum_{t\in T} F_{it}^{FC}\cdot (C_{H2} + CO_{2eq}^{H_2}\cdot CO_{2tax} + C_{liqH2}) + 0.8\cdot E_{battmax}\cdot C_{elec}\cdot \frac{1}{\eta_{batt}} \tag{4.4}$$

PEMFC stacks model
The equations 4.5 to 4.12 describe the behavior of the PEMFC stacks, at each time step t. The fuel consumption of the stack is contingent upon the current density of an individual cell within the PEMFC stack, and concurrently, the power output of the fuel cell stack is also reliant on the current density of the individual cells in the PEMFC stack. The relation between H_2 consumption vs current density vs output power is drawn from the commercial products for reference [128], [124].

Equation 4.5 refers to amount of hydrogen consumed at each time step t for the i^{th} stack as a function of the current density of an individual cell by means of the linearization coefficients k_{1f}andk_{2f}. $\delta_{it}^{FC}$and δ_{it}^{stup} are the binary variables that describe the on/off status of the i^{th} PEMFC stack and the startup of the PEMFC stack. F_{start} is the additional hydrogen consumption due to the start up of the PEMFC stack, which is assumed to be 10% of the consumption at the maximum rated power (F_{max}^{fc}) [113]. In equation 4.6, the power output of the PEMFC stack is related to the current density with the linearization coefficients $k_{1p}$and k_{2p}. The upper and lower limits of current density of the i^{th} stack are shown in equation 4.7. The binary variable x_i^{FC} in equations 4.7 and 4.8 expresses the inclusion of the i^{th} stack in the optimal system configuration. The sum of such variables x_i^{FC} defines the number of PEMFC stacks n_{FC} that should be included in the system (Equation 4.8).

The equation 4.9 limits the power generated by the i^{th} PEMFC stack in order to not exceed the minimum (k_{fcmin}) and maximum (k_{fcmax}) power load, expressed as a percentage of the rated power of the stack P_{fcmax}. The binary variable δ_{it}^{FC} in equation 4.9 is multiplied with the upper and lower power limits

of the stack to ensure that the stack operates between the given limits, or is switched off. At each time step, the load variation cannot exceed the maximum value Δ_{PFC} as reported in equation 4.10. The equation 4.11 is used to determine the number of start up phases that have occurred for the i^{th} PEMFC stack, i.e. $\sum \delta_{it}^{stup}$. The final equation 4.12 ensures that all the selected stacks deliver the same power at each time step.

$$F_{it}^{FC} = k_{1f} \cdot I_{it}^{FC} + k_{2f} \cdot \delta_{it}^{FC} + \delta_{it}^{stup} \cdot F_{start} \cdot F_{max}^{fc} \qquad \forall i \in I \qquad \forall t \in T \tag{4.5}$$

$$P_{it}^{fc} = k_{1p} \cdot I_{it}^{FC} + k_{2p} \cdot \delta_{it}^{FC} \qquad \forall i \in I \qquad \forall t \in T \tag{4.6}$$

$$I_{fcmin} \cdot x_i^{FC} \leq I_{it}^{FC} \leq I_{fcmax} \cdot x_i^{FC} \qquad \forall i \in I \qquad \forall t \in T \tag{4.7}$$

$$\sum_{i \in I} x_i^{FC} = n_{FC} \tag{4.8}$$

$$k_{fcmin} \cdot P_{fcmax} \cdot \delta_{it}^{FC} \leq P_{it}^{FC} \leq k_{fcmax} \cdot P_{fcmax} \cdot \delta_{it}^{FC} \qquad \forall i \in I \qquad \forall t \in T \tag{4.9}$$

$$\Delta_{PFC} \geq |P_{it}^{FC} - P_{i,t-1}^{FC}| \qquad \forall i \in I \qquad \forall t \in range(1, len(T)) \tag{4.10}$$

$$0 \leq \delta_{it}^{FC} - \delta_{i,t+1}^{FC} + \delta_{it}^{stup} \qquad \forall i \in I \qquad \forall t \in range(len(T) - 1) \tag{4.11}$$

$$P_{it}^{FC} = P_{1t}^{FC} \cdot x_i^{FC} \qquad \forall i \in I \qquad \forall t \in T \tag{4.12}$$

The equation 4.12 contains the product of a continuous and binary variable making the problem non-linear. To ensure that the formulation remains linear, big M method is used and the following equations replace 4.12 to ensure that all the selected stacks deliver the same power at each time step.

$$P_{it}^{FC} \leq M \cdot x_i^{FC} \qquad \forall i \in I \qquad \forall t \in T \tag{4.13}$$

$$P_{it}^{FC} \leq P_{1t}^{FC} \qquad \forall i \in I \qquad \forall t \in T \tag{4.14}$$

$$P_{it}^{FC} \geq P_{1t}^{FC} - (1 - x_i^{FC}) \cdot M \qquad \forall i \in I \qquad \forall t \in T \tag{4.15}$$

$$P_{it}^{FC} \geq 0 \qquad \forall i \in I \qquad \forall t \in T \tag{4.16}$$

Li-ion Battery Model

For the LFP battery, equations 4.17 to 4.21 define its operation at each time step t. The equation 4.17 defines the energy stored in the battery E_t^{batt} at each time step t as a function of the charging and discharging energy efficiency η_{batt}, the output power of the battery P_t^{batt+} and the input power of the battery P_t^{batt-}. To limit the complexity of the optimization model, the charging/discharging efficiency (η_{batt}) is set to be constant at varying C-rate (i.e. the ratio between the power output/input and the battery capacity $E_{battmax}$). Equation 4.18 ensures that the battery charge and discharge power do not exceed the maximum allowable C-rate. In equation 4.19 at each time step the energy stored in the battery cannot exceed the limits set on the maximum SOC, i.e. the ratio between the energy stored at time t (E_t^{batt}) and the installed battery capacity $E_{battmax}$ (eq. 4.22). The battery is assumed to be charged to 80% of it maximum capacity at the start of the trip using shore charging (equation 4.20). The equation 4.21 is the number of individual battery modules that are required to be installed.

$$E_t^{batt} = E_{t-1}^{batt} + (\eta_{batt} \cdot P_t^{batt-} - \frac{1}{\eta_{batt}} \cdot P_t^{batt+}) \cdot \Delta t \qquad \forall t \in T \tag{4.17}$$

$$P_t^{batt\pm} \leq |C_{ratemax} \cdot E_{battmax}| \qquad \forall t \in T \tag{4.18}$$

$$SOC_{min} \cdot E_{battmax} \leq E_t^{batt} \leq SOC_{max} \cdot E_{battmax} \qquad \forall t \in T \tag{4.19}$$

$$SOC_0 = 0.8 \tag{4.20}$$

$$E_{battmax} = n_{batt} \cdot E_{module} \tag{4.21}$$

$$SOC_t = \frac{E_t^{batt}}{E_{battmax}} \qquad \forall t \in T \tag{4.22}$$

Energy system constraints
To ensure that the energy system fulfills the power demand of the vessel $Load_t$ at each time step, the power balance equation 4.23 is set as a constraint in the optimization. An additional constraint has been setup in equation 4.24 to ensure that the alternative power system optimal design identified by solving the optimization model does not exceed the volume V_{ENG} of the currently installed power system(table 3.1). V_{FC} is the specific volume of the PEMFC stacks and V_{batt} is the specific volume of the LFP battery. An acceptable correction factor C_{ov} has also been introduced to account for the current limited state of development of FC systems [113].

$$\sum_{i \in I} P_{it}^{FC} + P_t^{batt+} = Load_t + P_t^{batt-} \qquad \forall t \in T \tag{4.23}$$

$$n_{FC} \cdot P_{fcmax} \cdot V_{FC} + E_{battmax} \cdot V_{batt} \leq V_{ENG} \cdot (1 + C_{ov}) \tag{4.24}$$

(ii) DG/PEMFC/LIB hybrid energy system

The objective function is similar to the one mentioned in equation 4.4, but is modified slightly with the addition of factors related to the installation of the Diesel Generator. n_{DG} is the number of installed diesel generators of rated power P_{ENGmax} and cost C_{DG}. F_{jt}^{DG} is the amount of marine gas oil consumed by the j^{th} generator, which is subject to the cost of the fuel C_{MGO}, storage costs (C_S^{MGO}) and carbon taxation similar to hydrogen (equation 4.25).

$$\begin{aligned} \underset{\mathrm{n}_{fc},\mathrm{n}_{batt},\mathrm{n}_{DG},\mathrm{P}_{it}^{FC},\mathrm{P}_t^{batt\pm},\mathrm{P}_{jt}^{DG}}{\text{Minimize}} \quad & \mathrm{J}(\mathrm{n}_{fc},\mathrm{n}_{batt},\mathrm{n}_{DG},\mathrm{P}_{it}^{FC},\mathrm{P}_t^{batt\pm},\mathrm{P}_{jt}^{DG}) = E_{battmax} \cdot C_{batt} + n_{FC} \cdot P_{fcmax} \cdot C_{FC} \\ & + n_{DG} \cdot P_{ENGmax} \cdot C_{DG} + 0.8 \cdot E_{battmax} \cdot C_{elec} \cdot \frac{1}{\eta_{batt}} + \sum_{i \in I} \sum_{t \in T} F_{it}^{FC} \cdot C_S^{LH2} + \sum_{j \in J} \sum_{t \in T} F_{jt}^{DG} \cdot C_S^{MGO} \\ & + \sum_{i \in I} \sum_{t \in T} F_{it}^{FC} \cdot (C_{H2} + CO_{2eq}^{H_2} \cdot CO_{2tax} + C_{liqH2}) + \sum_{j \in J} \sum_{t \in T} F_{jt}^{DG} \cdot (C_{MGO} + CO_{2eq}^{MGO} \cdot CO_{2tax}) \end{aligned} \tag{4.25}$$

All the equations from the PEMFC/LIB model 4.5 to 4.22 are valid for this model. The diesel generator constraints are further added on as below.

Diesel generator model
Equations 4.26 to 4.31 refer to the operation of the j^{th} Diesel Generator at time t. The equation 4.26 relates the MGO consumption to the output power of the ICE using a piece wise linear approximation using the linearization coefficients $k_{1dg}$to k_{6dg}. equation 4.27 is the output power of the ICE multiplied

by the alternator efficiency η_{DG}. Equation 4.28 refers to the upper (k_{ENGmin}) and lower (k_{ENGmax}) operating power limits of the ICE expressed as a percentage of the rated power of the ICE P_{ENGmax}. The binary variable x_{DG} in equations 4.28 and 4.29 expresses the inclusion of the j^{th} DG in the optimal system configuration. The sum of x_{DG} defines the number of DG sets that should be included in the system (equation 4.29). Equation 4.30 ensures that the increase in the DG load between time steps is not more than Δ_{DG}, which is the limit set by the manufacturer. The DG set can instantly drop it's output power from 100% to zero. Therefore equation 4.30 is only applicable to load increases. Equation 4.31 ensures that all the selected DG's deliver the same amount of power at each time step t.

$$F_{jt}^{DG} = \begin{cases} k_{1dg} \cdot P_{jt}^{ENG} + k_{2dg}, & \text{if } P_{jt}^{ENG} \leq 600 \\ k_{3dg} \cdot P_{jt}^{ENG} + k_{4dg}, & \text{if } 600 \leq P_{jt}^{ENG} \leq 680 \\ k_{5dg} \cdot P_{jt}^{ENG} + k_{6dg}, & \text{if } 680 \leq P_{jt}^{ENG} \leq 800 \end{cases} \tag{4.26}$$

$$P_{jt}^{DG} = P_{jt}^{ENG} \cdot \eta_{DG} \qquad \forall j \in J \qquad \forall t \in T \tag{4.27}$$

$$k_{ENGmin} \cdot P_{ENGmax} \cdot x_j^{DG} \leq P_{jt}^{ENG} \leq k_{ENGmax} \cdot P_{ENGmax} \cdot x_j^{DG} \qquad \forall j \in J \qquad \forall t \in T \tag{4.28}$$

$$\sum_{j \in J} x_j^{DG} = n_{DG} \tag{4.29}$$

$$\Delta_{ENG} \geq P_{jt}^{ENG} - P_{j,t-1}^{ENG} \qquad \forall j \in J \qquad \forall t \in T \tag{4.30}$$

$$P_{jt}^{DG} = P_{1,t}^{DG} \cdot x_j^{DG} \qquad \forall j \in J \qquad \forall t \in T \tag{4.31}$$

Similar to 4.12, the equation 4.31 is linearized using the Big M method to ensure that all the DGs deliver the same amount of power at each time step.

Constraints

The power balance constraint in equation 4.23 is updated with the inclusion of the diesel generator power in equation 4.32. Similarly, the volume constraint of the engine room in equation 4.24 is updated with the inclusion of the specific volume of the Diesel Generator V_{DG} in the equation 4.33.

$$\sum_{j \in J} P_{jt}^{DG} + \sum_{i \in I} P_{it}^{FC} + P_t^{batt+} = Load_t + P_t^{batt-} \qquad \forall t \in T \tag{4.32}$$

$$n_{DG} \cdot P_{DGmax} \cdot V_{DG} + n_{FC} \cdot P_{fcmax} \cdot V_{FC} + E_{battmax} \cdot V_{batt} \leq V_{ENG} \cdot (1 + C_{ov}) \tag{4.33}$$

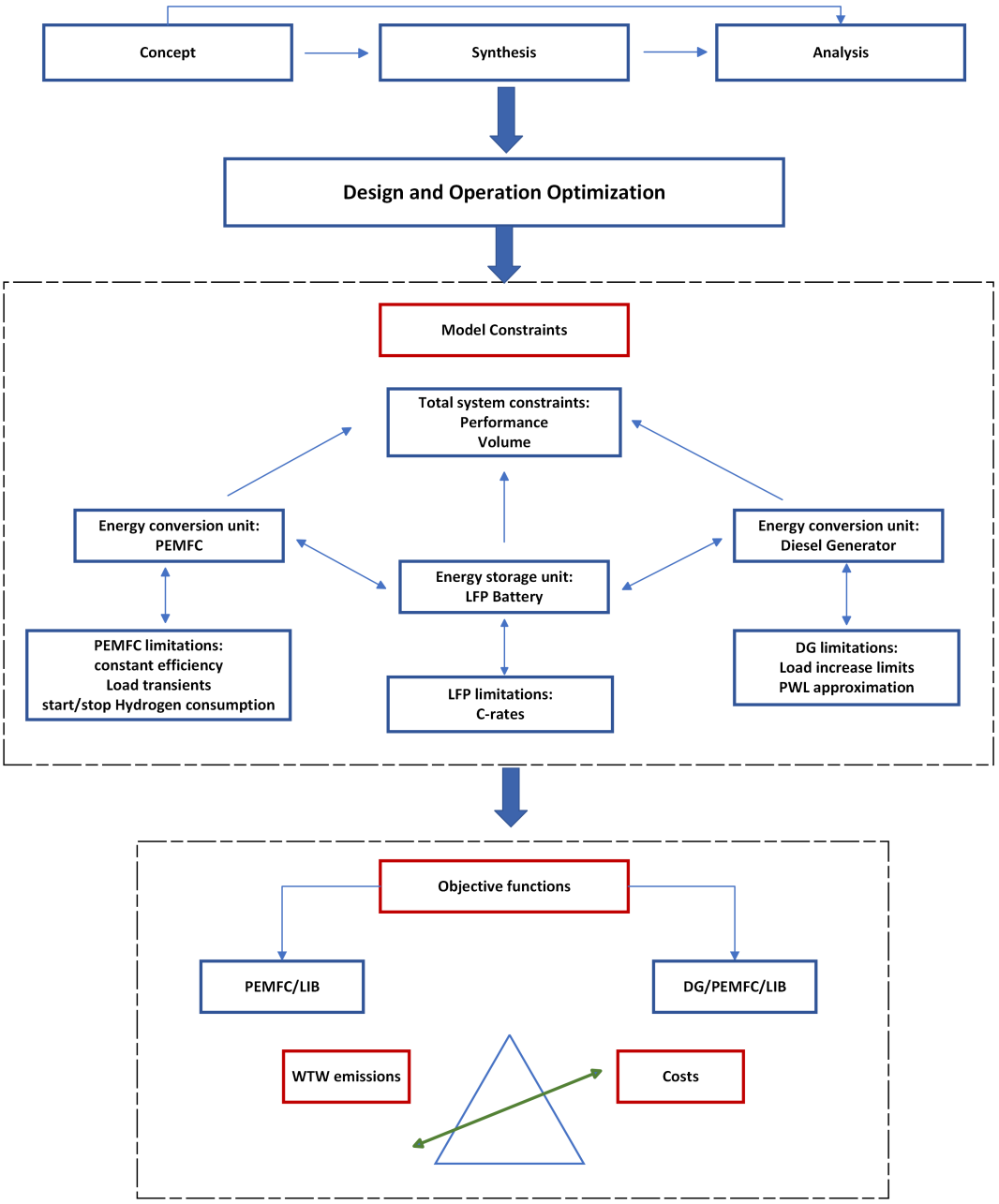

Figure 4.1: Flow chart of the synthesis/design/optimization approach of stage 1

4.1.4. Stage 2: Lifetime estimation of the installed components

In this phase, the lifetime of the installed PEMFC stacks and LFP battery obtained from section 4.1.3 is analysed for both the PEMFC/LIB and DG/PEMFC/LIB solutions. A single trip of the vessel is 102 hours. The vessel is assumed to be carrying out 5 such similar trips per month in this analysis. The vessel is assumed to be docked at the port for 5 days in a month where it undergoes maintenance and inspections where it is idle.

In this section, first the degradation modelling mechanisms of both the PEMFC stacks and the LFP battery are introduced. Further, the methodology for the lifetime estimation used in this study is elaborated on.

PEMFC Degradation Modelling equations

Equations 4.34 to 4.37 describe the performance degradation of the PEMFC stacks, which is defined as the voltage reduction of a single cell at equal current output, assuming that the behavior of a single cell can approximate the one of the entire PEMFC stack. The loss of voltage depends on: load variation (equation 4.34), start/stop cycles (equation 4.35), and the power levels of the i^{th} PEMFC stack (equation 4.36). For each time step t, equation 4.37 defines the total loss of voltage in a single cell, which has been set to be linearly depending on the operation of the variables of the i^{th} stack.

$$dV_{i,t+1}^{load} = |P_{it}^{FC} - P_{i,t+1}^{FC}| \cdot \Delta v_{load} \qquad \forall i \in I \qquad \forall t \in range(len(T) - 1) \tag{4.34}$$

$$dV_{it}^{stup} = \delta_{it}^{stup} \cdot \Delta v_{stup} \qquad \forall i \in I \qquad \forall t \in T \tag{4.35}$$

$$dV_{it}^{PFC} = k_{1dv} \cdot I_{it}^{FC} + k_{2dv} \qquad \forall i \in I \qquad \forall t \in T \tag{4.36}$$

$$dV_{it} = dV_{i,t}^{load} + dV_{it}^{stup} + dV_{it}^{PFC} \qquad \forall i \in I \qquad \forall t \in T \tag{4.37}$$

In equation 4.34, dV_{it}^{load} is the voltage reduction due to the load variations of the i^{th} single cell, proportional to the load variation by Δ_{load}. Similarly, equation 4.35 expresses the voltage reduction due to start up of the i^{th} PEMFC stack dV_{it}^{stup} as a constant value of voltage reduction Δ_{stup} according to the binary variable δ_{it}^{stup} which defines the happening of the startup phase and has been obtained from the equation 4.11.

The equation 4.36 defines the voltage loss due to operating power level which is a function of the current density of a single cell from equation 4.6. The degradation due to operating power level dV_{it}^{PFC} is expressed as a linear function of the current density I_{it}^{FC} by means of linearization coefficients k_{1dv} and k_{2dv}. The total voltage reduction dV_{it} is then calculated as a sum of the three different contributions in equation 4.37.

Performance loss of li-ion battery
The battery capacity obtained in the first stage optimization model has been updated to ensure that the battery maintains the necessary useful capacity till end of life (equation 4.38).

$$E_{battos} = \frac{E_{battmax}}{E_{EoL}} \tag{4.38}$$

Where E_{EoL} is the share of battery capacity at the end of lifetime.

From the literature study in section 2.5.2, two main degradation mechanisms have been identified as the main contribution to the capacity loss of the Li-ion battery: (i) Cycling aging, and (ii) calendar aging.

Cycling aging
To calculate the number of charge/discharge cycles that the battery has undergone, the cycle counting

algorithm by Gundogdu and Gladwin has been used in this study [129]. This algorithm is advantageous compared to the conventional rainflow approach as the rainflow algorithm can only be applied to extreme points (peaks and valleys), whereas this algorithm processes all the data at each time step. After the operation optimization of a single trip has been performed, the SOC data of the battery is used as input to count the number of cycles that the battery has undergone in a single trip. The algorithm is shown in figure 4.2.

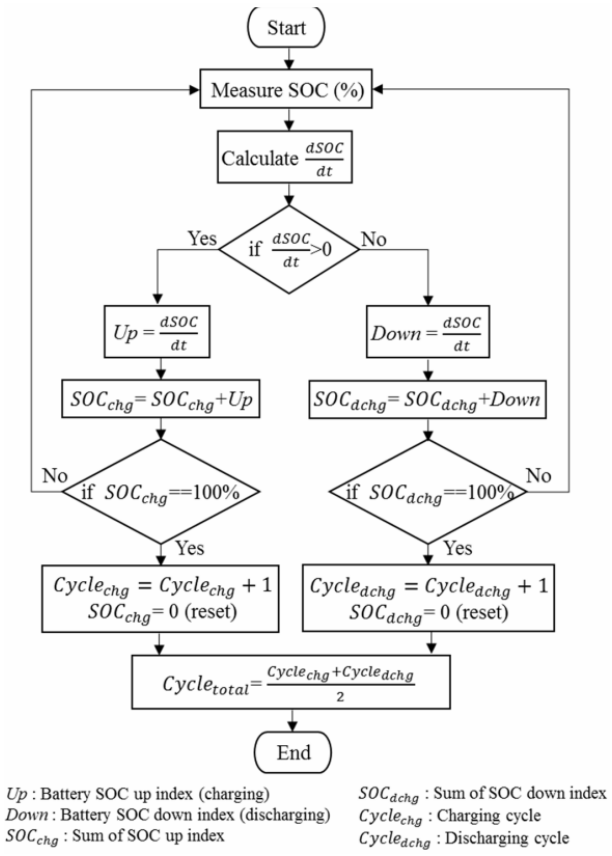

Figure 4.2: Cycle counting estimation method [129]

The method is described as following:

- In the first step, the change in battery SOC (dSOC/dt) is extracted for each time step. If the dSOC/dt is greater than zero, the battery is charging; if it is less than zero, the battery is discharging; or if it is equal to zero the battery is resting.
- The algorithm considers each positive and negative value of dSOC/dt as "Up" and "Down" indexes, respectively. In the second step, the sum of all up indexes forms the battery SOC charging data set SOC_{chg} and the sum of all down indexes forms the battery SOC discharging data set SOC_{dchg}.
- In the third, during the simulation when each SOC_{chg} and SOC_{dchg} equals to 100% the battery $Cycle_{chg}$ and discharge cycle $Cycle_{dchg}$ are incremented, independently. A full battery cycle is calculated as the average of battery charge and discharge cycles for the given period of time.
- the algorithm is repeated over the considered SOC data from the trip providing a total cycle count at the end.

To adapt the above model to this case study, certain modifications have been made as follows:

- Since the battery is being shore charged the initial SOC_{chg} is set as 0.8 before the start of the simulation.

- for simplicity, the partial charge and discharge cycles SOC_{chg} and SOC_{dchg} are added to the full charge and discharge cycles $Cycle_{chg}$ and $Cycle_{dchg}$ at the end of the trip.

The loss in capacity due to cycling aging after each month is defined as a percentage loss of the total number of cycles given by the battery manufacturer, i.e. 6250 cycles.

Calendar aging
Another crucial aspect contributing to the capacity loss of the battery is calendar aging as described in section 2.5.2. Ali, Beltran, Lindsey, *et al.*, came up with a calendar aging prediction model using studies in literature for the different Li-ion battery chemistries using the following equation 4.39 [130].

$$\text{Capacity Degradation} = a_1 e^{a_2 SOC} \cdot b_1 e^{b_2/T} \cdot t^{c_1} \tag{4.39}$$

where a_1, a_2, b_1, b_2 and c_1 are the fitting parameters, SOC is state of charge ranges from 0 to 1, T is the temperature in Kelvin and t in the time in days. the fitting parameters are shown in table 4.4 [130].

Table 4.4: Fitting parameter values for all six LIB chemistries [130]

	Fitting Parameters				
	a_1	a_2	b_1	b_2	c_1
NMC	0.03304	0.5036	385.3	-2708	0.51
LFP	0.00157	1.317	142300	-3492	0.48
LMO	0.3737	1.066	1410	-4421	0.8
NCA	0.0132	0.3442	10571	-2900	0.4
LCO	0.01329	0.9	4550	-3290	0.7
LTO	0.6129	0.5274	2191	-3970	0.5988

The LFP battery is assumed to be stored at the end SOC (SOC_{end}) after the trip for 5 days in a month where the vessel is not being operated at a temperature of 25°C/298.15K.

Hierarchical Multi-Objective Optimization

To minimize the degradation of the fuel cell from equations 4.34 to 4.37, a hierarchical multi-objective optimization method has been set up with two objectives. The first objective is the OPEX of a single trip in equations 4.40 (PEMFC/LIB solution) and 4.42 (DG/PEMFC/LIB solution). The second objective is to minimize the degradation due to voltage loss of the installed PEMFC cells as in equation 4.41.

A hierarchical or lexicographic approach assigns a priority to each objective, and optimizes for the objectives in decreasing priority order. During each of these optimization passes, it finds the best solution for the current objective, but only from among those that would not degrade the solution quality for higher-priority objectives. In this study, a higher priority (priority=2) has been assigned for the OPEX of a single trip, and lower priority (priority=1) has been assigned to the degradation of the fuel cell to not increase the OPEX of a single trip while minimizing the degradation of the fuel cell. Since all the PEMFC stacks are operating at the same power level, 2^{nd} objective is evaluated for a single stack.

$$\begin{aligned}\underset{\mathrm{P}_{it}^{FC},\mathrm{P}_{t}^{batt\pm}}{\text{Minimize}} \quad \mathrm{J}_1(\mathrm{P}_{it}^{FC},\mathrm{P}_{t}^{batt\pm}) = \sum_{i\in I}\sum_{t\in T} F_{it}^{FC}\cdot(C_{H2} + CO_{2eq}^{H_2}\cdot CO_{2tax} + C_{liqH2}) \\ +0.8\cdot E_{battmax}\cdot C_{elec}\cdot\frac{1}{\eta_{batt}}\end{aligned} \tag{4.40}$$

$$\underset{\mathrm{P}_{it}^{FC},\Delta\mathrm{P}_{it}^{FC},\delta_{it}^{stup}}{\text{Minimize}} \quad \mathrm{J}_2(\mathrm{P}_{it}^{FC},\Delta\mathrm{P}_{it}^{FC},\delta_{it}^{stup}) = \sum_{t\in T} dV_{1,t} \tag{4.41}$$

The OPEX objective is modified for the DG/PEMFC/LIB solution.

$$\begin{aligned}\underset{\mathrm{P}_{it}^{FC},\mathrm{P}_{t}^{batt\pm},\mathrm{P}_{jt}^{DG}}{\text{Minimize}} \quad & \mathrm{J}_1(\mathrm{P}_{it}^{FC},\mathrm{P}_{t}^{batt\pm},\mathrm{P}_{jt}^{DG}) = \sum_{i\in I}\sum_{t\in T} F_{it}^{FC}\cdot(C_{H2}+CO_{2eq}^{H_2}\cdot CO_{2tax}+C_{liqH2}) \\ & +\sum_{j\in J}\sum_{t\in T} F_{jt}^{DG}\cdot(C_{MGO}+CO_{2eq}^{MGO}\cdot CO_{2tax})+0.8\cdot E_{battmax}\cdot C_{elec}\cdot\frac{1}{\eta_{batt}}\end{aligned} \tag{4.42}$$

All the equations from 4.5 to 4.23 and 4.26 to 4.32 are valid for the operation optimization.

Methodology for Lifetime Estimation
The methodology used in this study for estimating the lifetime of the installed PEMFC and battery systems in both the solutions is shown in figure 4.3. Starting from month k=0, corresponding to new PEMFC and battery systems installed on-board, consecutive optimization runs have been run until either the PEMFC or Li-ion battery reach the end of their life. in order to limit the computational effort, it has been assumed that the first trip in the month is representative of the operation of all the trips in a month (5 trips).

The degradation of the installed LFP battery is evaluated after each month, and is not part of the trip operation optimization. After a single trip is executed in a month t, the voltage loss in the PEMFC and capacity loss in the Li-ion battery are calculated for the entire month. The next step is to update the cumulative voltage loss(equation 4.43) in the PEMFC ($dV_{cumulative}$) and the cumulative capacity loss of the battery (Q_{loss}) upto the current month. The State of health of both the PEMFC (SOH_{PEMFC}) and battery (SOH_{batt}) are evaluated and if either of them drop below 80% the optimization loop stops (equations 4.45 and 4.46).

If neither of the SOH's are below 80% the loop continues onto the next month. Here the reduction in battery capacity is updated, and the total voltage loss of the PEMFC is updated. The voltage loss of the PEMFC is compensated by increasing the output current density of the cell. This is achieved using the equation 4.44, which updates the coefficient of current density (k_{1p}) in equation 4.6, which in turn leads increase in hydrogen consumption to deliver the same amount of power (equation 4.5).

Updating the losses of PEMFC and battery

$$dV_{cumulative} += \left[\sum_{t\in T} dV_{1,t}\right]\cdot 5 \tag{4.43}$$

$$k_{1p} = k_{1deg}\cdot dV_{cumulative} + k_{2deg} \tag{4.44}$$

$$SOH_{PEMFC} = \frac{V_{ref,fc} - dV_{cumulative}}{V_{ref,fc}} \tag{4.45}$$

$$SOH_{batt} = \frac{E_{battos} - Q_{loss}}{E_{battos}} \tag{4.46}$$

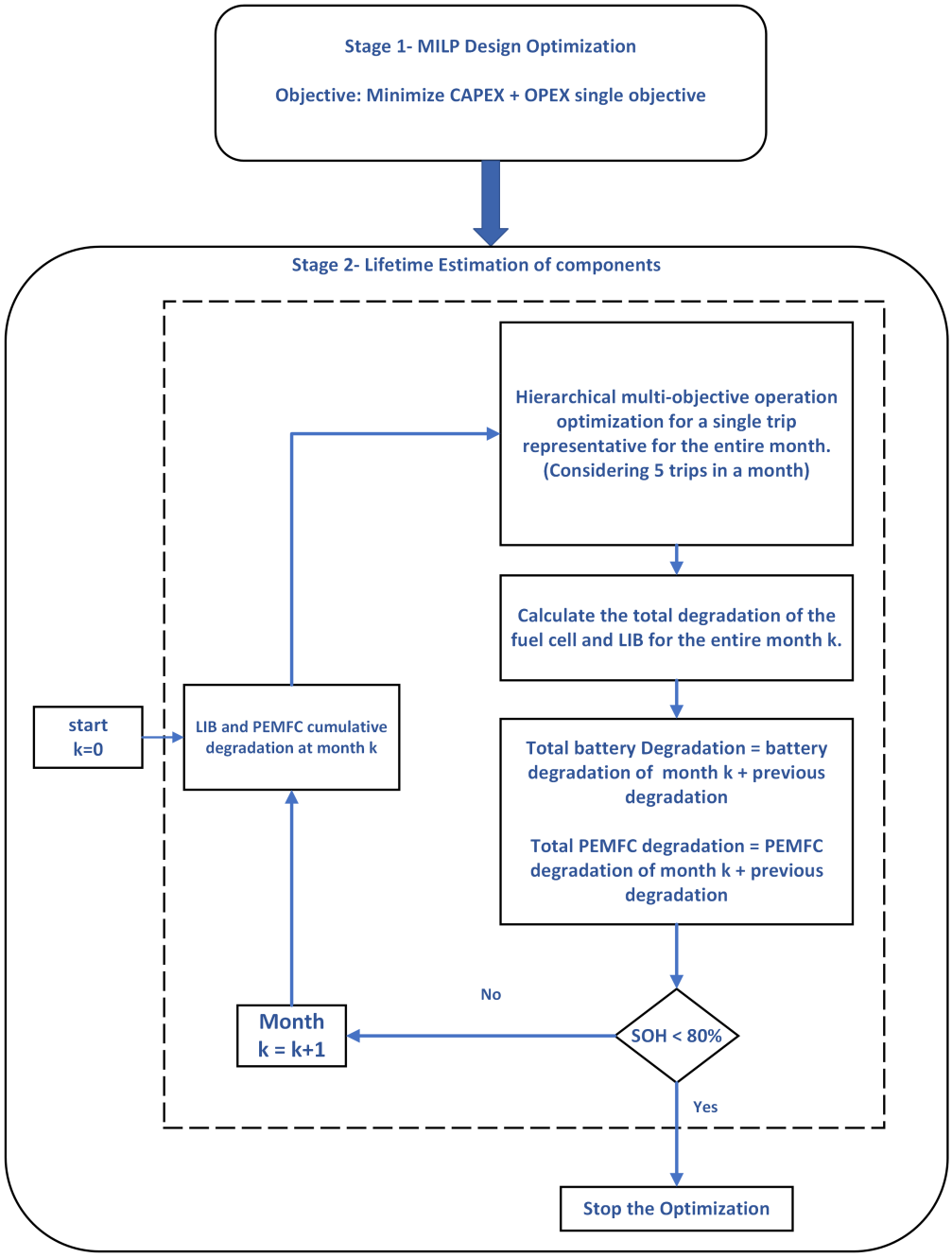

Figure 4.3: Methodology for Lifetime estimation of PEMFC and Li-ion Battery

5
Results and Discussion

This chapter presents the outcomes of the optimization stages proposed in Chapter 4, followed by a detailed discussion of the results. The input parameters of the optimization model presented in the table 4.2 have been updated with the actual values used in this model in table 5.1.

Table 5.1: Input optimization parameters

Parameter	Unit	Value	Reference
PEMFC Parameters			
C_{FC}	\$/kW	635	[87]
V_{FC}	m^3/kW	0.00396	[124]
Δ_{PFC}	%	10	[126], [113]
k_{1p}, k_{2p}	$kWcm^2$/A, kW	0.1245, 8.83	[124], [128], [126]
k_{1f}, k_{2f}	$kg \cdot cm^2/A$, kg	0.0074, 0.3236	[124], [128], [126], [131]
I_{fcmin}	A/cm^2	0	[128], [131], [126]
I_{fcmax}	A/cm^2	1500	[128], [131], [126]
k_{fcmin}	%	10	[113]
k_{fcmax}	%	90	[113]
P_{fcmax}	kW	150	[124]
F_{max}^{FC}	kg/hr	8.82	[124]
F_{start}	%	10	[113]
Δ_{load}	$\mu V/\Delta kW$	0.0441	[17], [132], [79]
Δ_{stup}	$\mu V/cycle$	23.91	[17], [132], [79]
$V_{ref,fc}$	V	0.979	[113], [126], [131], [128]
k_{1dv}, k_{2dv}	$\mu Vcm^2/A$, μV	0.0018, 9.4166	[17], [132], [79]
k_{1deg}, k_{2deg}	$kWcm^2/A\mu V$, $kWcm^2/A$	0.09866, 0.1245	[128], [17], [132], [79], [126]
Hydrogen Parameters			
H_2 grade	-	PEM, ALK, SMR, SMR+CCS, ATR+CCS	[64]
C_{H2}	\$/kg	8.4, 7.19, 2, 3.82, 3.77	[64]
$CO_{2eq}H_2$	$kgCO_{2eq}/kgH_2$	0, 0, 12.34, 2.5, 3	[65], [66]

Table 5.1 continued from previous page

C^S_{LH2}	\$/kg	200	[43]
C_{liqH2}	\$/kg	1	[54]
Battery Parameters			
C_{batt}	\$/kWh	150	[93]
η_{batt}	%	95	[89], [133], [134]
V_{batt}	m^3/kWh	0.01515	[123]
SOC_{min}	%	10	[123], [135]
SOC_{max}	%	90	[123], [135]
E_{module}	kWh	3.1	[123]
$C_{ratemax}$	C	1	[123], [89]
Diesel Generator Parameters			
C_{DG}	\$/kW	300	[100], [101]
k_{ENGmin}	%	11	[125]
k_{ENGmax}	%	100	[125]
η_{DG}	%	95	[125]
P_{ENGmax}	kW	800	[125]
V_{DG}	m^3/kW	0.0296	[125]
k_{1dg}, k_{3dg}, k_{5dg}	kg/kW	0.00292, 0.0031875, 0.003375	[125]
k_{2dg}, k_{4dg}, k_{6dg}	kg	0.238, 0.0775, -0.05	[125]
Δ_{DG}	%	33	[125]
Marine Gas Oil (MGO) Parameters			
C_{MGO}	\$/kg	0.844	[136]
C^S_{MGO}	\$/kg	1.3	[137]
CO^{MGO}_{2eq}	$kgCO_{2eq}/kgMGO$	4.211	[67]
Other Parameters			
CO_{2tax}	$\$/kgCO_{2eq}$	0.0963	[138]
V_{ENG}	m^3	135	-
Δt	time	1 min	-
C_{ov}	-	0.2	[126], [113]
C_{elec}	\$/kWh	0.095	[139]
$Load_t$	kW	from dataset	-
M	-	100000	-

5.1. Stage 1: Design Optimization and emission analysis across various grades of hydrogen

In this section the design optimization of the two hybrid energy systems, i.e. (i) PEMFC/LIB hybrid system, and (ii) DG/PEMFC/LIB hybrid system across the various grades of hydrogen has been presented.

5.1.1. PEMFC/LIB hybrid energy system

Based on the methodology proposed in chapter 4, the optimal sizes of the hybrid energy system consisting of PEMFC and battery system have been optimized for. The search space for the optimization has been set as table 5.2.

Table 5.2: Search space of design optimization of PEMFC/LIB

Description	Variables	Value	
		min	max
Number of 150kW PEMFC stacks	n_{FC}	0	8
Number of 3.1kWh LFP modules	n_{batt}	0	97

Irrespective of the costs and emission intensities of the various grades of hydrogen the optimal system configuration of the PEMFC/LIB hybrid energy system remains the same across all the grades. The system configuration is as follows.

Table 5.3: PEMFC/LIB solution

Component	Variable	Value	Total Capacity
150kW PEMFC stacks	n_{FC}	7	1050 kW
3.1 kWh LFP modules	n_{batt}	29	89.90 kWh

To verify that the model is working as intended to find the optimal design of hybrid system verification tests have been conducted as shown in appendix C.

The output power of a single PEMFC stack is depicted in Figure 5.1. Given that all PEMFC stacks are operating at an identical output power level, the output power of the remaining stacks is same as that illustrated in Figure 5.1. The installed battery charge/discharge power vs SOC is shown in figure 5.2. The power schedule of the different installed components is shown in the figure 5.3.

As seen from the figure 5.3, majority of the power is supplied by the PEMFC stacks. The reason for this is due to limited transient loading needed to be handled by the battery. The load profile has been linearly interpolated from 5 minutes to 1 minute, meaning that the load change between time steps is smaller compared to the 5 minute profile, and this can be handled by the fuel cells, resulting in a smaller battery capacity. Further checks are needed with the exact profile to verify that the current configuration can handle the different load transients.

To verify, that the optimal number of stacks have been selected, the number of available stacks has been reduced to 6 in appendix C.1, and the upper limit on the battery capacity is removed which resulted in a massive increase in the required battery capacity to 8128.20kWh. This is due to the cost of components, length of the trip, and the battery being utilized to compensate for the difference in power during transients.

The CAPEX, OPEX and total emissions for a single trip of the hybrid energy system across the various grades of hydrogen are shown in the figure 5.4. The quantity of hydrogen consumed across all the different hydrogen grades is 4784.14 kg for the entire trip. The break up of different costs is given in the table 5.4.

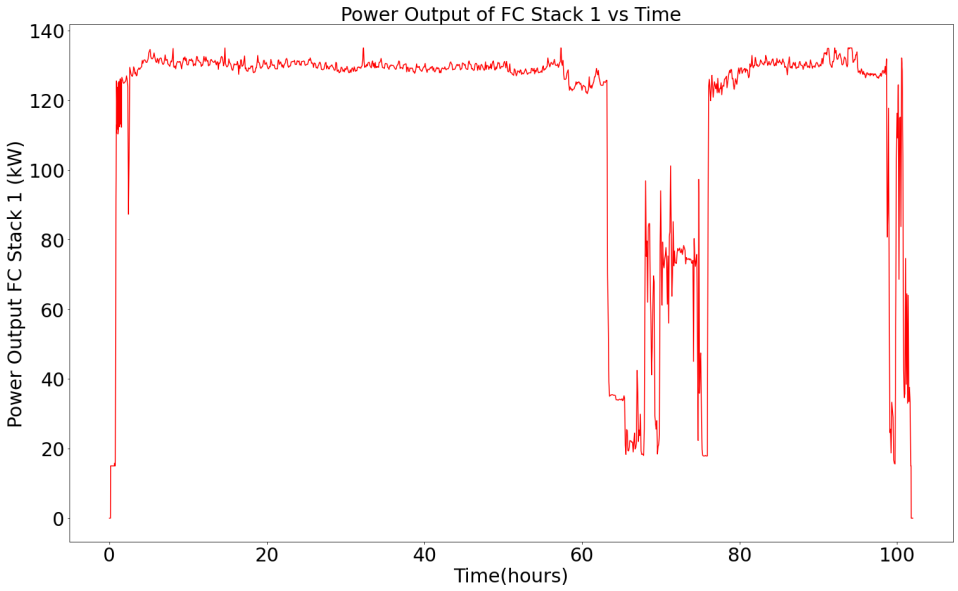

Figure 5.1: Output power of a individual PEMFC stack in the PEMFC/LIB hybrid system

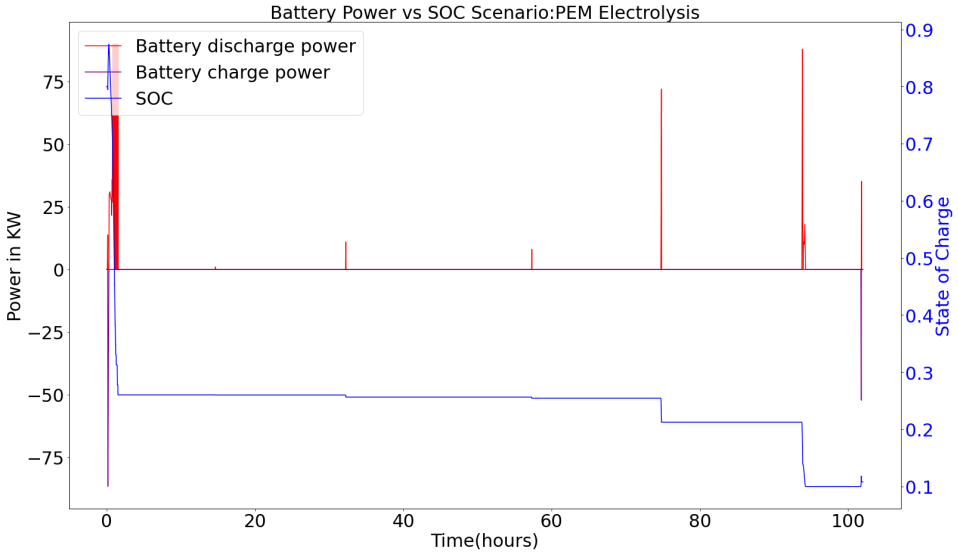

Figure 5.2: Battery charge/discharge power vs SOC in the PEMFC/LIB hybrid system

Table 5.4: Cost break-up of the PEMFC/LIB solution across various grades of hydrogen.

Hydrogen Grade	**PEMFC cost $**	**Battery Cost $**	**H_2 storage cost $**	**H_2 cost $**	**liquefaction cost $**	**Emission cost $**	**Batt charging cost $**
PEM				40186.77		0	
ALK				34397.97		0	
SMR	666750.00	13485.00	956827.97	9568.28	4784.14	5667.48	7.19
SMR+CCS				18275.41		1148.19	
ATR+CCS				18036.21		1377.83	

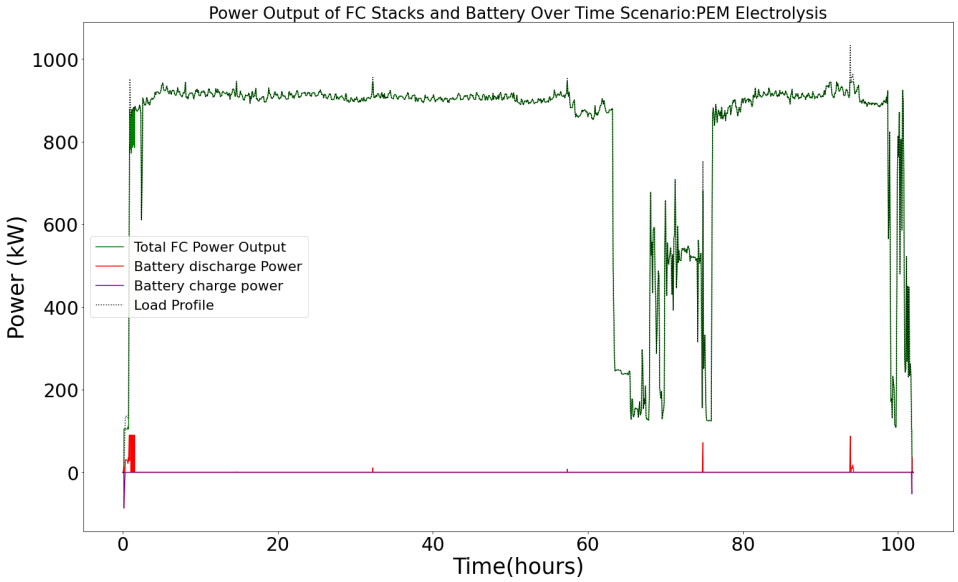

Figure 5.3: Power schedule of the installed components in the PEMFC/LIB solution

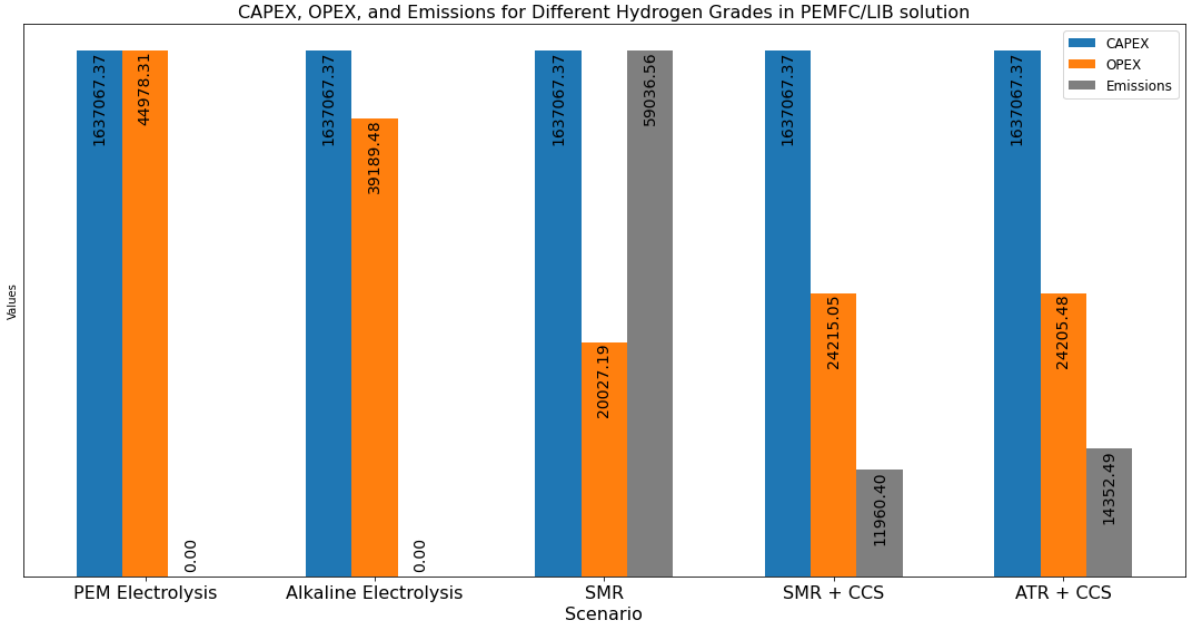

Figure 5.4: CAPEX (in $), OPEX (in $) and CO_{2eq} (in kg) emissions of the PEMFC/LIB hybrid energy system for various grades of hydrogen

Evaluation of cost and emission trade-offs of the PEMFC/LIB solution

As can be seen from the figure 5.4, the CAPEX costs of the hybrid energy system are $ 1637067.37, and the OPEX varies based on the costs and emission intensities of the various grades of hydrogen. A significant contributor to the CAPEX is the high cost of storing liquefied hydrogen on-board as shown in table 5.4. With respect to the OPEX, hydrogen produced using electrolysis (PEM and ALK) is still significantly expensive than fossil sources of hydrogen that even include carbon capture.

The MGO consumed across the entire trip with respect to the original power train configuration consisting of 1.8MW ICE is 19.7 tons, leading to total emissions of 82.95 tons of CO_{2eq}. A total emission reduction of 100% is possible with the use of electrolytic hydrogen. But this leads to an OPEX increase from $ 18,923.91 (using MGO) to $ 44,978.8 using PEM hydrogen and $ 39,189.30 using ALK hydrogen,

which is a 137% increase and 107% increase respectively.

The highest emitting PEMFC/LIB solution is the usage of hydrogen produced using SMR. This leads to a total emissions of 59.03 tons, which is a reduction of 28% total emissions. The OPEX of this solution is $ 20,027.09 which is a minor increase of 5.8%. The solutions using hydrogen produced using carbon capture provide a good trade-off between emission reduction and costs. The SMR+CCS hydrogen leads to an increase in costs of 27%, but a reduction in emissions of almost 85%, while the ATR+CCS hydrogen leads to an increase in costs of 27% and reduction in emissions of 83%.

5.1.2. DG/PEMFC/LIB hybrid energy system

Similar to the above subsection 5.1.1, the optimal sizes of the hybrid energy system configuration of the DG/PEMFC/LIB has been optimized for. The search spaces for the optimization has been set as table 5.5

Table 5.5: Search space of design optimization DG/PEMFC/LIB

Description	Variables	Value	
		min	max
Number of 800kW DG sets	n_{DG}	0	2
Number of 150kW PEMFC stacks	n_{FC}	0	7
Number of 3.1kWh LFP modules	n_{batt}	0	97

The search space limits for the PEMFC have been set based on the results from the PEMFC/LIB solution, and as the peak power demand of the trip is around 1000kW, 2 DG sets would be sufficient to satisfy the power demand.

Similar to the PEMFC/LIB solution, irrespective of the costs and emission intensities of the various grades of hydrogen the optimal system configuration of the DG/PEMFC/LIB hybrid energy system remains the same across all the grades. The system configuration is as follows.

Table 5.6: DG/PEMFC/LIB solution

Component	Variable	Value	Total Capacity
800kW DG sets	n_{DG}	1	800 kW
150kW PEMFC stacks	n_{FC}	2	300 kW
3.1 kWh LFP modules	n_{batt}	47	145.70 kWh

Verification tests were performed in appendix C.2. The selection of 2 DG's and battery despite it being the less expensive solution was due to the SOC of the battery at the start of the trip being set to 0.8 and the battery capacity was limited to 300 kWh.

The output power of the installed Diesel Generator and one of the PEMFC stacks (as all the stacks deliver the same power) is shown in the figures 5.5 and 5.6. It has been observed that the power split between the installed components is similar across all the different grades of hydrogen.

The battery charge/discharge power vs SOC and the power schedule of the different installed components is shown in figures 5.7 and 5.8. The battery is being utilized at the start of the trip for the DG and PEMFC stacks to reach the optimal power based on the transient constraints set, and once they reach the optimal power, the battery is being discharged across the length of the trip until around hour 60 to reduce the H_2 consumption. There are no rules set in place on how the battery needs to be discharged if there are no excessive demands that the PEMFC stacks and DG can't handle. The DG in this part of the trip is being operated at it's maximum rated power due to the high costs of the hydrogen storage. Around hour 60, the PEMFC stacks are switched-off and the DG set is being operated at higher % of

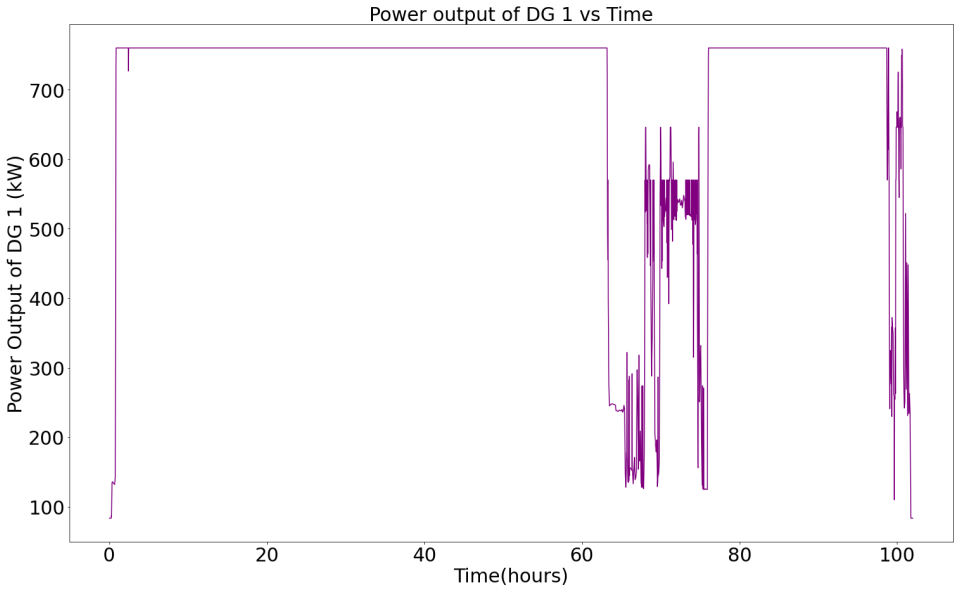

Figure 5.5: Output power of DG in DG/PEMFC/LIB solution

Figure 5.6: Output power of PEMFC in DG/PEMFC/LIB solution

it's rated power(better efficiency) to charge the battery back up to the maximum SOC limit. Further on, after the power demands are back to normal, the DG set operates at it's maximum rated power, and the battery is discharged to reduce the H_2 consumption.

The CAPEX, OPEX and total emissions for a single trip of the hybrid energy system across the various grades of hydrogen are shown in figure 5.9. The quantity of hydrogen consumed across all the different hydrogen grades is 685.02 kg, and MGO consumed is 14,095.43 kg. The break up of the different cost components is given in table 5.7

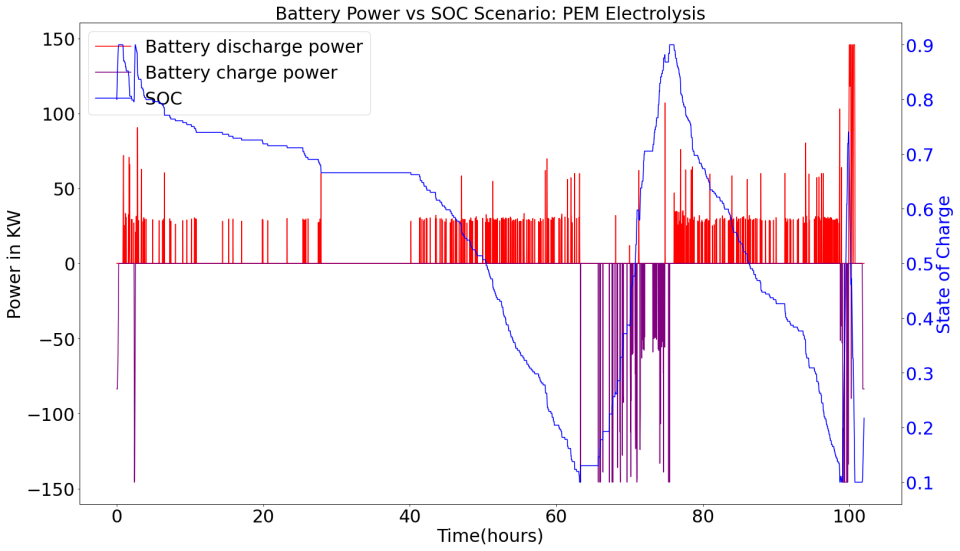

Figure 5.7: Battery charge/discharge power vs SOC in DG/PEMFC/LIB solution

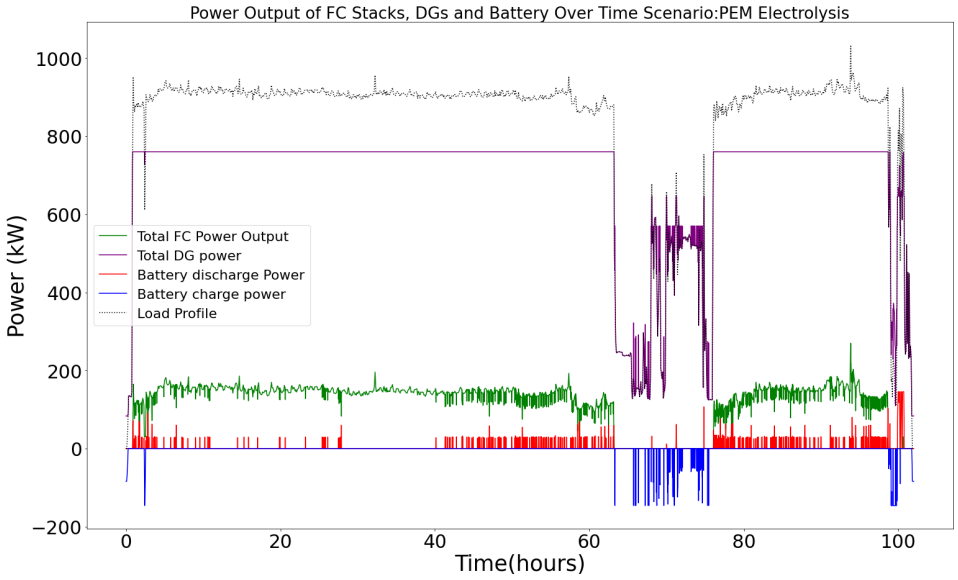

Figure 5.8: Power output of the installed components in the DG/PEMFC/LIB solution

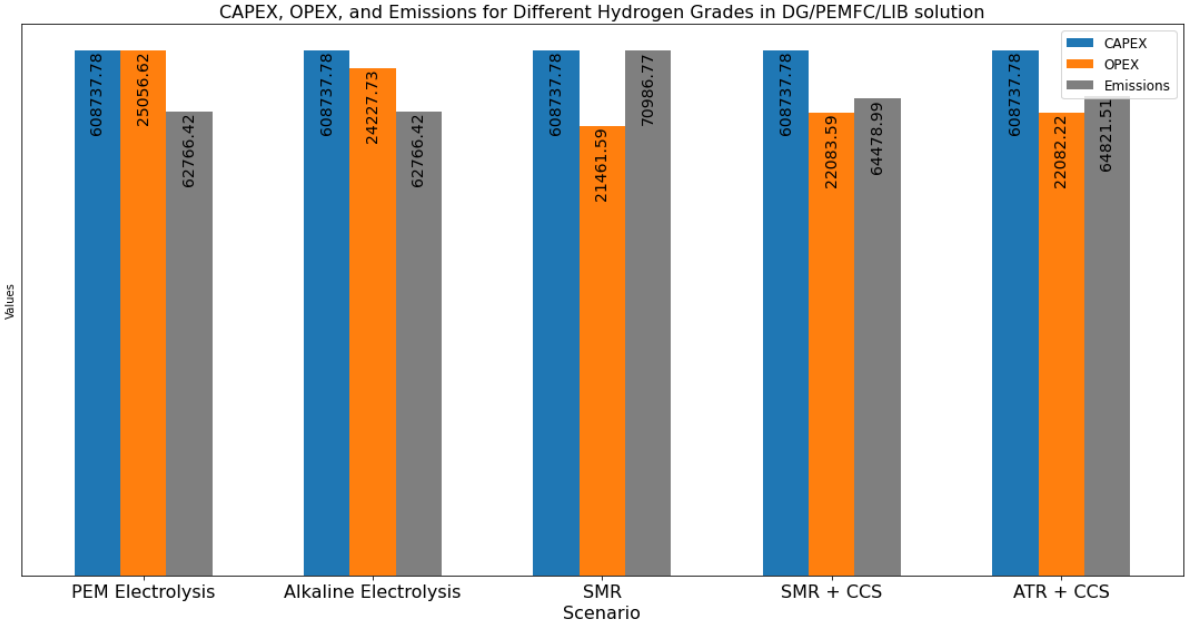

Figure 5.9: CAPEX (in $), OPEX (in $) and CO_{2eq} (in kg) emissions of the DG/PEMFC/LIB hybrid energy system for various grades of hydrogen

Table 5.7: Cost break-up of the DG/PEMFC/LIB solution across various grades of hydrogen

Hydrogen Grade	DG Cost $	PEMFC cost $	Battery Cost $	MGO storage cost $	H2 storage cost $	H2 cost $	H2 liquefaction cost $	MGO cost $	Total emission cost $	Batt charging cost $
PEM						5754.15			6025.61	
ALK						4925.28			6025.61	
SMR	240000	190500	21855	19377.06	137003.56	1370.04	685.02	12580.19	6814.75	11.66
SMR+CCS						2616.77			6190.01	
ATR+CCS						2582.52			6222.90	

Evaluation of cost and emission tradeoff's of the DG/PEMFC/LIB solution

As can be seen from the figure 5.9, the CAPEX of this hybrid energy system is same across all the different grades of hydrogen, i.e. $ 608737.78, which is 62.8% less expensive than the PEMFC/LIB hybrid energy system.

Among the different grades of hydrogen, due to high cost of the electrolytic hydrogen, the OPEX is higher if PEM and ALK hydrogen are used. The OPEX if PEM hydrogen is used is $ 25,056.62, and if ALK hydrogen is used is $ 24,227.75 which is a 32% and 28% increase respectively. The emissions for the entire trip are reduced from 82.5 tons to 62.76 tons which is a $\approx$ 24% reduction in emissions.

Among the fossil sources of hydrogen, the SMR leads to the highest amount of emissions of 70.98 tons, which is a 13.6% reduction in emissions from the original configuration. The OPEX is the lowest for this solution at $ 21,461.65 which is an increase of 13.43%. The better trade-off between emissions and costs can be achieved by using Fossil hydrogen using CCS. The SMR+CCS solution leads to a $\approx$17% increase in OPEX while reducing the emissions by 21.85%. The ATR+CCS solution also gives similar results, a 16.68% increase in OPEX and 21.42% reduction in emissions.

Impact of Storage costs of liquefied hydrogen on-board

One of the factors holding back the PEMFC stacks from being operated at a higher power is the high cost of liquefied hydrogen storage. For this analysis, the costs of liquefied hydrogen storage and MGO storage has been removed from the total cost objective function(equation 4.25). In the figure 5.10, it is evident that the PEMFC stacks are being operated at a higher % of their max rated power compared to figure 5.8, due to which there has been an increase in the amount of hydrogen consumed from 685kg to 1359 kg for SMR hydrogen. This massive increase in hydrogen consumption is not observed for the other grades of hydrogen.

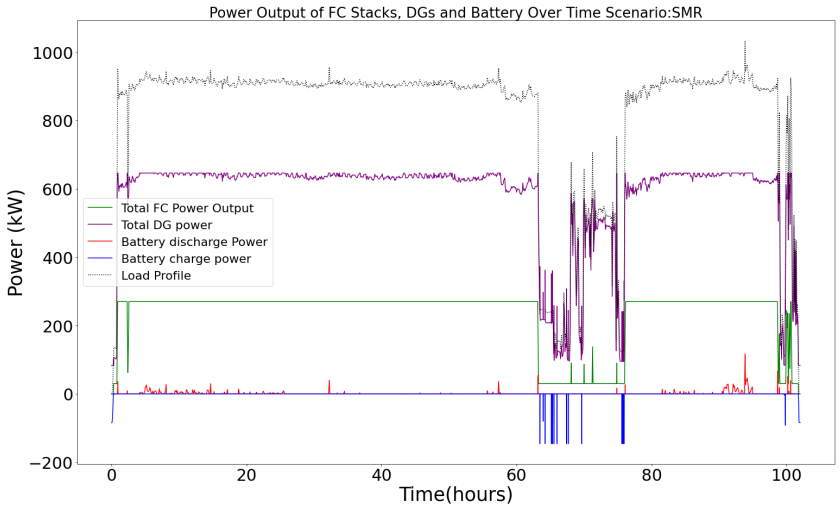

Figure 5.10: Power output of the installed components in the DG/PEMFC/LIB solution without storage costs (SMR Hydrogen)

5.2. Stage 2: Lifetime Estimation of Components

In this subsection, the estimated lifetime of the installed PEMFC and LFP battery components has been elaborated on for both the (i) PEMFC/LIB hybrid energy system and (ii) DG/PEMFC/LIB hybrid energy system. The methodology used for the lifetime estimation has been described in the section 4.1.4.

Before the start of the analysis, to ensure that the installed battery retains the necessary capacity for operation till end of life the battery capacity is increased according to equation 4.38 for both the solutions. The modified system configurations are as below:

Table 5.8: Modified PEMFC/LIB solution

Component	Variable	Value	Total Capacity
150kW PEMFC stacks	n_{FC}	7	1050 kW
3.1 kWh LFP modules	n_{batt}	37	114.70 kWh

Table 5.9: Modified DG/PEMFC/LIB solution

Component	Variable	Value	Total Capacity
800kW DG sets	n_{DG}	1	800 kW
150kW PEMFC stacks	n_{FC}	2	300 kW
3.1 kWh LFP modules	n_{batt}	59	182.90 kWh

The increase in CAPEX due to increase in the battery capacity is \$3720(PEMFC/LIB) and \$5580(DG/PEMFC/LIB). The volume constraints 4.33 and 4.24 have been verified for both the systems. For the lifetime estimation of components, only the price of PEM electrolysis hydrogen has been used as the input.

5.2.1. Lifetime of components in the PEMFC/LIB solution

In this subsection, the voltage loss of the PEMFC stacks and the number of cycles that the battery undergoes in a single trip are evaluated. Further along, the lifetime of the components and the increase in hydrogen consumption has been observed.

The power schedule of the components of both the single objective OPEX optimization and the multi-objective hierarchical optimization with the voltage loss of a single cell representative of the entire stack as the 2^{nd} objective is shown in the figures 5.11 and 5.12. Similarly the charge/discharge power vs SOC of the battery is shown in the figure 5.13, 5.14

Table 5.10: Voltage loss comparison of single objective vs multi-objective optimization in the PEMFC/LIB solution

Voltage Loss (in μV)	Single-Objectve	Multi-Objective	% Reduction
start-up voltage loss	23.91	23.91	0
transient loading voltage loss	153.81	79.12	48.55
operating power voltage loss	1118.52	1118.54	0
Total loss of voltage loss	1297.24	1221.57	5.83

From the table 5.10, it is observed that the major contribution to the voltage loss of the PEMFC stack is due to operating power of the PEMFC stack which is similar for both the methods. Since the fuel cell stacks undergo only a single start-stop cycle across the entire trip, it is also the same for both the methods. The voltage loss due to transient loading has been reduced by 48.55% from the single objective to the multi objective method. The overall voltage loss is reduced from 1297.24 μV to 1221.57 μV.

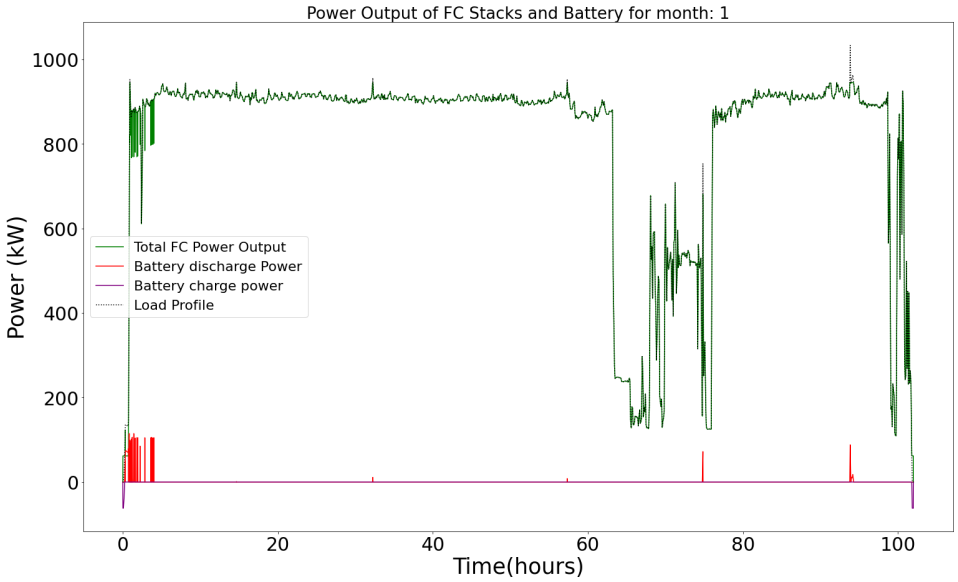

Figure 5.11: Power schedule of the installed PEMFC/LIB components in the single objective OPEX optimization

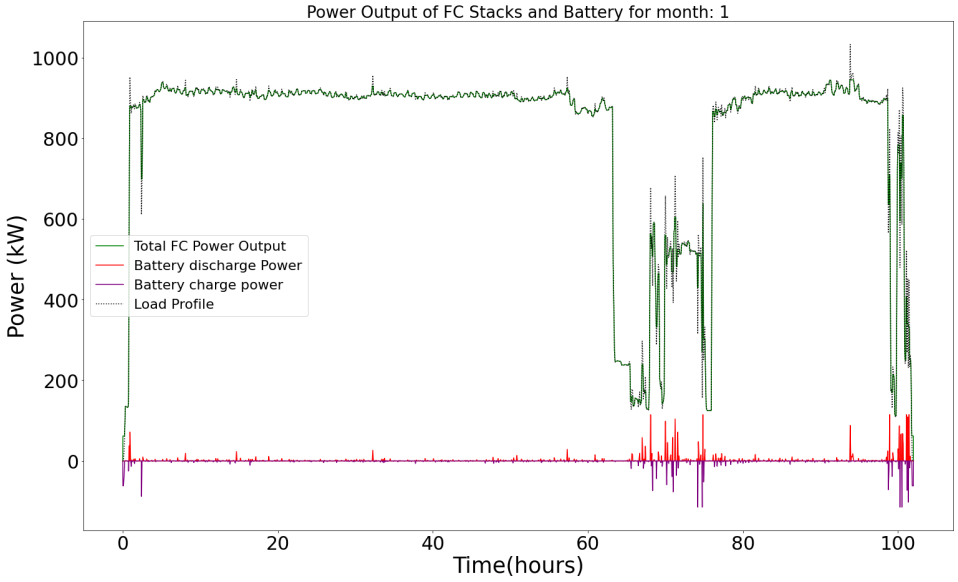

Figure 5.12: Power schedule of the installed PEMFC/LIB components in the multi objective OPEX and PEMFC degradation optimization

The number of battery cycles have been counted based on the SOC history of the battery after the trip according to the algorithm proposed by Gundogdu and Gladwin [129], and have increased from 0.88 cycles for the entire trip in the single objective optimization to 1.56 in the multi-objective optimization. This is due to the transient loading on the fuel cell being limited by the battery system.

The OPEX of the trip also didn't increase as expected of hierarchical multi-objective optimization where the lower priority objective (PEMFC voltage loss) does not degrade the optimal value of the higher priority objective (OPEX). It is $ 44,975.25 for the multi-objective optimization and $ 44,973.05 for the single objective optimization.

Lifetime of the installed PEMFC and LIB system

The operation optimization of the vessel has been performed for 1 trip representative of each month to reduce the computational burden and the voltage loss of the PEMFC stack and the battery cycles are

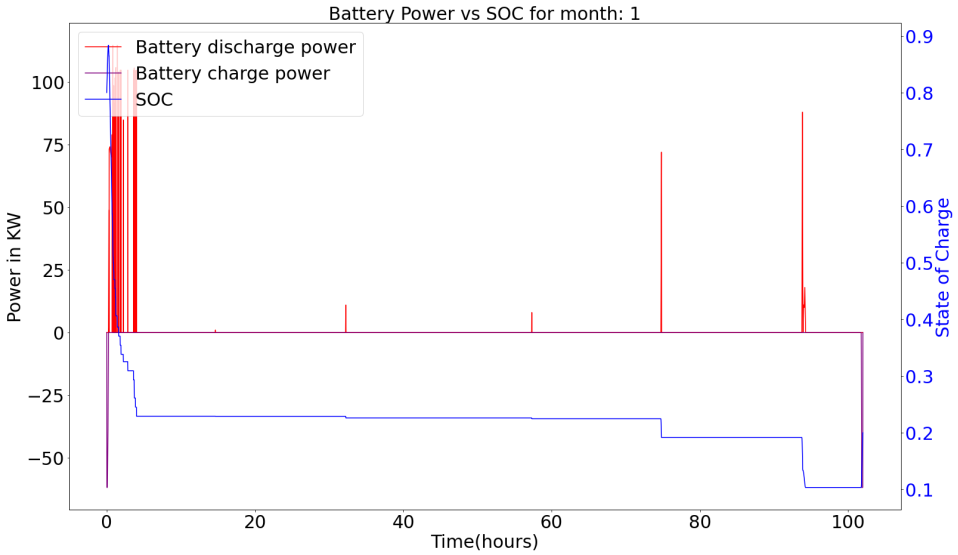

Figure 5.13: Battery power vs SOC: single objective OPEX optimization

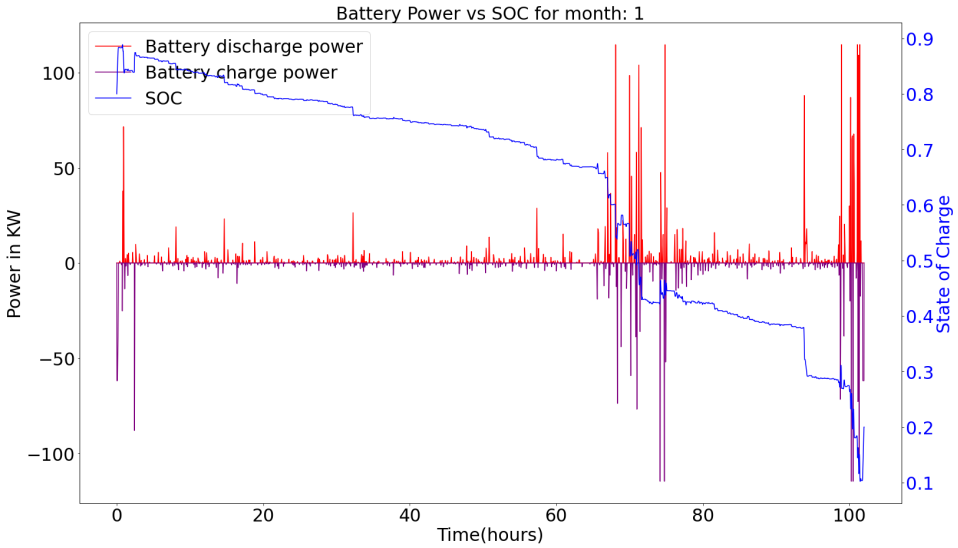

Figure 5.14: Battery power vs SOC in the multi objective OPEX and PEMFC degradation optimization

calculated. The calendar aging of the battery is evaluated for each month according to the equation 4.39 and the fitting parameters in 4.4. The battery is assumed to be stored at 25°C for 5 days in a month, at the SOC obtained after the end of the trip (SOC_{end}).

The resulting PEMFC and battery lifetime are shown in the figures 5.15 and 5.16. For the single objective optimization the PEMFC reaches 80% SOH at the 31^{st} month, whereas at the same time, the battery still is at 81% SOH, and it can last for an additional 1-2 months (figure 5.15). For the multi-objective optimization the battery reaches its end of life at the 29^{th} month where the SOH is at 80% and the PEMFC is still at a SOH of 82%, meaning that the PEMFC stack can last for an additional 3-4 months (figure 5.16).

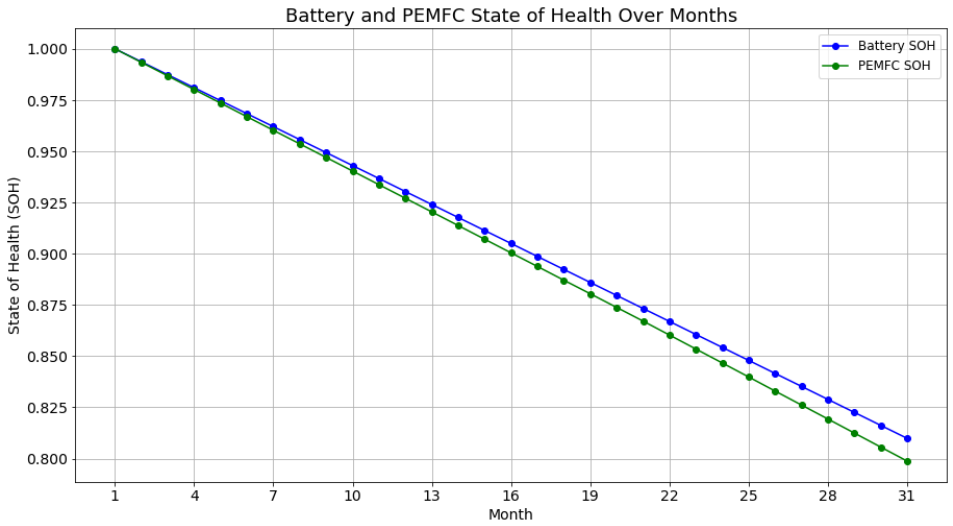

Figure 5.15: PEMFC and Battery SOH for single objective optimization in PEMFC/LIB solution

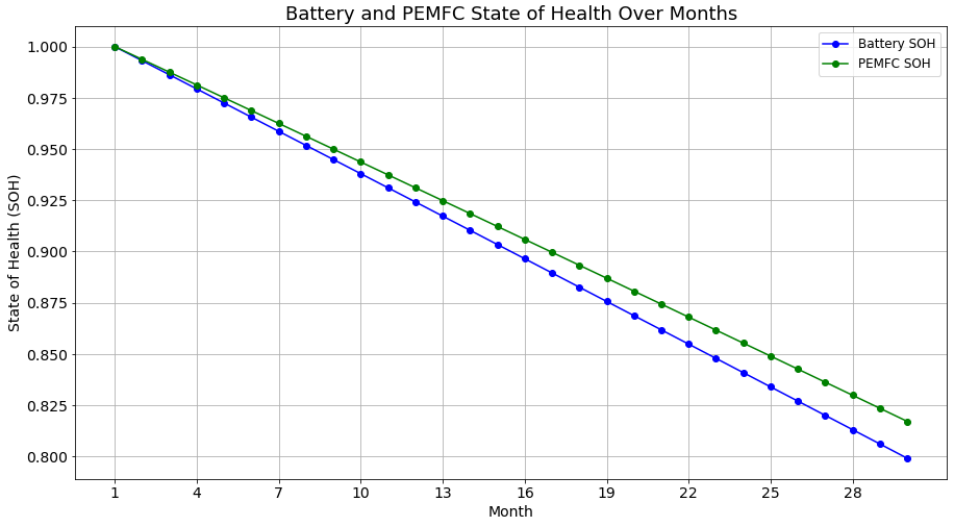

Figure 5.16: PEMFC and Battery SOH for multi-objective optimization in the PEMFC/LIB solution

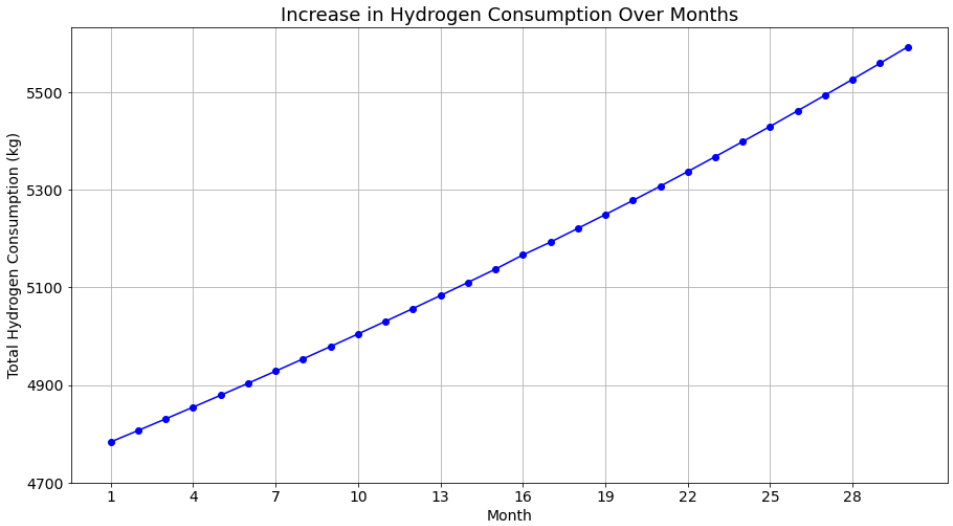

Figure 5.17: Increase in H_2 consumption for single objective optimization-PEMFC/LIB solution

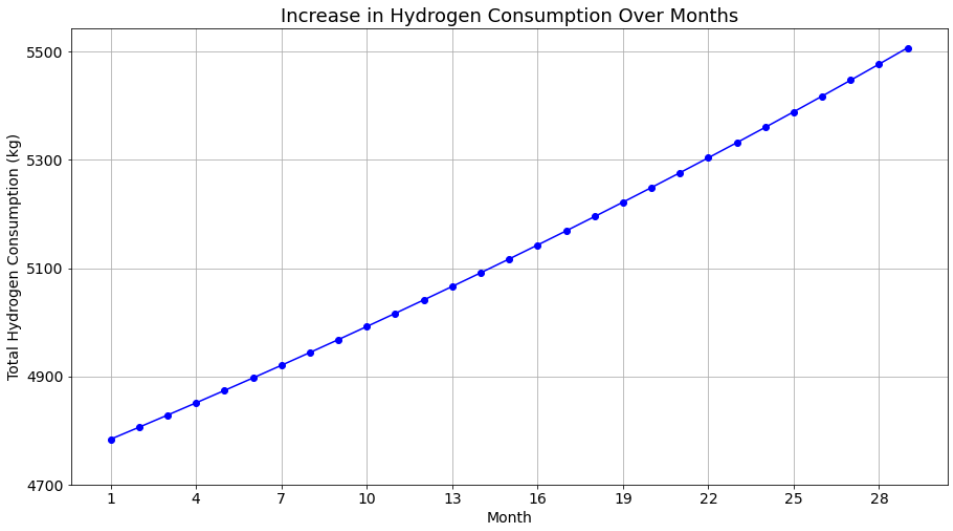

Figure 5.18: Increase in H_2 consumption for multi-objective optimization-PEMFC/LIB solution

The voltage loss of the PEMFC stack, leads to an increase in the current density to deliver the same power, which in turn leads to an increase in hydrogen consumption (equation 4.5). There is a significant increase in H_2 consumption due to the degradation of the PEMFC stack as can be seen in the figures 5.17 and 5.18. At the start of the plant lifetime the H_2 consumed for the entire trip is 4783.39 kg, where as towards the end of life of the stack, this has increased to 5592.96 kg in the single objective optimization which is a 16.92%(809.57kg) increase. In-case of the multi-objective optimization this has increased to 5507.33kg which is a 15.13%(723.94kg) increase.

This increase in H_2 consumption needs to be accounted for by the vessel owner at the new build stage due to the high costs of liquefied hydrogen storage. There is a $161,914 increase in the hydrogen storage costs due to the PEMFC and battery degradation.

5.2.2. Lifetime of components in the DG/PEMFC/LIB solution

Similar to the above subsection 5.2.1, first the voltage loss of the PEMFC stacks and the number of cycles that the battery undergoes in a single trip are evaluated. Further along, the lifetime of the components and the increase in hydrogen consumption has been observed.

The power schedule of the components of both the single objective OPEX optimization and the multi-objective optimization with the voltage loss of the single cell representative of the entire stack as the 2^{nd} objective is shown in figures 5.19 and 5.20. Similarly the charge/discharge power vs SOC of the battery is shown in the figures 5.21 and 5.22.

From the table 5.11, it can be seen that the major contributor to the voltage loss is the operation of the PEMFC stack which is the same for both the single objective and multi-objective optimization methods at 876.60 μV. In both the methods the fuel cell stack is switched on/off twice as can be seen from the figures 5.19 and 5.20, due to which the voltage loss is 47.82 μV. The major reduction in the voltage loss is due to the reduction in transient loading of the PEMFC stack in the multi objective optimization. It has reduced significantly from 556.67 μV to 26.09 μV which is a 95% reduction. The total voltage loss for a single trip has reduced from 1479.08 μV to 950 μV.

Comparing the figures 5.21 vs 5.22, it can be seen that the battery is discharging strategically to limit the transient loading on the PEMFC stack. The number of battery cycles has increased from 2.37 in the single objective optimization to 2.62 in the multi-objective optimization. The total OPEX of the entire trip has remained the same for both the methods at $25,035.50.

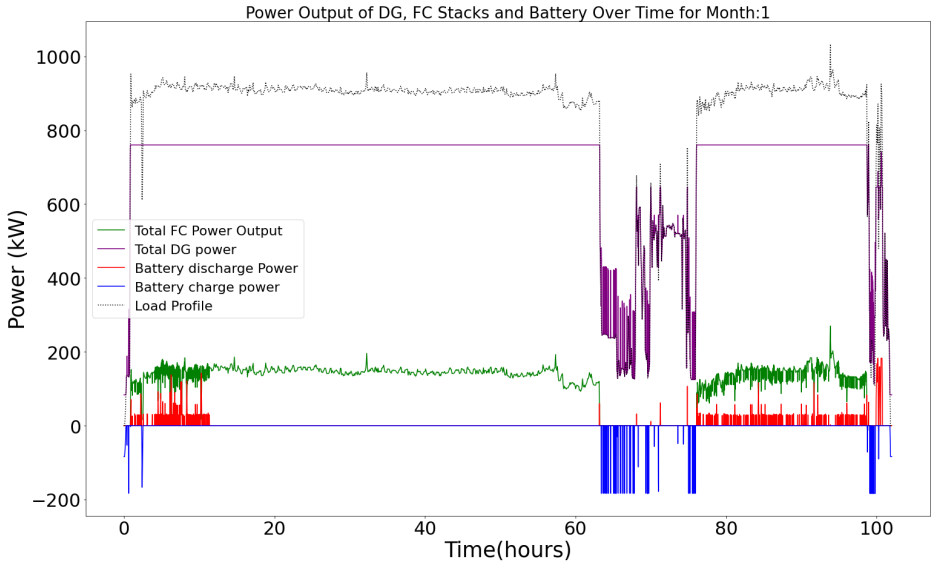

Figure 5.19: Power schedule of the installed components in the single objective OPEX optimization-DG/PEMFC/LIB solution

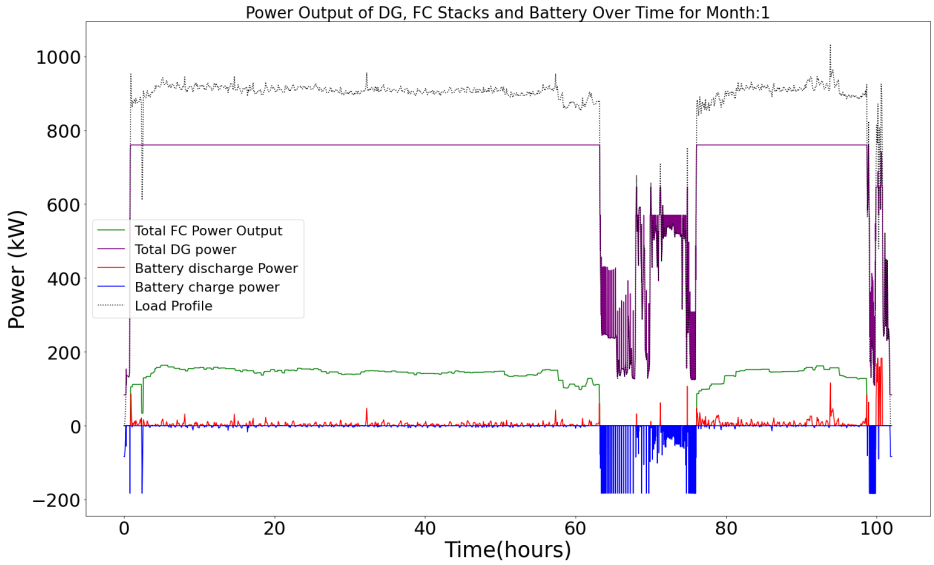

Figure 5.20: Power schedule of the installed components in the multi objective OPEX and PEMFC degradation optimization-DG/PEMFC/LIB solution

Table 5.11: Voltage loss comparison of single objective vs multi-objective operation optimization in the DG/PEMFC/LIB solution

Voltage Loss (in μV)	**Single-Objectve**	**Multi-Objective**	**% Reduction**
start-up voltage loss	47.82	47.82	0
transient loading voltage loss	554.67	26.09	95.29
operating power voltage loss	876.60	876.63	0
Total loss of voltage loss	1479.08	950.54	35.73

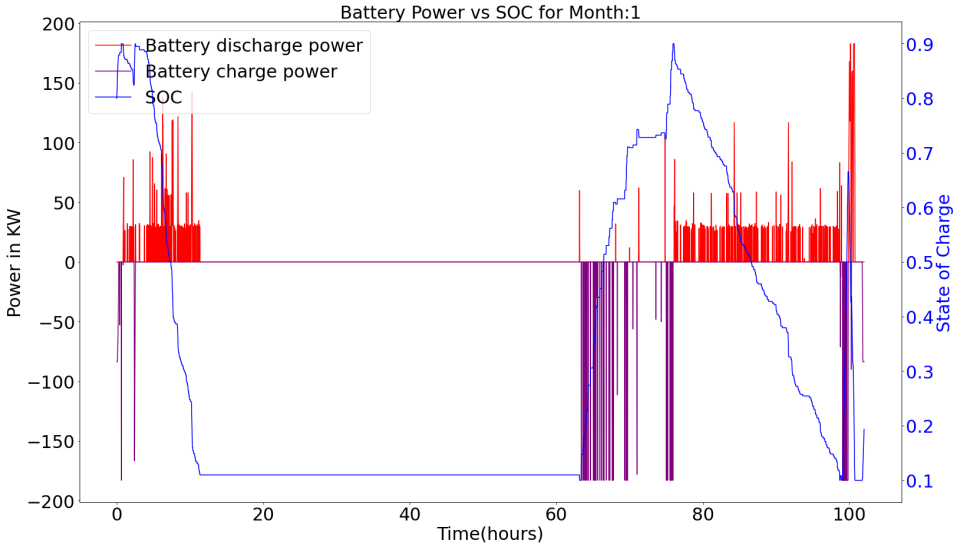

Figure 5.21: Battery charge/discharge power vs SOC: single objective OPEX optimization-DG/PEMFC/LIB solution

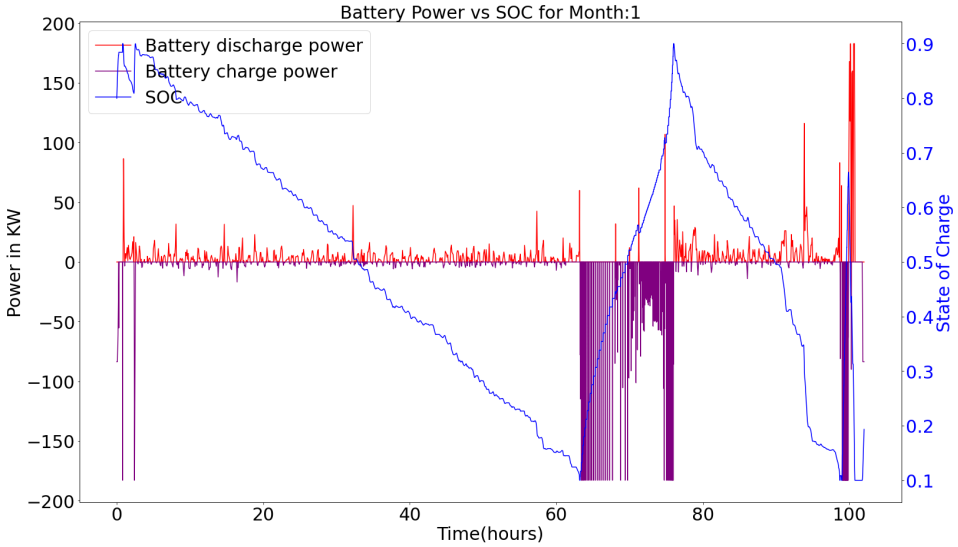

Figure 5.22: Battery charge/discharge power vs SOC in the multi objective OPEX and PEMFC degradation optimization-DG/PEMFC/LIB solution

Lifetime of the installed PEMFC and LIB

The procedure to evaluate the lifetime of the PEMFC and battery are similar to the above subsection. The resulting plant lifetime is shown in the figures 5.23 and 5.24. For a single objective optimization, the PEMFC stack reaches it's end-of-life at the 27^{th} month and the battery is at a SOH of 80% and can last for an additional 1 month. In case of the multi-objective method, the battery reaches it's end of life at the 26^{th} month, and the PEMFC is still at a SOH of 87%. To evaluate the exact time at which the PEMFC stack reaches it's end of life, the battery is replaced at the end of the 26^{th} month. The resulting plant lifetime evaluation is shown in figure 5.25. It can be clearly seen that the PEMFC stacks would last for 42 months after which they need to be replaced.

The resulting increase in H_2 due to the degradation of the PEMFC stack and battery is shown in figure 5.26 & 5.27. The H_2 consumption per trip increases from 681.74kg in the first month to 799.84kg in

the single objective method, and 750.98kg in the hierarchical method at the end of life. This increase in hydrogen consumption of 70kg(multi-objective method) can easily be accounted for in the design stage by the vessel owner compared to the PEMFC/LIB solution.

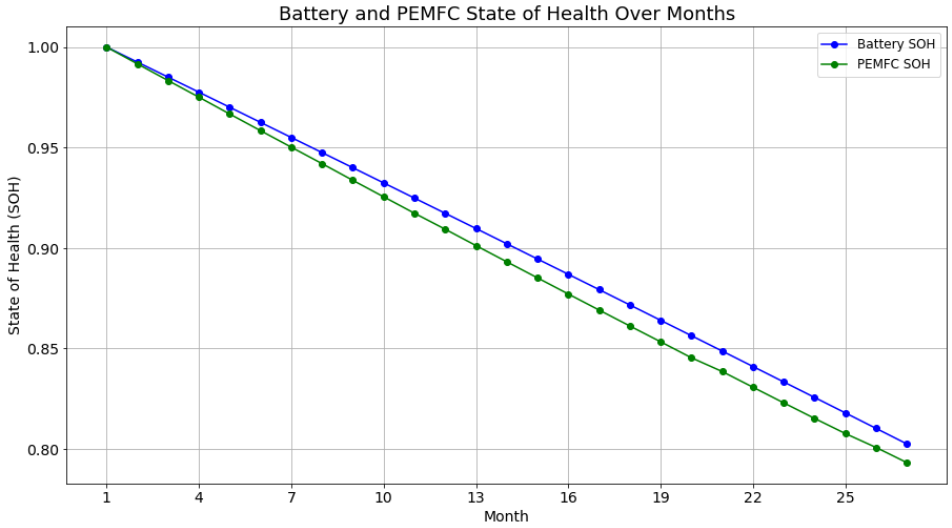

Figure 5.23: PEMFC and Battery SOH for single objective OPEX optimization in the DG/PEMFC/LIB solution

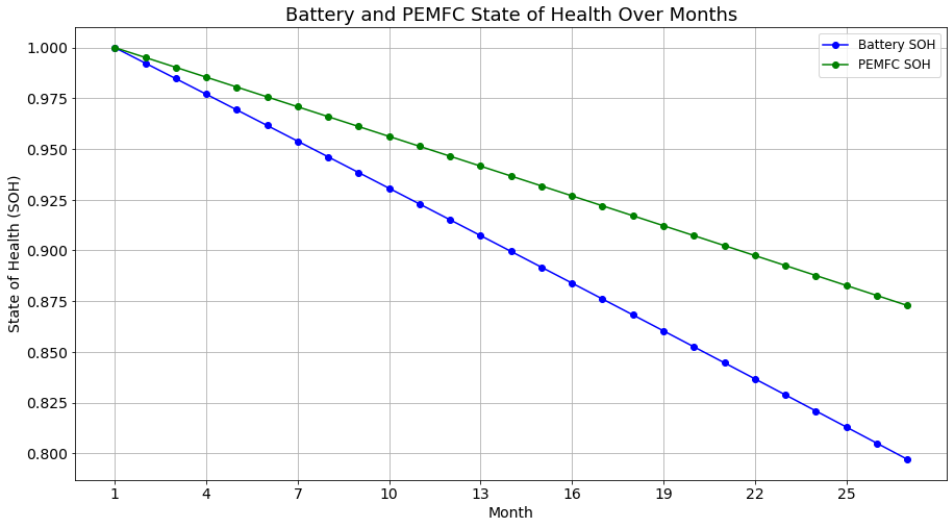

Figure 5.24: PEMFC and Battery SOH for multi-objective optimization in the DG/PEMFC/LIB solution

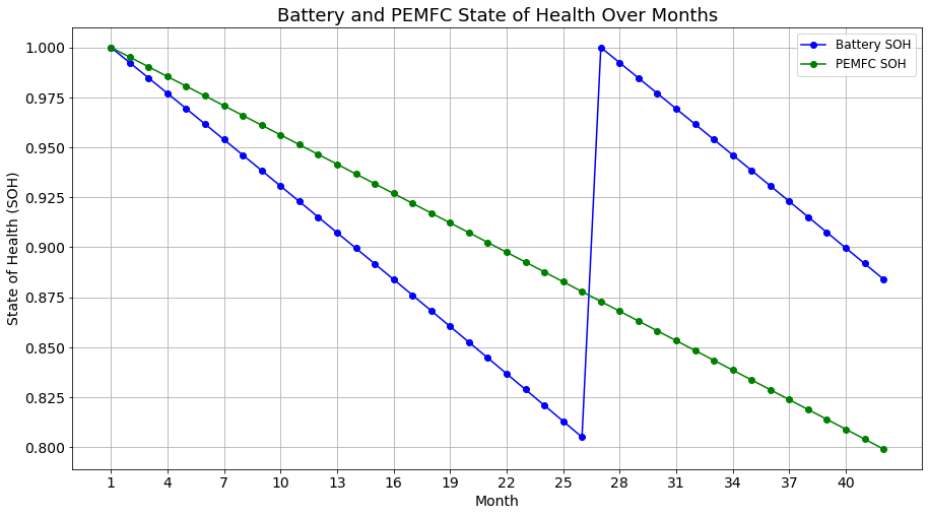

Figure 5.25: PEMFC and Battery SOH for multi-objective optimization in the DG/PEMFC/LIB solution with battery replaced at it's end of life

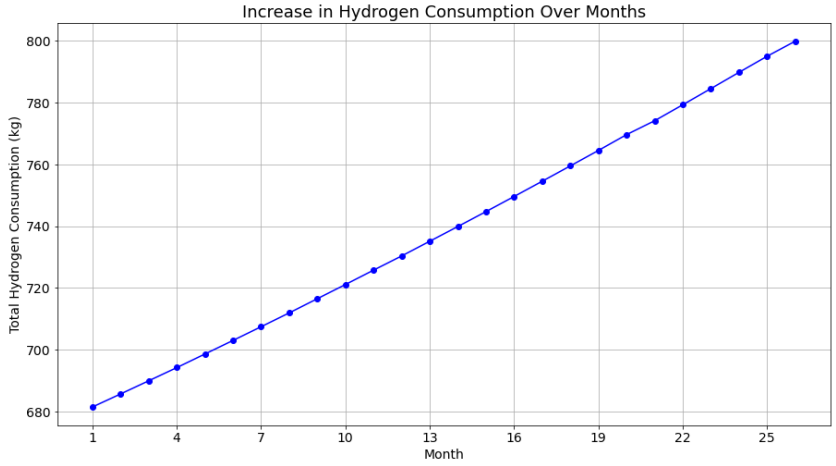

Figure 5.26: H_2 consumption increase for single objective optimization-DG/PEMFC/LIB solution

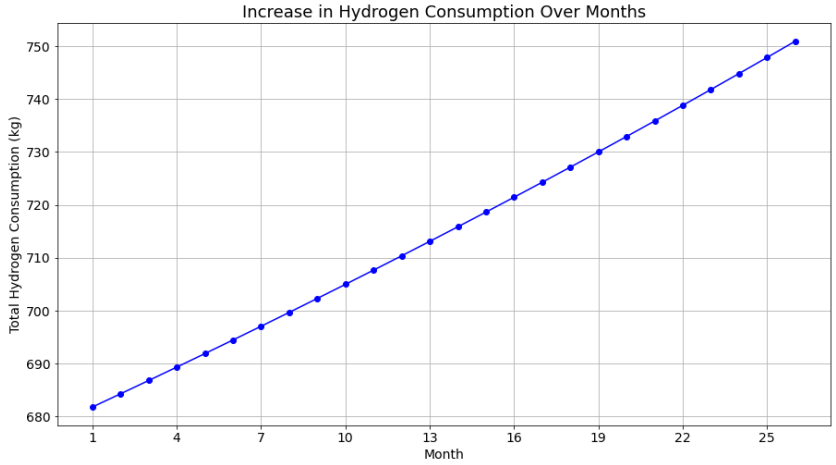

Figure 5.27: H_2 consumption increase for multi-objective optimization-DG/PEMFC/LIB solution

6
Conclusions and Recommendations

In this chapter, the conclusions of the report are explained and discussed. These are based on the results of the previous chapters. The conclusions will give an answer to the main and sub-research questions. After the conclusions, recommendations for future work are given.

6.1. Conclusions

This thesis investigated two different hybrid energy systems (i) PEMFC/LIB, and (ii) DG/PEMFC/LIB to look into the cost and emission trade-off's of using different grades of hydrogen considering their production emissions, and also estimate the lifetime of the installed components.

The main research question framed in chapter 1 of the study was:

How to optimize the design and operation of a ship hybrid energy system to minimize the costs considering the WTW emissions associated with the fuels and what is the lifetime of the installed components?

The following sub-research questions that were framed to answer the above question. hereby, all the questions have been answered.

1. ***What are the emissions associated with the different types of hydrogen and Marine Fuels?***

   The hydrogen production emissions depend on the carbon capture rate for fossil sources and grid emission intensity for electrolysis. The production of H_2 using natural gas without CCS leads to emissions of 11-12 kg CO_{2eq}/kg H_2 which is the most common method of production. With CCS the emissions vary between 1.5-6.2 kg CO_{2eq}/kg H_2. The emissions from coal gasification is the highest at 22-26kg CO_{2eq}/kg H_2.

   It is important to note that WTW emissions components can vary significantly depending on the source of the fuel, the method of extraction, the efficiency of transportation and conversion technologies, and the specific end-use conditions.

   The Well-to-Wake emissions of the different marine fuels have been obtained from the study by Comer and Osipova [67]. In this thesis, the use of Marine Gas Oil(MGO) in a Medium Speed Diesel (MSD) ICE is considered. The associated emissions are 4.211kg CO_{2eq}/kg MGO consumed.

2. ***What are the different aging modelling methods of PEMFC and Li-ion batteries?***

   The main sources of PEMFC degradation are: operation at low or high current, galvanostatic decay, load cycling, and start/stop phases. PEMFC stack aging is modeled through three approaches: impedance estimation, remaining useful life estimation, and stack voltage degradation model. Stack voltage degradation model is often used to limit the computational effort required in solving complex energy system models, although such modelling approach is less accurate with respect to other methods and depends on the experimental data.

   Two main causes of Li-ion battery aging have been identified: (i) Calendar aging, and (ii) cycling aging. To calculate the number of charge/discharge cycles that a battery has undergone, the cycle

counting algorithm by Gundogdu and Gladwin [129] is used. This is advantageous compared to the conventional rainflow approach as the rainflow algorithm can only be applied to extreme points (peaks and valleys), whereas this algorithm processes all the data at each time step. To find the capacity loss of various Li-ion battery chemistries due to calendar aging, different studies in literature have been analysed by Ali, Beltran, Lindsey, *et al.*, and a model is proposed to calculate the capacity degradation based on battery storage temperature, SOC, and number of storage days[130].

3. ***What are the different mathematical optimization techniques that are currently being utilized in the hybrid energy system design and operation of ships?***

   Mathematical optimization has become a crucial tool that engineers use to determine the power plant configuration. The choice of the optimization technique depends on the complexity of the system, the number of variables and constraints, and the specific objectives of the optimization. The most common optimization algorithms used in sizing of hybrid systems are MILP and (meta)heuristics such as genetic algorithms(NSGA-II) and swarm optimization(MOPSO) techniques and the sizing problem is generally a multi-objective problem, that optimizes for minimizing operational and capital costs and reduced emissions.

   In this review, studies which combined both the optimal sizing and control of the ship, to avoid sub-optimal solutions during the design stage were looked at. Factors such as battery and fuel cell degradations along with maintenance and replacement costs were also considered for the optimization problems. Other sizing studies were modelled considering the future uncertainties in fuels, converters and storage devices. Most of the studies assume the fuels to be based on renewable sources of electricity and optimize for the emissions from the Tank to Wake.

4. ***How can the hybrid energy system be modelled for the design and lifetime estimation of PEMFC and LIB components?***

   For the design of the two hybrid energy systems, MILP approach was taken to model the power components and the weight and volume constraints due to them allowing to account for large sets of design and operational variables without excessively increasing the computational effort. The PEMFC was modelled using linear equations relating current density, stack power output, and H_2 consumption. The battery power is constrained with the C-rate of the manufacturer, and the Diesel Generator was modelled using a Piece-wise linear (PWL) approximation of the output power and Marine Gas Oil (MGO) consumption.

   The design results obtained in the first stage have been used as input to the second stage to reduce the computational complexity. A hierarchical multi-objective optimization has been set up, with the primary objective to be the OPEX of a single trip, and the secondary objective to be the degradation of the PEMFC. To model the degradation of the PEMFC, a stack voltage degradation model has been considered and modelled as linear equations; (i) operational power, (ii) start/stops, and (iii) transients. The battery aging is not part of the operation optimization, but the trip SOC data is used to calculate the number of cycles, and the calendar aging effects of the battery have also been modelled.

5. ***What are the costs and emission trade-offs associated with the PEMFC/LIB hybrid vs DG/PEMFC/LIB hybrid energy system?***

   For the design of the hybrid systems hydrogen from 5 different sources has been considered, namely SMR, SMR+CCS, PEM, ALK and ATR+CCS. The resulting design has not varied across the different grades of hydrogen for both the hybrid system configurations. The CAPEX of the DG/PEMFC/LIB hybrid system was 62.8% less expensive than the PEMFC/LIB solution.

   In the PEMFC/LIB solution, using electrolytic hydrogen results in zero WTW emissions and an increase in OPEX compared to the original configuration of 137%(PEM) and 107%(ALK) respectively. The OPEX using SMR hydrogen resulted in the lowest costs(5.8% increase) and highest emissions(59 tons). The hydrogen with CCS provides a good trade-off between costs and emissions. The OPEX is increased by 27% and an emission reduction of 85% is achievable.

In the DG/PEMFC/LIB solution, the results are similar, with electrolytic hydrogen having the low emissions and high OPEX. A 24% reduction in emissions and a cost increase of 32%(PEM) and 28%(ALK) respectively. The use of SMR hydrogen resulted in the lowest OPEX, a 13.43% increase and high emissions(70.1 tons). The hydrogen with CCS results in a 17% increase in OPEX and a 21% reduction in emissions.

The use of SMR hydrogen even with high production emissions of 12 $kgCO_{2eq}/kgH_2$ reduces the total emissions of the trip due to the high efficiency of the PEMFC stack at Beginning of Life. Another key factor holding back the increased use of hydrogen is the high cost of liquefied hydrogen storage. If shore power is not available to charge the batteries, they can be charged using the other components on-board, and as the cost of charging the batteries using shore charging is not expensive.

6. ***What is the estimated lifetime of the PEMFC and batteries?***

   For the lifetime estimation, only the price of hydrogen produced using PEM electrolysis has been considered.

   In the PEMFC/LIB solution, the PEMFC lifetime can be increase from 31 months to 34 months using the hierarchical optimization. But the battery lifetime reduces from 33 months to 29 months due to the increase cycling aging. Due to the degradation of the PEMFC and battery there is massive increase in hydrogen consumption from 4783 kg to 5592 kg(Single Objective) and 5503(multi objective) at the end of life.

   In the DG/PEMFC/LIB solution, there is a reduction in the voltage loss due to transient loading in the hierarchical optimization, due to which the PEMFC lifetime has been extended from 27 months to 42 months and the battery lifetime is reduced from 28 to 26 months. There is not a massive increase in the hydrogen consumption in this case.

6.2. Future Recommendations

The potential for conducting additional research in this area is discussed here, along with some issues that could use some attention.

Uncertainties in Prices

In this study, deterministic design and operation optimization of the hybrid system has been conducted using fixed fuel and component prices. It is reasonable to use fixed component prices, as these are immutable and only relevant at the design stage of the project, impacting costs primarily when components require replacement at the end of their lifespan. However, fuel, carbon, and electricity costs are subject to change over time, differing from the fixed rates assumed at the design stage. Consequently, for a comprehensive life-cycle cost analysis of the system, it is crucial to account for these uncertainties in the long-term operation optimization along with the degradation of power components.

Monte Carlo Analysis (MCA) is a useful method that can facilitate uncertainty-based modeling for such long-term operation optimization. To implement Monte Carlo Analysis for optimizing hybrid systems over the long term, assign probability distributions to the uncertain parameters. Then, run a series of simulations drawing random samples from these distributions to model a variety of operational scenarios along with the lifetime estimation method presented in this study. Analyze these results to guide decision-making and optimization, ensuring strategies account for the full range of potential uncertainties and their impacts on system performance.

Power Component ratings

This study employs fixed ratings for the PEMFC, Li-ion battery, and Diesel Generator components for the optimization of the hybrid energy system. To enhance the model's accuracy and ensure optimal component selection, it is possible to include components from various manufacturers, each with their unique performance characteristics. This approach allows for a more comprehensive evaluation and selection process, ensuring the best fit from the available options is chosen based on performance and integration capabilities.

Maintenance and component replacement costs

In this optimization study, during the lifetime estimation of the system, the maintenance and replacement costs of the power components have not been considered and are to be included into the model to get a comprehensive life-cycle cost analysis.

Fuel Storage Restrictions

In this study, the volume and weight storage restrictions of the hydrogen and Marine Gas Oil (MGO) storage have not been considered. Since the existing vessel is being operated on MGO already there would be no additional storage tanks needed to be built. The necessary modifications and volume and weight storage restrictions associated with incorporating liquefied hydrogen storage need to be included in the optimization model.

Operational Profile

A single operational profile has been used in this study with a sampling frequency of 5 minutes which was linearly interpolated to a time step $\Delta t = 1$ min. This has led to a smaller battery capacity in the PEMFC/LIB solution because the PEMFC stacks were able to handle the load transients. The results can be verified/improved by using the exact load profile of vessel with a smaller time steps, for example $\Delta t = 5$ seconds which leads to higher computational complexity. Therefore a balance needs to be achieved in terms of computational complexity and accuracy of the results. The smaller time steps might also lead to an increase in PEMFC degradation due to transient loading.

Additionally, since the general cargo vessel operates between different European Ports, different operational profiles need to be used to perform a sensitivity analysis in order to ensure that the obtained hybrid configuration is suitable.

Additional renewable technologies

This study was limited to PEMFC hybrid energy systems. But additional de-carbonization power sources can be included in the optimization model such as Solid Oxide Fuel Cells (SOFC) which have better combined heat and power efficiencies compared to PEMFC, different battery chemistries, Dual Fuel ICE etc..

Bibliography

[1] *Maritime Decarbonization Strategy 2022 | Mærsk Mc-Kinney Møller Center for Zero Carbon Shipping*, Dec. 2022. [Online]. Available: https://www.zerocarbonshipping.com/publications/maritime-decarbonization-strategy/.

[2] *Review of maritime transport 2022, United Nations conference on trade and development(UNCTAD)*, 2022. [Online]. Available: https://unctad.org/system/files/official-document/rmt2022_en.pdf.

[3] O. Z. Sharaf and M. F. Orhan, "An overview of fuel cell technology: Fundamentals and applications," *Renewable and sustainable energy reviews*, vol. 32, pp. 810–853, 2014. [Online]. Available: https://doi.org/10.1016/j.rser.2014.01.012.

[4] Z. Yan, J. L. Hitt, J. A. Turner, and T. E. Mallouk, "Renewable electricity storage using electrolysis," *Proceedings of the National Academy of Sciences*, vol. 117, no. 23, pp. 12 558–12 563, 2020.

[5] A. J. Appleby, "Fuel cell handbook," 1988.

[6] A. E. Lutz, R. S. Larson, and J. O. Keller, "Thermodynamic comparison of fuel cells to the carnot cycle," *International Journal of Hydrogen Energy*, vol. 27, no. 10, pp. 1103–1111, 2002. DOI: https://doi.org/10.1016/S0360-3199(02)00016-2.

[7] L. van Biert and K. Visser, "Fuel cells systems for sustainable ships," in *Sustainable Energy Systems on Ships*, Elsevier, 2022, pp. 81–121. DOI: https://doi.org/10.1016/B978-0-12-824471-5.00010-4.

[8] L. Van Biert, K. Mrozewski, and P. Hart, "Public final report: Inventory of the application of fuel cells in the maritime sector (fcmar)," *Maritime Knowledge Centre (MKC): London, UK*, 2021.

[9] J. Töpler, "Hydrogen as energy-storage-medium and fuel-a strong partner of renewable energies," *Renewable Energy and Environmental Sustainability*, vol. 1, p. 31, 2016.

[10] C. Dall'Armi, "Energy modelling and optimization of PEM fuel cells power plants in view of shipping decarbonization," 2023.

[11] P. Thounthong, V. Chunkag, P. Sethakul, B. Davat, and M. Hinaje, "Comparative study of fuel-cell vehicle hybridization with battery or supercapacitor storage device," *IEEE transactions on vehicular technology*, vol. 58, no. 8, pp. 3892–3904, 2009.

[12] R. Geertsma, R. Negenborn, K. Visser, and J. Hopman, "Design and control of hybrid power and propulsion systems for smart ships: A review of developments," *Applied Energy*, vol. 194, pp. 30–54, 2017.

[13] O. B. Inal, J.-F. Charpentier, and C. Deniz, "Hybrid power and propulsion systems for ships: Current status and future challenges," *Renewable and Sustainable Energy Reviews*, vol. 156, p. 111 965, 2022.

[14] M. Jaurola, A. Hedin, S. Tikkanen, and K. Huhtala, "Optimising design and power management in energy-efficient marine vessel power systems: A literature review," *Journal of Marine Engineering & Technology*, vol. 18, no. 2, pp. 92–101, 2019.

[15] D. Bosich, G. Giadrossi, S. Pastore, and G. Sulligoi, "Weighted bandwidth method for stability assessment of complex dc power systems on ships," *Energies*, vol. 15, no. 1, p. 258, 2021.

[16] R. Prenc, A. Cuculi, and I. Baumgartner, "Advantages of using a dc power system on board ship," *Pomorski zbornik*, vol. 52, no. 1, pp. 83–97, 2016.

[17] P. Wu and R. Bucknall, "Hybrid fuel cell and battery propulsion system modelling and multi-objective optimisation for a coastal ferry," *International journal of hydrogen energy*, vol. 45, no. 4, pp. 3193–3208, 2020. [Online]. Available: https://doi.org/10.1016/j.ijhydene.2019.11.152.

[18] A. Innes and J. Monios, "Identifying the unique challenges of installing cold ironing at small and medium ports–the case of aberdeen," *Transportation Research Part D: Transport and Environment*, vol. 62, pp. 298–313, 2018.

[19] J. E. Gutierrez-Romero, J. Esteve-Pérez, and B. Zamora, "Implementing onshore power supply from renewable energy sources for requirements of ships at berth," *Applied energy*, vol. 255, p. 113 883, 2019.

[20] M. E. Radwan, J. Chen, Z. Wan, T. Zheng, C. Hua, and X. Huang, "Critical barriers to the introduction of shore power supply for green port development: Case of djibouti container terminals," *Clean Technologies and Environmental Policy*, vol. 21, pp. 1293–1306, 2019.

[21] B. De Jager, T. Van Keulen, and J. Kessels, *Optimal control of hybrid vehicles*. Springer, 2013.

[22] *Hydrogen as a marine fuel - an introduction*. London, England: Society for Gas as a Marine Fuel, Feb. 2023, ISBN: 9781739870379.

[23] S. Lagouvardou, H. N. Psaraftis, and T. Zis, "A literature survey on market-based measures for the decarbonization of shipping," *Sustainability*, vol. 12, no. 10, p. 3953, 2020.

[24] E. A. Bouman, E. Lindstad, A. I. Rialland, and A. H. Strømman, "State-of-the-art technologies, measures, and potential for reducing ghg emissions from shipping–a review," *Transportation Research Part D: Transport and Environment*, vol. 52, pp. 408–421, 2017.

[25] IRENA, "A pathway to decarbonise the shipping sector by 2050," *International Renewable Energy Agency*, 2021.

[26] J. Faber, H. Wang, D. Nelissen, B. Russell, D. Amand, *et al.*, "Marginal abatement costs and cost effectiveness of energy-efficiency measures," *International Maritime Organization, London, UK*, 2011.

[27] H. Lindstad and G. S. Eskeland, "Low carbon maritime transport: How speed, size and slenderness amounts to substantial capital energy substitution," *Transportation Research Part D: Transport and Environment*, vol. 41, pp. 244–256, 2015.

[28] Z. L. Yang, D. Zhang, O. Caglayan, *et al.*, "Selection of techniques for reducing shipping nox and sox emissions," *Transportation Research Part D: Transport and Environment*, vol. 17, no. 6, pp. 478–486, 2012.

[29] D. Konovalov, E. Trushliakov, M. Radchenko, H. Kobalava, and V. Maksymov, "Research of the aerothermopressor cooling system of charge air of a marine internal combustion engine under variable climatic conditions of operation," in *Grabchenkos International Conference on Advanced Manufacturing Processes*, Springer, 2019, pp. 520–529.

[30] F. Tillig, W. Mao, and J. Ringsberg, "Systems modelling for energy-efficient shipping," Chalmers University of Technology, Tech. Rep., 2015.

[31] M. N. Nyanya, H. B. Vu, A. Schönborn, and A. I. Ölçer, "Wind and solar assisted ship propulsion optimisation and its application to a bulk carrier," *Sustainable Energy Technologies and Assessments*, vol. 47, p. 101 397, 2021.

[32] T. Chou, V. Kosmas, M. Acciaro, and K. Renken, "A comeback of wind power in shipping: An economic and operational review on the wind-assisted ship propulsion technology," *Sustainability*, vol. 13, no. 4, p. 1880, 2021.

[33] L. van Biert, M. Godjevac, K. Visser, and P. Aravind, "A review of fuel cell systems for maritime applications," *Journal of Power Sources*, vol. 327, pp. 345–364, 2016.

[34] T. Zis, R. J. North, P. Angeloudis, W. Y. Ochieng, and M. G. Harrison Bell, "Evaluation of cold ironing and speed reduction policies to reduce ship emissions near and at ports," *Maritime Economics & Logistics*, vol. 16, pp. 371–398, 2014.

[35] Y. Zhao, Y. Fan, K. Fagerholt, and J. Zhou, "Reducing sulfur and nitrogen emissions in shipping economically," *Transportation Research Part D: Transport and Environment*, vol. 90, p. 102 641, 2021.

[36] M. Lamas and C. Rodriguez, "Emissions from marine engines and nox reduction methods," *Journal of maritime research*, vol. 9, no. 1, pp. 77–81, 2012.

[37] M. H. Simonsen, E. Larsson, W. Mao, and J. W. Ringsberg, "State-of-the-art within ship weather routing," in *International Conference on Offshore Mechanics and Arctic Engineering*, American Society of Mechanical Engineers, vol. 56499, 2015, V003T02A053.

[38] T. P. Zis, H. N. Psaraftis, and L. Ding, "Ship weather routing: A taxonomy and survey," *Ocean Engineering*, vol. 213, p. 107 697, 2020.

[39] U. Eberle, M. Felderhoff, and F. Schueth, "Chemical and physical solutions for hydrogen storage," *Angewandte Chemie International Edition*, vol. 48, no. 36, pp. 6608–6630, 2009.

[40] Q. Lai, M. Paskevicius, D. A. Sheppard, *et al.*, "Hydrogen storage materials for mobile and stationary applications: Current state of the art," *ChemSusChem*, vol. 8, no. 17, pp. 2789–2825, 2015.

[41] A. Züttel, "Materials for hydrogen storage," *Materials today*, vol. 6, no. 9, pp. 24–33, 2003.

[42] I. T. Azkarate, H. A. L. Barthélémy, P. H. Hooker, *et al.*, "Research priority workshop on hydrogen safety," *Petten, Netherlands*, 2018.

[43] H. K. Shin and S. K. Ha, "A review on the cost analysis of hydrogen gas storage tanks for fuel cell vehicles," *Energies*, vol. 16, no. 13, p. 5233, 2023.

[44] H. Barthélémy, "Hydrogen storage–industrial prospectives," *International journal of hydrogen energy*, vol. 37, no. 22, pp. 17 364–17 372, 2012.

[45] D. Stolten and B. Emonts, *Hydrogen Science and Engineering, 2 Volume Set: Materials, Processes, Systems, and Technology*. John Wiley & Sons, 2016, vol. 1.

[46] H. Barthélémy, M. Weber, and F. Barbier, "Hydrogen storage: Recent improvements and industrial perspectives," *International Journal of Hydrogen Energy*, vol. 42, no. 11, pp. 7254–7262, 2017.

[47] Z. Wang, Y. Wang, S. Afshan, and J. Hjalmarsson, "A review of metallic tanks for h2 storage with a view to application in future green shipping," *International Journal of Hydrogen Energy*, vol. 46, no. 9, pp. 6151–6179, 2021.

[48] E. Rivard, M. Trudeau, and K. Zaghib, "Hydrogen storage for mobility: A review," *Materials*, vol. 12, no. 12, p. 1973, 2019.

[49] M. C. Galassi, D. Baraldi, B. A. Iborra, and P. Moretto, "Cfd analysis of fast filling scenarios for 70 mpa hydrogen type iv tanks," *International Journal of Hydrogen Energy*, vol. 37, no. 8, pp. 6886–6892, 2012.

[50] M. Heitsch, D. Baraldi, and P. Moretto, "Numerical investigations on the fast filling of hydrogen tanks," *International Journal of Hydrogen Energy*, vol. 36, no. 3, pp. 2606–2612, 2011.

[51] A. Bernardini, I. Lavagnini, C. DallArmi, *et al.*, "The reship project: Renewable energy for ship propulsion," in *Technology and Science for the Ships of the Future*, IOS Press, 2022, pp. 692–701.

[52] E. (EMSA), *Study on the use of fuel cells in shipping*, Jan. 2017. [Online]. Available: `https://www.emsa.europa.eu/publications/item/2921-emsa-study-on-the-use-of-fuel-cells-in-shipping.html`.

[53] L. Van Hoecke, L. Laffineur, R. Campe, P. Perreault, S. W. Verbruggen, and S. Lenaerts, "Challenges in the use of hydrogen for maritime applications," *Energy & Environmental Science*, vol. 14, no. 2, pp. 815–843, 2021.

[54] S. Z. Al Ghafri, S. Munro, U. Cardella, *et al.*, "Hydrogen liquefaction: A review of the fundamental physics, engineering practice and future opportunities," *Energy & environmental science*, vol. 15, no. 7, pp. 2690–2731, 2022.

[55] H. Central, *Kawasaki completes worlds first liquefied hydrogen receiving terminal [video]*, Jan. 2021. [Online]. Available: `https://hydrogen-central.com/kawasaki-completes-worlds-first-liquefied-hydrogen-receiving-terminal/`.

[56] J. W. Pratt, "Feasibility of the sf-breeze: A zero-emission hydrogen fuel cell high-speed passenger ferry.," Sandia National Lab.(SNL-CA), Livermore, CA (United States), Tech. Rep., 2017.

[57] N. M. CleanTech, "Norwegian future value chains for liquid hydrogen," *Report. URL: https://maritimecleantech.no/wp-content/uploads/2016/11/Report-liquid-hydrogen. pdf*, 2019.

[58] L. Klebanoff, J. Pratt, and C. LaFleur, "Comparison of the safety-related physical and combustion properties of liquid hydrogen and liquid natural gas in the context of the sf-breeze high-speed fuel-cell ferry," *International Journal of Hydrogen Energy*, vol. 42, no. 1, pp. 757–774, 2017.

[59] A. Habibic, *Worlds first liquid hydrogen bunkering facility for fuelling zero-emission ships revealed*, Nov. 2021. [Online]. Available: https://www.offshore-energy.biz/worlds-first-liquid-hydrogen-bunkering-facility-for-fuelling-zero-emission-ships-revealed/.

[60] F. Ustolin, A. Campari, and R. Taccani, "An extensive review of liquid hydrogen in transportation with focus on the maritime sector," *Journal of Marine Science and Engineering*, vol. 10, no. 9, p. 1222, 2022.

[61] C. DallArmi, D. Micheli, and R. Taccani, "Comparison of different plant layouts and fuel storage solutions for fuel cells utilization on a small ferry," *InternatIonal journal of hydrogen energy*, vol. 46, no. 26, pp. 13 878–13 897, 2021.

[62] A. Iulianelli and A. Basile, *Advances in hydrogen production, storage and distribution*. Elsevier, 2014.

[63] IEA, *Towards hydrogen definitions based on their emissions intensity*, Apr. 2023. [Online]. Available: https://www.iea.org/reports/towards-hydrogen-definitions-based-on-their-emissions-intensity.

[64] S&PGlobal, *Platts hydrogen price wall*. [Online]. Available: https://www.spglobal.com/commodityinsights/PlattsContent/_assets/_files/en/specialreports/energy-transition/platts-hydrogen-price-wall/index.html.

[65] D. McFarlane, D. Rodriguez, and E. Abramson, *The carbon intensity of hydrogen production*, Oct. 2022. [Online]. Available: https://www.carbonsolutionsllc.com/hydrogen-lca/.

[66] D. McFarlane, D. Rodriguez, and E. Abramson, *Hydrogen a climate solution*, Oct. 2022. [Online]. Available: https://www.carbonsolutionsllc.com/hydrogen-a-climate-solution/.

[67] B. Comer and L. Osipova, *Update: Accounting for well-to-wake carbon dioxide equivalent emissions in maritime transportation climate policies*, Aug. 2021. [Online]. Available: https://theicct.org/wp-content/uploads/2021/08/update-well-to-wake-co2-aug21-1.pdf.

[68] W. Grot, *Fluorinated ionomers*. William Andrew, 2011.

[69] B. V. Sasank, N. Rajalakshmi, and K. Dhathathreyan, "Performance analysis of polymer electrolyte membrane (pem) fuel cell stack operated under marine environmental conditions," *Journal of Marine Science and Technology*, vol. 21, pp. 471–478, 2016.

[70] W.-M. Yan, X.-D. Wang, S.-S. Mei, X.-F. Peng, Y.-F. Guo, and A. Su, "Effects of operating temperatures on performance and pressure drops for a 256 cm2 proton exchange membrane fuel cell: An experimental study," *Journal of Power Sources*, vol. 185, no. 2, pp. 1040–1048, 2008.

[71] A. Pietra, M. Gianni, N. Zuliani, S. Malabotti, and R. Taccani, "Experimental characterization of a pem fuel cell for marine power generation," in *E3S Web of Conferences*, EDP Sciences, vol. 334, 2022, p. 05 002.

[72] H. Q. Nguyen and B. Shabani, "Proton exchange membrane fuel cells heat recovery opportunities for combined heating/cooling and power applications," *Energy Conversion and Management*, vol. 204, p. 112 328, 2020.

[73] M. R. Islam, B. Shabani, G. Rosengarten, and J. Andrews, "The potential of using nanofluids in pem fuel cell cooling systems: A review," *Renewable and Sustainable Energy Reviews*, vol. 48, pp. 523–539, 2015.

[74] M. H. Bargal, M. A. Abdelkareem, Q. Tao, J. Li, J. Shi, and Y. Wang, "Liquid cooling techniques in proton exchange membrane fuel cell stacks: A detailed survey," *Alexandria Engineering Journal*, vol. 59, no. 2, pp. 635–655, 2020.

[75] Z. Du, C. Liu, J. Zhai, *et al.*, "A review of hydrogen purification technologies for fuel cell vehicles," *Catalysts*, vol. 11, no. 3, p. 393, 2021.

[76] J. Wu, X. Z. Yuan, J. J. Martin, *et al.*, "A review of pem fuel cell durability: Degradation mechanisms and mitigation strategies," *Journal of Power Sources*, vol. 184, no. 1, pp. 104–119, 2008.

[77] J. Péron, Y. Nedellec, D. J. Jones, and J. Roziére, "The effect of dissolution, migration and precipitation of platinum in nafionő-based membrane electrode assemblies during fuel cell operation at high potential," *Journal of Power Sources*, vol. 185, no. 2, pp. 1209–1217, 2008.

[78] L. Franck-Lacaze, C. Bonnet, E. Choi, *et al.*, "Ageing of pemfcs due to operation at low current density: Investigation of oxidative degradation," *international journal of hydrogen energy*, vol. 35, no. 19, pp. 10 472–10 481, 2010.

[79] T. Fletcher, R. Thring, and M. Watkinson, "An energy management strategy to concurrently optimise fuel consumption & pem fuel cell lifetime in a hybrid vehicle," *international journal of hydrogen energy*, vol. 41, no. 46, pp. 21 503–21 515, 2016.

[80] S. Zhang, X. Yuan, H. Wang, *et al.*, "A review of accelerated stress tests of mea durability in pem fuel cells," *International journal of hydrogen energy*, vol. 34, no. 1, pp. 388–404, 2009.

[81] G. Wang, F. Huang, Y. Yu, S. Wen, and Z. Tu, "Degradation behavior of a proton exchange membrane fuel cell stack under dynamic cycles between idling and rated condition," *International journal of hydrogen energy*, vol. 43, no. 9, pp. 4471–4481, 2018.

[82] S. Cleghorn, D. Mayfield, D. Moore, *et al.*, "A polymer electrolyte fuel cell life test: 3 years of continuous operation," *Journal of Power Sources*, vol. 158, no. 1, pp. 446–454, 2006.

[83] M. Mayur, M. Gerard, P. Schott, and W. G. Bessler, "Lifetime prediction of a polymer electrolyte membrane fuel cell under automotive load cycling using a physically-based catalyst degradation model," *Energies*, vol. 11, no. 8, p. 2054, 2018.

[84] C. Lorenzo, D. Bouquain, S. Hibon, and D. Hissel, "Synthesis of degradation mechanisms and of their impacts on degradation rates on proton-exchange membrane fuel cells and lithium-ion nickel–manganese–cobalt batteries in hybrid transport applications," *Reliability Engineering & System Safety*, vol. 212, p. 107 369, 2021.

[85] E. Brightman and G. Hinds, "In situ mapping of potential transients during start-up and shutdown of a polymer electrolyte membrane fuel cell," *Journal of Power Sources*, vol. 267, pp. 160–170, 2014.

[86] M. Yue, S. Jemei, R. Gouriveau, and N. Zerhouni, "Review on health-conscious energy management strategies for fuel cell hybrid electric vehicles: Degradation models and strategies," *International Journal of Hydrogen Energy*, vol. 44, no. 13, pp. 6844–6861, 2019.

[87] A. Kampker, H. Heimes, M. Kehrer, S. Hagedorn, P. Reims, and O. Kaul, "Fuel cell system production cost modeling and analysis," *Energy Reports*, vol. 9, pp. 248–255, 2023.

[88] FuelCellWorks, *Toyota motor corp.. to increase production capacity for fuel cell vehicles tenfold*, Nov. 2020. [Online]. Available: `https://fuelcellsworks.com/news/toyota-motor-corp-increase-production-capacity-for-fuel-cell-vehicles-tenfold/`.

[89] E. (EMSA), *Study on electrical energy storage for ships*, May 2020. [Online]. Available: `https://www.emsa.europa.eu/publications/item/3895-study-on-electrical-energy-storage-for-ships.html`.

[90] J. T. Frith, M. J. Lacey, and U. Ulissi, "A non-academic perspective on the future of lithium-based batteries," *Nature Communications*, vol. 14, no. 1, p. 420, 2023.

[91] B. University, *Bu-808: How to prolong lithium-based batteries*, Mar. 2022. [Online]. Available: `https://batteryuniversity.com/article/bu-808-how-to-prolong-lithium-based-batteries`.

[92] B. University, *BU-1003a: Battery Aging in an electric vehicle (EV)*, Aug. 2019. [Online]. Available: `https://batteryuniversity.com/article/bu-1003a-battery-aging-in-an-electric-vehicle-ev`.

[93] IEA, *Global EV Outlook 2023-catching up with climate ambitions*. Apr. 2023. [Online]. Available: `https://www.iea.org/reports/global-ev-outlook-2023`.

[94] M. Hannan, S. Wali, P. Ker, *et al.*, "Battery energy-storage system: A review of technologies, optimization objectives, constraints, approaches, and outstanding issues," *Journal of Energy Storage*, vol. 42, p. 103 023, 2021.

[95] B. University, *Bu-216: Summary table of lithium-based batteries*, Dec. 2021. [Online]. Available: https://batteryuniversity.com/article/bu-216-summary-table-of-lithium-based-batteries.

[96] P. Miller, "State of the art and future developments in lithiumion battery packs for passenger car applications united kingdom," *Johnson Matthey Technol. Rev*, vol. 59, pp. 4–13, 2015.

[97] H. K. Fathy, J. A. Reyer, P. Y. Papalambros, and A. Ulsov, "On the coupling between the plant and controller optimization problems," in *Proceedings of the 2001 American Control Conference.(Cat. No. 01CH37148)*, IEEE, vol. 3, 2001, pp. 1864–1869.

[98] E. Silvas, T. Hofman, N. Murgovski, L. P. Etman, and M. Steinbuch, "Review of optimization strategies for system-level design in hybrid electric vehicles," *IEEE Transactions on Vehicular Technology*, vol. 66, no. 1, pp. 57–70, 2016.

[99] A. Panday and H. O. Bansal, "A review of optimal energy management strategies for hybrid electric vehicle," *International Journal of Vehicular Technology*, vol. 2014, 2014.

[100] A. Ritari, J. Huotari, and K. Tammi, "Marine vessel powertrain design optimization: Multiperiod modeling considering retrofits and alternative fuels," *Proceedings of the Institution of Mechanical Engineers, Part M: Journal of Engineering for the Maritime Environment*, p. 14 750 902 221 145 747, 2023.

[101] F. Baldi, S. Brynolf, and F. Maréchal, "The cost of innovative and sustainable future ship energy systems," *ECOS*, 2019.

[102] O. Balland, S. O. Erikstad, and K. Fagerholt, "Concurrent design of vessel machinery system and air emission controls to meet future air emissions regulations," *Ocean Engineering*, vol. 84, pp. 283–292, 2014.

[103] N. L. Trivyza, A. Rentizelas, and G. Theotokatos, "A novel multi-objective decision support method for ship energy systems synthesis to enhance sustainability," *Energy Conversion and Management*, vol. 168, pp. 128–149, 2018.

[104] J. Zhu, L. Chen, B. Wang, and L. Xia, "Optimal design of a hybrid electric propulsive system for an anchor handling tug supply vessel," *Applied energy*, vol. 226, pp. 423–436, 2018.

[105] K. Deb, A. Pratap, S. Agarwal, and T. Meyarivan, "A fast and elitist multiobjective genetic algorithm: Nsga-ii," *IEEE transactions on evolutionary computation*, vol. 6, no. 2, pp. 182–197, 2002.

[106] C. C. Coello and M. S. Lechuga, "Mopso: A proposal for multiple objective particle swarm optimization," in *Proceedings of the 2002 Congress on Evolutionary Computation. CEC'02 (Cat. No. 02TH8600)*, IEEE, vol. 2, 2002, pp. 1051–1056.

[107] A. Dolatabadi and B. Mohammadi-Ivatloo, "Stochastic risk-constrained optimal sizing for hybrid power system of merchant marine vessels," *IEEE Transactions on Industrial Informatics*, vol. 14, no. 12, pp. 5509–5517, 2018.

[108] Z. Wang, L. Chen, F. Guo, and B. Wang, "Optimal design of hybrid electric propulsive system for a mini polar cruise," in *The 31st International Ocean and Polar Engineering Conference*, OnePetro, 2021.

[109] X. Bao, X. Xu, Y. Zhang, Y. Xiong, and C. Shang, "Optimal sizing of battery energy storage system in a shipboard power system with considering energy management optimization," *Discrete Dynamics in Nature and Society*, vol. 2021, pp. 1–12, 2021.

[110] A. Prasanthi, H. Shareef, M. Asna, A. A. Ibrahim, and R. Errouissi, "Optimization of hybrid energy systems and adaptive energy management for hybrid electric vehicles," *Energy Conversion and Management*, vol. 243, p. 114 357, 2021.

[111] X. Wang, U. Shipurkar, A. Haseltalab, H. Polinder, F. Claeys, and R. R. Negenborn, "Sizing and control of a hybrid ship propulsion system using multi-objective double-layer optimization," *Ieee Access*, vol. 9, pp. 72 587–72 601, 2021.

[112] S. Karagiorgis, S. Nasiri, and H. Polinder, "Implementation of ship hybridisation: Sizing a hybrid crew transfer vessel considering uncertainties," in *Proceedings of the International Naval Engineering Conference*, vol. 16, 2022, p. 49.

[113] D. Pivetta, C. DallArmi, and R. Taccani, "Multi-objective optimization of hybrid pemfc/li-ion battery propulsion systems for small and medium size ferries," *International Journal of Hydrogen Energy*, vol. 46, no. 72, pp. 35 949–35 960, 2021.

[114] S. Xie, X. Hu, Q. Zhang, X. Lin, B. Mu, and H. Ji, "Aging-aware co-optimization of battery size, depth of discharge, and energy management for plug-in hybrid electric vehicles," *Journal of power sources*, vol. 450, p. 227 638, 2020.

[115] A. Haseltalab, L. van Biert, H. Sapra, B. Mestemaker, and R. R. Negenborn, "Component sizing and energy management for sofc-based ship power systems," *Energy Conversion and Management*, vol. 245, p. 114 625, 2021.

[116] F. Baldi, L. Wang, M. Pérez-Fortes, and F. Maréchal, "A cogeneration system based on solid oxide and proton exchange membrane fuel cells with hybrid storage for off-grid applications," *Frontiers in Energy Research*, vol. 6, p. 139, 2019.

[117] F. Baldi, S. Moret, K. Tammi, and F. Maréchal, "The role of solid oxide fuel cells in future ship energy systems," *Energy*, vol. 194, p. 116 811, 2020.

[118] M. Yoo, L. Lessard, M. Kermani, and F. Maréchal, "Osmose lua: A unified approach to energy systems integration with life cycle assessment," in *12th International conference PSE 2015 and 25th International conference ESCAPE*, vol. 2015, 2015, pp. 6–9.

[119] S. Sukumar, M. Marsadek, A. Ramasamy, and H. Mokhlis, "Grey wolf optimizer based battery energy storage system sizing for economic operation of microgrid," in *2018 IEEE International Conference on Environment and Electrical Engineering and 2018 IEEE Industrial and Commercial Power Systems Europe (EEEIC/I&CPS Europe)*, IEEE, 2018, pp. 1–5.

[120] M. Li, L. Wang, Y. Wang, and Z. Chen, "Sizing optimization and energy management strategy for hybrid energy storage system using multiobjective optimization and random forests," *IEEE Transactions on Power Electronics*, vol. 36, no. 10, pp. 11 421–11 430, 2021.

[121] D. Stapersma, "Diesel engines, volume 1: Performance analysis," *Royal Netherlands Naval College*, 2002.

[122] G. A. Livanos, G. Theotokatos, and D.-N. Pagonis, "Techno-economic investigation of alternative propulsion plants for ferries and roro ships," *Energy Conversion and Management*, vol. 79, pp. 640–651, 2014.

[123] EAS, *Easy marine 80ah lfp battery module*. [Online]. Available: `https://eas-batteries.com/system/files/attachments/Data%20sheet%20EASy%20Marine%20rev.3.2_2.pdf`.

[124] ZEPP.SOLUTIONS, *Zepp.x150: Ultra high power density fuel cell system (150kw)*, Oct. 2022. [Online]. Available: `https://zepp.solutions/en/x150/`.

[125] Wartsila, *Wärtsilä 20 product guide*. [Online]. Available: `https://www.wartsila.com/marine/products/engines-and-generating-sets/diesel-engines/wartsila-20`.

[126] C. DallArmi, D. Pivetta, and R. Taccani, "Health-conscious optimization of long-term operation for hybrid pemfc ship propulsion systems," *Energies*, vol. 14, no. 13, p. 3813, 2021.

[127] *Mixed integer programming (mip) programming-a primer for basics*, Aug. 2023. [Online]. Available: `https://www.gurobi.com/resources/mixed-integer-programming-mip-a-primer-on-the-basics/`.

[128] Nedstack, *PRODUCT DATA SHEET FCS 3-XXL Gen 2.9*, Jul. 2022. [Online]. Available: `https://nedstack.com/sites/default/files/2022-07/nedstack-fcs-13-xxl-gen-2.9-datasheet-rev01.pdf`.

[129] B. Gundogdu and D. T. Gladwin, "A fast battery cycle counting method for grid-tied battery energy storage system subjected to microcycles," in *2018 International Electrical Engineering Congress (iEECON)*, IEEE, 2018, pp. 1–4.

[130] H. Ali, H. Beltran, N. J. Lindsey, and M. Pecht, "Assessment of the calendar aging of lithium-ion batteries for a long-termspace missions," *Frontiers in Energy Research*, vol. 11, p. 1 108 269, 2023.

[131] J. Zhang, *PEM fuel cell electrocatalysts and catalyst layers: fundamentals and applications*. Springer Science & Business Media, 2008. [Online]. Available: `https://doi.org/10.1007/978-1-84800-936-3`.

[132] L. Balestra and I. Schjølberg, "Modelling and simulation of a zero-emission hybrid power plant for a domestic ferry," *International Journal of Hydrogen Energy*, vol. 46, no. 18, pp. 10 924–10 938, 2021.

[133] T. S. Schmidt, M. Beuse, X. Zhang, *et al.*, "Additional emissions and cost from storing electricity in stationary battery systems," *Environmental science & technology*, vol. 53, no. 7, pp. 3379–3390, 2019.

[134] T. Terlouw, T. AlSkaif, C. Bauer, and W. Van Sark, "Multi-objective optimization of energy arbitrage in community energy storage systems using different battery technologies," *Applied energy*, vol. 239, pp. 356–372, 2019.

[135] J. Groot, *State-of-health estimation of Li-ion batteries: Ageing models*. Chalmers Tekniska Hogskola (Sweden), 2014.

[136] Ship and Bunker, *Rotterdam bunker prices*. [Online]. Available: `https://shipandbunker.com/prices/emea/nwe/nl-rtm-rotterdam#MGO`.

[137] TNO, *Tno power-2-fuel cost analysis - smartport*, Sep. 2020. [Online]. Available: `https://smartport.nl/wp-content/uploads/2020/09/Cost-Analysis-Power-2-Fuel_def_2020.pdf`.

[138] A. Mengden, *Carbon taxes in europe*, Oct. 2023. [Online]. Available: `https://taxfoundation.org/data/all/eu/carbon-taxes-in-europe-2023/#timeline`.

[139] *Ember. (January 4, 2024). Average monthly electricity wholesale price in the Netherlands from January 2019 to December 2023 (in euros per megawatt-hour) [Graph]. In Statista*, en, Accessed: 2023-01-15. [Online]. Available: `https://www-statista-com.tudelft.idm.oclc.org/statistics/1314549/netherlands-monthly-wholesale-electricity-price/`.

[140] H. Yumiya, M. Kizaki, and H. Asai, "Toyota fuel cell system (tfcs)," *World Electric Vehicle Journal*, vol. 7, no. 1, pp. 85–92, 2015.

[141] L. Micoli, T. Coppola, and M. Turco, "A case study of a solid oxide fuel cell plant on board a cruise ship," *Journal of Marine Science and Application*, vol. 20, no. 3, pp. 524–533, 2021.

A

Research Paper

Design and Operation Optimization of Hybrid Energy Systems for a General Cargo Vessel: WTW Emission Analysis and Plant Lifetime Estimation

Arun Datta Beeravelli [a], Foivos Mylonopoulos [a], Andrea Coraddu [a], Henk Polinder [a],

[a] *Department of Maritime and Transport Technology, Delft University of Technology, Mekelweg 2, 2628 CD, Delft, Zuid Holland, The Netherlands*

Abstract

The International Maritime Organization (IMO) has set out to cut emissions from shipping to net zero by 2050. One of the key technologies in reducing the shipping emissions is the PEMFC hybrid energy systems. PEMFC fuelled by hydrogen is operationally a zero emission solution. A key issue is the production emission intensity of the hydrogen both from fossil and non-fossil sources. The current study aims to optimize the design and operation of a general cargo vessel using a Mixed-Integer Linear programming (MILP) approach considering the emission intensities of the fuels for two hybrid energy systems: (i) PEMFC/LIB, and (ii)DG/PEMFC/LIB to analyse the cost and emission trade-offs. The configurations of both hybrid systems do not vary across all the grades of hydrogen and the DG/PEMFC/LIB hybrid system is 62.8% less expensive than the PEMFC/LIB configuration. In the PEMFC/LIB system the use of electrolytic hydrogen leads to a OPEX increase of 137%. SMR+CCS leads to an emission reduction of 85% with a OPEX increase of 27%. The maximum emission reduction possible is 24% using electrolytic hydrogen with an OPEX increase of 30% in the DG/PEMFC/LIB system. The other major problem is the estimated lifetime of the fuel cell and battery components. A hierarchical multi-objective operation optimization is set up considering the PEMFC degradation and OPEX . For the degradation of the PEMFC, a stack voltage degradation model is used and for the battery both the calendar and cycling aging impacts are considered. The estimated lifetime of the PEMFC has been increased to 42 months in the DG/PEMFC/LIB solution with the battery lasting 26 months.

Key words: Hybrid Energy System, Mixed Integer Linear Programming (MILP), Li-ion batteries (LIB), Proton Exchange Membrane Fuel Cell (PEMFC), Degradation, Well-to-Wake (WTW) emissions

1 Introduction

The Global Shipping industry is responsible for transporting 90% of global commerce and is responsible for 3% if global green house gas emissions. The International Maritime Organization(IMO) has set out to cut annual greenhouse gas emissions from international shipping by 40% by 2030 and to reach net zero by 2050.

Fuel cell technologies are proposed as alternative power systems to help decarbonize the shipping industry. In particular low temperature-Proton exchange membrane fuel cells (LT-PEMFC) are the most mature technology for shipping applications with advantages such as better transient loading capabilities, quick start-up/shut-down times and good power densities [1], [2]. PEMFC are usually coupled with electrical energy storage systems (EESS) such as batteries into hybrid power trains to improve the system response to load changes and allow the PEMFC to operate in the best of load conditions to reduce stresses on the membrane to reduce the degradation [3], [4]. The power systems can be connected in series, parallel, or series-parallel hybrid if an internal combustion engines (ICE) is also considered [5], [6]. The advantages of hybrid energy systems along with emission reduction, reliability and redundancy are the transient load response, adaptation to various operation modes, reduction in fuel consumption, and reduced noise and vibrations [7].

LT-PEMFC are fuelled exclusively by hydrogen, which operationally is a zero emission solution since the only output is water. A key issue is the production emission intensity of the hydrogen. At the end of 2021, almost 47% of global hydrogen production is from natural gas, 27% from coal, 22% from oil, and only 4% from electrolysis. with 33% of the electricity produced worldwide being renewable, less that 1% of global hydrogen produced worldwide using electrolysis is considered green [8]. It is important to consider the production emissions of hy-

drogen during design stage of the hybrid energy system to provide a holistic view to the vessel owner and aid in decision making.

Another key factor affecting the decision making ability of vessel owners in the adoption of PEMFC hybrid energy systems is the expected plant lifetime due to the degradation of the installed PEMFC and battery systems and increase in hydrogen consumption due to the reduced efficiency of the PEMFC stack.

1.1 System Level design of hybrid power plants

Having more than one source of power, hybrid powertrains give birth to a large design space for the physical system and increase the complexity of the control algorithm. The coupling (dependence) between the parameters of the physical system (e.g., topology) and the parameters of the control algorithm transforms the problem into a multilevel problem that, if solved sequentially, is by definition sub-optimal [9]. Therefore, the physical system and the control algorithm should be designed in an integrated manner to obtain an optimal system design [10]. For the plant design and control problem, there are three coordination architectures as listed below.

- alternating plant and control design, i.e., first, the plant is optimally designed. Using this outcome, the controller is optimally designed. Subsequently, the plant is optimized again, etc. The coordinator alternates between optimizing the plant and optimizing the control until the coupled variables have converged;
- control design nested within plant design, i.e., every evaluation of a plant requires the full optimization of the controller design;
- simultaneous plant and controller design (i.e., solving (2) all in one).

the control strategies for energy management of hybrid vehicles can be categorized into two, namely rule based and optimization based [11]. Rule-based control strategies are fundamental control schemes that depend on mode of operation. They can be easily implemented with real-time supervisory control to manage the power flow in a hybrid drive train. The rules are determined based on human intelligence, heuristics, or mathematical models and generally without prior knowledge of a drive cycle [11]. In optimization based control strategies, the goal of a controller is to minimize the cost function. The cost function (objective function) for an HEV may include the emission, fuel consumption, and torque depending on the application. The optimization can be either be global or real time [11].

1.2 Optimization studies

Baldi, Brynolf, and Maréchal's study used a MILP model to analyze the cost of reducing GHG emissions in maritime vessels. They found that reducing emissions by up to 75% would cost 50-70% more than the IMO's targets. Full de-carbonization could raise costs by 280-340% over business as usual scenario. Retrofits were not considered [12]. In [13], a model for concurrent optimization of machinery system design and emission control installation was developed. Interactions and compatibility issues between controls and between controls and machinery systems have been taken into consideration. Satisfying power demand at all time and complying with emission regulations were modeled as main constraints while the solution was driven by costs.

For the sizing optimization of anchor handling tug supply vessel, Zhu, Chen, Wang, *et al.* used NSGA-II (introduced by Deb, Pratap, Agarwal, *et al.*) to search the design space. In this study the optimization was done for a Diesel ICE-Battery hybrid system in which shore power was used to charge the battery. The pareto solutions of NSGA-II are compared against (multi-objective particle swarm optimization) MOPSO[16], the solutions generated by NSGA-II solutions were less distributed [14]. In [14], the outer search space for component sizing uses Multiobjective particle swarm optimization(MOPSO), and in the inner layer of control for energy management uses AECMS(adaptive equivalent consumption minimization strategy). Real time HIL tests were also conducted for this study to test the effectiveness of the optimization. the optimal solution of the proposed methods was also found to be significantly superior to single-level optimizations.

Dolatabadi and Mohammadi-Ivatloo present a risk-based stochastic model for determining the optimal sizing of a hybrid PV/diesel/storage power system for merchant marine vessels. It considers the influence of solar radiation intermittency and utilizes a scenario reduction technique to reduce computational complexity, balancing the expected cost of system sizing with the risk of high costs in worse scenarios using the CVaR methodology [17]. In [18], Wang, Chen, Guo, *et al.* propose a hybrid diesel engine/battery/shore power propulsive system for a polar cruise and a tri-objective optimization considering annual fuel consumption, lifecycle cost and annual pure electric time is carried out. The results show that 0.27% fuel reduction and 37.48% annual pure electric time are gained by sacrificing 7.85% lifecycle cost compared with the conventional diesel electric propulsive system. In [19], Bao, Xu, Zhang, *et al.* use Mixed integer quadratic programming (MIQP), for energy storage system (ESS) sizing and power system scheduling optimization which are simultaneously conducted.

Wang, Shipurkar, Haseltalab, *et al.* developed a nested plant and control design architecture for a PEMFC-ICE-Battery hybrid vessel. In the external plant design optimization layer, NSGA-II multi-objective optimization was used to reduce CAPEX, OPEX and emissions by varying the size of components. In the inner layer MILP

was used to design the optimal control strategy to minimize OPEX based on the size of the components generated by the NSGA-II algorithm [20]. This study was further extended by Karagiorgis, Nasiri, and Polinder to include uncertainty of fuel and electricity prices into the model for retrofitting a vessel [21].

For the PEMFC and battery hybridization of a coastal ferry Wu and Bucknall used a similar nested optimization architecture, where in the external layer, MILP was used in minimization of emissions and cost. The component sizes generated in the external layer are passed from the outer layer into the inner layer for the optimization of energy management (power split) to reduce costs, which was done using deterministic dynamic programming (DDP). In this study the degradation effects of the PEMFC and battery are also modelled [22]. In [23], Pivetta, Dall'Armi, and Taccani considered the performance degradation of PEM fuel cells in the multi-objective optimization problem using MILP. The proposed algorithm resulted in a 65% reduction in fuel cell degradation, but an increase of battery capacity by 136%. In [24], battery degradation effects were considered in the sizing optimization.

2 Case Study

A short sea general cargo vessel ANKIE has been chosen for this study. General cargo or multi-purpose vessels are designed for flexibility and carry a huge variety of cargo. The vessel operates between multiple European Ports, and a single power profile has been acquired for the vessel operating between the Netherlands and Finland. The key characteristics of the vessel are listed in the table 1.

Table 1
Main Characteristics of ANKIE General Cargo Vessel

Parameter	**Value**
Name	ANKIE
Build year	2007
Engine	Wartsila 9L20, 1.8MW @ 1000RPM
Propeller Type	Controllable Pitch Propeller
Length × Width	89.9 m × 12.5 m
Dead Weight Tonnage (DWT)	3638 T
MGO Tank Capacity	285 m^3
Engine Room Volume	465 m^3
Speed	10.5 knots

The power profile of the vessel is shown in the figure 1. The vessel starts travelling on 16-April-2022 in the morning 07:20, and ends its journey on 20-April-2022 at 13:20. The total duration of the trip is 102 hours and the original load profile of the ship has been acquired with a sampling period of 5 minutes. The load profile has been linearly interpolated to a sampling period of 1 minute intervals for better accuracy. Across the entire length of the trip the vessel consumes 19.7 tonnes of Marine Gas Oil(MGO).

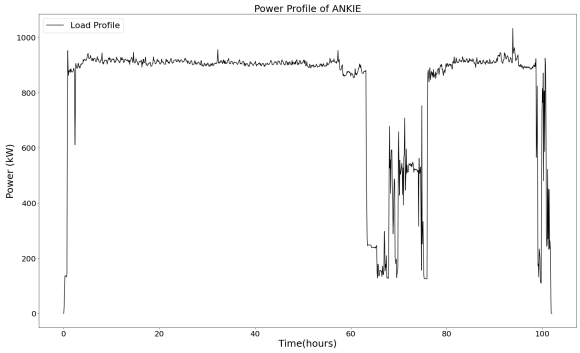

Fig. 1. Propulsive power demand of the general cargo vessel ANKIE chosen as case study for the PEMFC hybrid energy system

2.1 *Proposed hybrid configurations*

In this study two hybrid energy systems in series configuration are proposed for a general cargo vessel: (i) PEMFC/LIB, and (ii) DG/PEMFC/LIB. The cost and emission trade-off's against various grades of hydrogen and the estimated lifetime of the installed PEMFC and LFP battery components are evaluated for both the configurations.

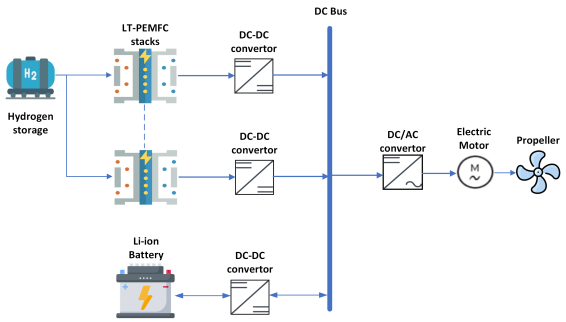

Fig. 2. PEMFC/LIB hybrid energy system

In this study LFP chemistry has been chosen due to it's safety that is required for Maritime applications. EASy Marine®80Ah LFP Battery Module has been selected [25]. PEMFC stacks of 150kW rated power from ZEPP solutions are considered for this study [26]. Liquefied hydrogen is considered due to its better storage energy density. For the selection of the diesel generator, the current OEM of the installed ICE-Wartsila has been chosen, and using the engine configurator tool on the website, a 50Hz, MGO fuelled, IMO Tier 3 diesel generator has been selected. From the options provided, the smallest Diesel generator has been selected which is the Wartsila 4L20 [27].

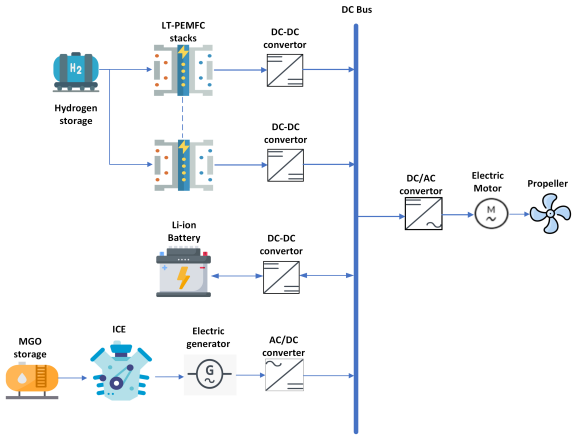

Fig. 3. DG/PEMFC/LIB hybrid energy system

3 Methodology and Modelling

This thesis draws from the scholarly contributions of Pivetta, Dall'Armi, and Taccani, serving as a crucial framework for the exploration and analysis presented herein [23], [28], [29].

The methodology has been developed in different optimization phases. Firstly a deterministic design and operation MILP optimization has been run in-order to determine the optimal sizes of the energy conversion and storage units of the energy systems and their optimal operation over a single trip along with the emission analysis across various grades of hydrogen. Afterwards, a further operation optimization has been performed consecutively taking into account the performance degradation of the PEMFC and LIB installed until the end of life is reached.

In 3.1, 3.2 the two methodology phases (i.e. the two optimization problems) are described, with particular reference to the objective function(s) of the problems, the main constraints describing the components operation, and the ones setting the energy system power balances and limits on the volume of the engine room.

3.1 Stage 1: Design optimization and emission analysis across various grades of Hydrogen

The first phase of the optimization is aimed at determining the optimal size of the energy conversion and storage units, along with the emission and cost analysis for the various grades of hydrogen that are available. To design the hybrid energy system configuration, the entire system operation is optimized for a single trip (figure 1).

A single objective optimization has been set to define the optimal design and operation of the hybrid propulsion system that allows for the minimization of total costs.

Since there are two different types of hybrid energy systems that are being designed, this subsection is further split into two: (i) PEMFC/LIB hybrid energy system, and (ii) DG/PEMFC/LIB hybrid energy system.

3.1.1 (i) PEMFC/LIB hybrid system

In the equation 1, representing the objective of total cost, $E_{battmax}$ represents the required battery capacity, C_{batt} is the cost of batteries per kWH, n_{FC} is the number of installed PEMFC stacks of rated power P_{fcmax} and cost C_{FC}. F_{it}^{FC} is the amount of hydrogen consumed by the i^{th} PEMFC stack at time t, and C_{H2} is the cost of different grades of hydrogen per kg. The hydrogen consumed is subject to carbon tax according to EU ETS (CO_2tax), and the cost of using liquefied hydrogen is also included in the objective function (C_{liqH2}). The objective function also consists of the costs of liquefied hydrogen storage (C_S^{LH2}) which is part of the CAPEX. The final part of the objective function is the cost (C_{elec}) of shore charging the installed battery.

$$\underset{\mathbf{n}_{fc},\mathbf{n}_{batt},\mathbf{P}_{it}^{FC},\mathbf{P}_{t}^{batt\pm}}{\text{Minimize}} \quad \mathbf{J}(\mathbf{n}_{fc},\mathbf{n}_{batt},\mathbf{P}_{it}^{FC},\mathbf{P}_{t}^{batt\pm}) =$$
$$E_{battmax}\cdot C_{batt} + n_{FC}\cdot P_{fcmax}\cdot C_{FC} + \sum_{i\in I}\sum_{t\in T} F_{it}^{FC}\cdot C_S^{LH2}$$
$$+\sum_{i\in I}\sum_{t\in T} F_{it}^{FC}\cdot (C_{H2} + CO_{2eq}^{H_2}\cdot CO_{2tax} + C_{liqH2})$$
$$+0.8\cdot E_{battmax}\cdot C_{elec}\cdot \frac{1}{\eta_{batt}} \tag{1}$$

PEMFC stacks model
The equations 2 to 9 describe the behavior of the PEMFC stacks, at each time step t. The fuel consumption of the stack is contingent upon the current density of an individual cell within the PEMFC stack, and concurrently, the power output of the fuel cell stack is also reliant on the current density of the individual cells in the PEMFC stack. The relation between H_2 consumption vs current density vs output power is drawn from the commercial products for reference [30], [26].

Equation 2 refers to amount of hydrogen consumed at each time step t for the i^{th} stack as a function of the current density of an individual cell by means of the linearization coefficients k_{1f}andk_{2f}. $\delta_{it}^{FC}$and δ_{it}^{stup} are the binary variables that describe the on/off status of the i^{th} PEMFC stack and the startup of the PEMFC stack. F_{start} is the additional hydrogen consumption due to the start up of the PEMFC stack, which is assumed to be 10% of the consumption at the maximum rated power (F_{max}^{fc}) [23]. In equation 3, the power output of the PEMFC stack is related to the current density with the linearization coefficients $k_{1p}$and k_{2p}. The upper and

lower limits of current density of the i^{th} stack are shown in equation 4. The binary variable x_i^{FC} in equations 4 and 5 expresses the inclusion of the i^{th} stack in the optimal system configuration. The sum of such variables x_i^{FC} defines the number of PEMFC stacks n_{FC} that should be included in the system (Equation 5).

The equation 6 limits the power generated by the i^{th} PEMFC stack in order to not exceed the minimum (k_{fcmin}) and maximum (k_{fcmax}) power load, expressed as a percentage of the rated power of the stack P_{fcmax}. The binary variable δ_{it}^{FC} in equation 6 is multiplied with the upper and lower power limits of the stack to ensure that the stack operates between the given limits, or is switched off. At each time step, the load variation cannot exceed the maximum value Δ_{PFC} as reported in equation 7. The equation 8 is used to determine the number of start up phases that have occurred for the i^{th} PEMFC stack, i.e. $\sum \delta_{it}^{stup}$. The final equation 9 ensures that all the selected stacks deliver the same power at each time step.

$$F_{it}^{FC} = k_{1f} \cdot I_{it}^{FC} + k_{2f} \cdot \delta_{it}^{FC} + \delta_{it}^{stup} \cdot F_{start} \cdot F_{max}^{fc} \qquad \forall i \in I \qquad \forall t \in T \tag{2}$$

$$P_{it}^{fc} = k_{1p} \cdot I_{it}^{FC} + k_{2p} \cdot \delta_{it}^{FC} \qquad \forall i \in I \qquad \forall t \in T \tag{3}$$

$$I_{fcmin} \cdot x_i^{FC} \leq I_{it}^{FC} \leq I_{fcmax} \cdot x_i^{FC} \qquad \forall i \in I \qquad \forall t \in T \tag{4}$$

$$\sum_{i \in I} x_i^{FC} = n_{FC} \tag{5}$$

$$k_{fcmin} \cdot P_{fcmax} \cdot \delta_{it}^{FC} \leq P_{it}^{FC} \leq k_{fcmax} \cdot P_{fcmax} \cdot \delta_{it}^{FC} \qquad \forall i \in I \qquad \forall t \in T \tag{6}$$

$$\Delta_{PFC} \geq |P_{it}^{FC} - P_{i,t-1}^{FC}| \qquad \forall i \in I \qquad \forall t \in range(1, len(T)) \tag{7}$$

$$0 \leq \delta_{it}^{FC} - \delta_{i,t+1}^{FC} + \delta_{it}^{stup} \qquad \forall i \in I \qquad \forall t \in range(len(T) - 1) \tag{8}$$

$$P_{it}^{FC} = P_{1t}^{FC} \cdot x_i^{FC} \qquad \forall i \in I \qquad \forall t \in T \tag{9}$$

The equation 9 contains the product of a continuous and binary variable making the problem non-linear. To ensure that the formulation remains linear, big M method is used to replace equation 9 and the following equations have been introduced.

$$P_{it}^{FC} \leq M \cdot x_i^{FC} \qquad \forall i \in I \qquad \forall t \in T \tag{10}$$

$$P_{it}^{FC} \leq P_{1t}^{FC} \qquad \forall i \in I \qquad \forall t \in T \tag{11}$$

$$P_{it}^{FC} \geq P_{1t}^{FC} - (1 - x_i^{FC}) \cdot M \qquad \forall i \in I \qquad \forall t \in T \tag{12}$$

$$P_{it}^{FC} \geq 0 \qquad \forall i \in I \qquad \forall t \in T \tag{13}$$

Li-ion Battery Model

For the LFP battery, equations 14 to 18 define its operation at each time step t. The equation 14 defines the energy stored in the battery E_t^{batt} at each time step t as a function of the charging and discharging energy efficiency η_{batt}, the output power of the battery P_t^{batt+} and the input power of the battery P_t^{batt-}. To limit the complexity of the optimization model, the charging/discharging efficiency (η_{batt}) is set to be constant at varying C-rate (i.e. the ratio between the power output/input and the battery capacity $E_{battmax}$). Equation 15 ensures that the battery charge and discharge power do not exceed the maximum allowable C-rate. In equation 16 at each time step the energy stored in the battery cannot exceed the limits set on the maximum SOC, i.e. the ratio between the energy stored at time t (E_t^{batt}) and the installed battery capacity $E_{battmax}$ (eq. **??**). The battery is assumed to be charged to 80% of it maximum capacity at the start of the trip using shore charging (equation 17). The equation 18 is the number of individual battery modules that are required to be installed.

$$E_t^{batt} = E_{t-1}^{batt} + (\eta_{batt} \cdot P_t^{batt-} - \frac{1}{\eta_{batt}} \cdot P_t^{batt+}) \cdot \Delta t \qquad \forall t \in T \tag{14}$$

$$P_t^{batt\pm} \leq |C_{ratemax} \cdot E_{battmax}| \qquad \forall t \in T \tag{15}$$

$$SOC_{min} \cdot E_{battmax} \leq E_t^{batt} \leq SOC_{max} \cdot E_{battmax} \qquad \forall t \in T \tag{16}$$

$$SOC_0 = 0.8 \tag{17}$$

$$E_{battmax} = n_{batt} \cdot E_{module} \tag{18}$$

Energy system constraints
To ensure that the energy system fulfills the power demand of the vessel $Load_t$ at each time step, the power balance equation 19 is set as a constraint in the optimization. An additional constraint has been setup in equation 20 to ensure that the alternative power system optimal design identified by solving the optimization model does not exceed the volume V_{ENG} of the currently installed power system(table 1). V_{FC} is the specific volume of the PEMFC stacks and V_{batt} is the specific volume of the LFP battery. An acceptable correction factor C_{ov} has also been introduced to account for the current limited state of development of FC systems [23].

$$\sum_{i\in I} P_{it}^{FC} + P_t^{batt+} = Load_t + P_t^{batt-} \qquad \forall t \in T \tag{19}$$

$$n_{FC} \cdot P_{fcmax} \cdot V_{FC} + E_{battmax} \cdot V_{batt} \leq V_{ENG} \cdot (1 + C_{ov}) \tag{20}$$

3.1.2 (ii) DG/PEMFC/LIB hybrid energy system

The objective function is similar to the one mentioned in equation 1, but is modified slightly with the addition of factors related to the installation of the Diesel Generator. n_{DG} is the number of installed diesel generators of rated power P_{ENGmax} and cost C_{DG}. F_{jt}^{DG} is the amount of marine gas oil consumed by the j^{th} generator, which is subject to the cost of the fuel C_{MGO}, storage costs (C_S^{MGO}) and carbon taxation similar to hydrogen (equation 21).

$$\begin{aligned}
\underset{\mathbf{n}_{fc},\mathbf{n}_{batt},\mathbf{n}_{DG},\mathbf{P}_{it}^{FC},\mathbf{P}_t^{batt\pm},\mathbf{P}_{jt}^{DG}}{\text{Minimize}} \quad & \mathbf{J}(\mathbf{n}_{fc},\mathbf{n}_{batt},\mathbf{n}_{DG},\\
\mathbf{P}_{it}^{FC},\mathbf{P}_t^{batt\pm},\mathbf{P}_{jt}^{DG}) = {} & E_{battmax}\cdot C_{batt} + n_{FC}\cdot P_{fcmax}\cdot C_{FC}\\
& + n_{DG}\cdot P_{ENGmax}\cdot C_{DG} + 0.8\cdot E_{battmax}\cdot C_{elec}\cdot\frac{1}{\eta_{batt}}\\
& + \sum_{i\in I}\sum_{t\in T} F_{it}^{FC}\cdot C_S^{LH2} + \sum_{j\in J}\sum_{t\in T} F_{jt}^{DG}\cdot C_S^{MGO}\\
& + \sum_{i\in I}\sum_{t\in T} F_{it}^{FC}\cdot (C_{H2} + CO_{2eq}^{H_2}\cdot CO_{2tax} + C_{liqH2})\\
& + \sum_{j\in J}\sum_{t\in T} F_{jt}^{DG}\cdot (C_{MGO} + CO_{2eq}^{MGO}\cdot CO_{2tax})
\end{aligned} \tag{21}$$

All the equations from the PEMFC/LIB model 2 to **??** are valid for this model. The diesel generator constraints are further added on as below.

Diesel generator model
Equations 22 to 27 refer to the operation of the j^{th} Diesel Generator at time t. The equation 22 relates the MGO consumption to the output power of the ICE using a piece wise linear approximation using the linearization coefficients $k_{1dg}$to k_{6dg}. equation 23 is the output power of the ICE multiplied by the alternator efficiency η_{DG}. Equation 24 refers to the upper (k_{ENGmin}) and lower (k_{ENGmax}) operating power limits of the ICE expressed as a percentage of the rated power of the ICE P_{ENGmax}. The binary variable x_{DG} in equations 24 and 25 expresses the inclusion of the j^{th} DG in the optimal system configuration. The sum of x_{DG} defines the number of DG sets that should be included in the system (equation 25). Equation 26 ensures that the increase in the DG load between time steps is not more than Δ_{DG}, which is the limit set by the manufacturer. The DG set can instantly drop it's output power from 100% to zero. Therefore equation 26 is only applicable to load increases. Equation 27 ensures that all the selected DG's deliver the same amount of power at each time step t.

$$F_{jt}^{DG} = \begin{cases} k_{1dg}\cdot P_{jt}^{ENG} + k_{2dg}, & \text{if } P_{jt}^{ENG} \leq 600 \\ k_{3dg}\cdot P_{jt}^{ENG} + k_{4dg}, & \text{if } 600 \leq P_{jt}^{ENG} \leq 680 \\ k_{5dg}\cdot P_{jt}^{ENG} + k_{6dg}, & \text{if } 680 \leq P_{jt}^{ENG} \leq 800 \end{cases} \tag{22}$$

$$P_{jt}^{DG} = P_{jt}^{ENG}\cdot\eta_{DG} \qquad \forall j\in J \qquad \forall t\in T \tag{23}$$

$$\begin{aligned} k_{ENGmin}\cdot P_{ENGmax}\cdot x_j^{DG} \leq P_{jt}^{ENG} \\ \leq k_{ENGmax}\cdot P_{ENGmax}\cdot x_j^{DG} \\ \forall j\in J \qquad \forall t\in T \end{aligned} \tag{24}$$

$$\sum_{j\in J} x_j^{DG} = n_{DG} \tag{25}$$

$$\Delta_{ENG} \geq P_{jt}^{ENG} - P_{j,t-1}^{ENG} \qquad \forall j\in J \qquad \forall t\in T \tag{26}$$

$$P_{jt}^{DG} = P_{1,t}^{DG}\cdot x_j^{DG} \qquad \forall j\in J \qquad \forall t\in T \tag{27}$$

Similar to equation 9, the equation 27 is linearized using the big M method.

Energy system constraints
The power balance constraint in equation 19 is updated with the inclusion of the diesel generator power in equation 28. Similarly, the volume constraint of the engine room in equation 20 is updated with the inclusion of the specific volume of the Diesel Generator V_{DG} in the equation 29.

$$\sum_{j\in J} P_{jt}^{DG} + \sum_{i\in I} P_{it}^{FC} + P_t^{batt+} = Load_t + P_t^{batt-} \qquad \forall t\in T \tag{28}$$

$$n_{DG} \cdot P_{DGmax} \cdot V_{DG} + n_{FC} \cdot P_{fcmax} \cdot V_{FC} + E_{battmax} \cdot V_{batt} \leq V_{ENG} \cdot (1 + C_{ov}) \quad (29)$$

3.2 Stage 2: Lifetime estimation of the installed components

In this phase, the lifetime of the installed PEMFC stacks and LFP battery obtained from section 3.1 is analysed for both the PEMFC/LIB and DG/PEMFC/LIB solutions. A single trip of the vessel is 102 hours. The vessel is assumed to be carrying out 5 such similar trips per month in this analysis. The vessel is assumed to be docked at the port for 5 days in a month where it undergoes maintenance and inspections where it is idle.

In this section, first the degradation modelling mechanisms of both the PEMFC stacks and the LFP battery are introduced. Further, the methodology for the lifetime estimation used in this study is elaborated on.

3.2.1 PEMFC Degradation

Equations 30 to 33 describe the performance degradation of the PEMFC stacks, which is defined as the voltage reduction of a single cell at equal current output, assuming that the behavior of a single cell can approximate the one of the entire PEMFC stack. The loss of voltage depends on: load variation (equation 30), start/stop cycles (equation 31), and the power levels of the i^{th} PEMFC stack (equation 32). For each time step t, equation 33 defines the total loss of voltage in a single cell, which has been set to be linearly depending on the operation of the variables of the i^{th} stack.

$$dV_{i,t+1}^{load} = |P_{it}^{FC} - P_{i,t+1}^{FC}| \cdot \Delta v_{load} \quad \forall i \in I \quad \forall t \in range(len(T) - 1) \quad (30)$$

$$dV_{it}^{stup} = \delta_{it}^{stup} \cdot \Delta v_{stup} \quad \forall i \in I \quad \forall t \in T \quad (31)$$

$$dV_{it}^{PFC} = k_{1dv} \cdot I_{it}^{FC} + k_{2dv} \quad \forall i \in I \quad \forall t \in T \quad (32)$$

$$dV_{it} = dV_{i,t}^{load} + dV_{it}^{stup} + dV_{it}^{PFC} \quad \forall i \in I \quad \forall t \in T \quad (33)$$

In equation 30, dV_{it}^{load} is the voltage reduction due to the load variations of the i^{th} single cell, proportional to the load variation by Δ_{load}. Similarly, equation 31 expresses the voltage reduction due to start up of the i^{th} PEMFC stack dV_{it}^{stup} as a constant value of voltage reduction Δ_{stup} according to the binary variable δ_{it}^{stup} which defines the happening of the startup phase and has been obtained from the equation 8.

The equation 32 defines the voltage loss due to operating power level which is a function of the current density of a single cell from equation 3. The degradation due to operating power level dV_{it}^{PFC} is expressed as a linear function of the current density I_{it}^{FC} by means of linearization coefficients k_{1dv} and k_{2dv}. The total voltage reduction dV_{it} is then calculated as a sum of the three different contributions in equation 33.

3.2.2 Li-ion battery degradation

The battery capacity obtained in the first stage optimization model has been updated to ensure that the battery maintains the necessary useful capacity till end of life (equation 34).

$$E_{battos} = \frac{E_{battmax}}{E_{EoL}} \quad (34)$$

Where E_{EoL} is the share of battery capacity at the end of lifetime (80%).

Two main degradation mechanisms have been identified as the main contribution to the capacity loss of the Li-ion battery: (i) Cycling aging, and (ii) calendar aging.

(i) Cycling aging
To calculate the number of charge/discharge cycles that the battery has undergone, the cycle counting algorithm by Gundogdu and Gladwin has been used in this study [31]. After the operation optimization of a single trip has been performed, the SOC data of the battery is used as input to count the number of cycles that the battery has undergone in a single trip. The algorithm is shown in figure 4.

To adapt the above model to this case study, certain modifications have been made as follows:

- Since the battery is being shore charged the initial SOC_{chg} is set as 0.8 before the start of the simulation.
- for simplicity, the partial charge and discharge cycles SOC_{chg} and SOC_{dchg} are added to the full charge and discharge cycles $Cycle_{chg}$ and $Cycle_{dchg}$ at the end of the trip.

The loss in capacity due to cycling aging after each month is defined as a percentage loss of the total number of cycles given by the battery manufacturer, i.e. 6250 cycles.

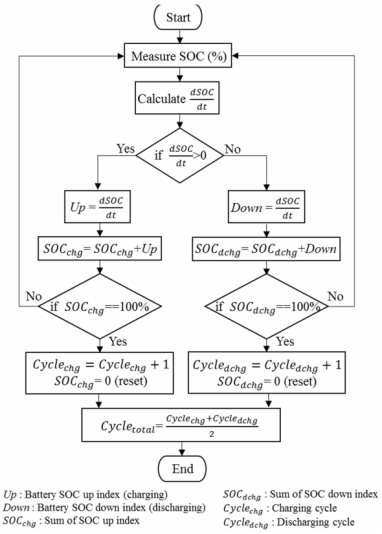

Fig. 4. Cycle counting estimation method [31]

(ii) Calendar aging

Another crucial aspect contributing to the capacity loss of the battery is calendar aging. Ali, Beltran, Lindsey, *et al.*, came up with a calendar aging prediction model using studies in literature for the different Li-ion battery chemistries using the following equation 35 [32].

$$\text{Capacity Degradation} = a_1 e^{a_2 SOC} \cdot b_1 e^{b_2/T} \cdot t^{c_1} \quad (35)$$

where a_1, a_2, b_1, b_2 and c_1 are the fitting parameters, SOC is state of charge ranges from 0 to 1, T is the temperature in Kelvin and t in the time in days [32].

The LFP battery is assumed to be stored at the end SOC (SOC_{end}) after the trip for 5 days in a month where the vessel is not being operated at a temperature of 25°C/298.15K.

3.2.3 Hierarchical Multi-Objective Optimization

To minimize the degradation of the fuel cell from equations 30 to 33, a hierarchical multi-objective optimization method has been set up with two objectives. The first objective is the OPEX of a single trip in equations 36 (PEMFC/LIB solution) and 38 (DG/PEMFC/LIB solution). The second objective is to minimize the degradation due to voltage loss of the installed PEMFC cells as in equation 37.

A hierarchical or lexicographic approach assigns a priority to each objective, and optimizes for the objectives in decreasing priority order. During each of these optimization passes, it finds the best solution for the current objective, but only from among those that would not degrade the solution quality for higher-priority objectives.

In this study, a higher priority (priority=2) has been assigned for the OPEX of a single trip, and lower priority (priority=1) has been assigned to the degradation of the fuel cell to not increase the OPEX of a single trip while minimizing the degradation of the fuel cell. Since all the PEMFC stacks are operating at the same power level, 2^{nd} objective is evaluated for a single stack.

$$\begin{aligned}\underset{\mathbf{P}_{it}^{FC}, \mathbf{P}_{t}^{batt\pm}}{\text{Minimize}} \quad & \mathbf{J_1}(\mathbf{P}_{it}^{FC}, \mathbf{P}_{t}^{batt\pm}) = \\ & \sum_{i\in I}\sum_{t\in T} F_{it}^{FC} \cdot (C_{H2} + CO_{2eq}^{H_2} \cdot CO_{2tax} + C_{liqH2}) \\ & +0.8 \cdot E_{battmax} \cdot C_{elec} \cdot \frac{1}{\eta_{batt}}\end{aligned} \quad (36)$$

$$\underset{\mathbf{P}_{it}^{FC}, \Delta\mathbf{P}_{it}^{FC}, \delta_{it}^{stup}}{\text{Minimize}} \quad \mathbf{J_2}(\mathbf{P}_{it}^{FC}, \Delta\mathbf{P}_{it}^{FC}, \delta_{it}^{stup}) = \sum_{t\in T} dV_{1,t} \quad (37)$$

The OPEX objective is modified for the DG/PEMFC/LIB solution.

$$\begin{aligned}\underset{\mathbf{P}_{it}^{FC}, \mathbf{P}_{t}^{batt\pm}, \mathbf{P}_{jt}^{DG}}{\text{Minimize}} \quad & \mathbf{J_1}(\mathbf{P}_{it}^{FC}, \mathbf{P}_{t}^{batt\pm}, \mathbf{P}_{jt}^{DG}) = \\ & \sum_{i\in I}\sum_{t\in T} F_{it}^{FC} \cdot (C_{H2} + CO_{2eq}^{H_2} \cdot CO_{2tax} + C_{liqH2}) \\ & + \sum_{j\in J}\sum_{t\in T} F_{jt}^{DG} \cdot (C_{MGO} + CO_{2eq}^{MGO} \cdot CO_{2tax}) \\ & +0.8 \cdot E_{battmax} \cdot C_{elec} \cdot \frac{1}{\eta_{batt}}\end{aligned} \quad (38)$$

All the equations from 2 to 19 and 22 to 28 are valid for the operation optimization.

3.2.4 Methodology for Lifetime Estimation

The methodology used in this study for estimating the lifetime of the installed PEMFC and battery systems in both the solutions is shown in figure 5. Starting from month k=0, corresponding to new PEMFC and battery systems installed on-board, consecutive optimization runs have been run until either the PEMFC or Li-ion battery reach the end of their life. in order to limit the computational effort, it has been assumed that the first trip in the month is representative of the operation of all the trips in a month (5 trips).

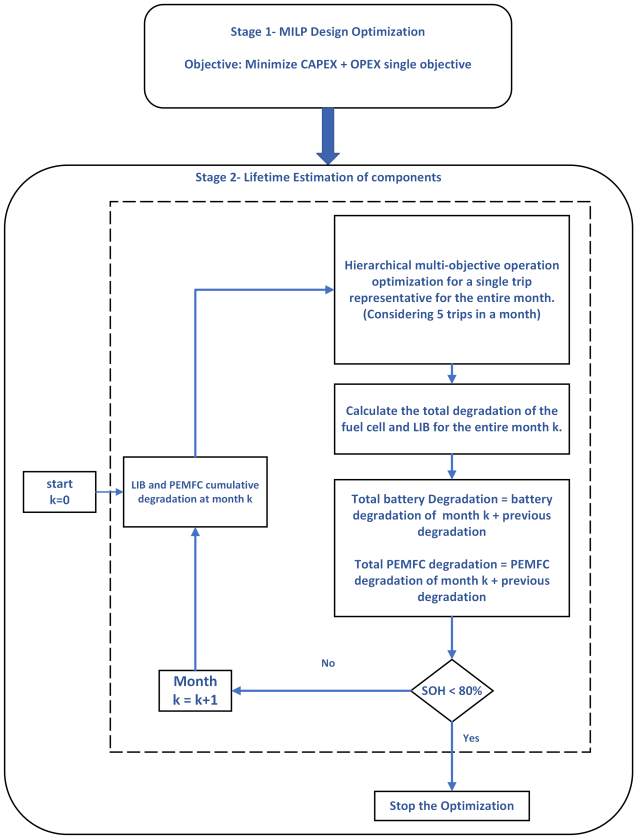

Fig. 5. Methodology for Lifetime estimation of PEMFC and Li-ion Battery

The degradation of the installed LFP battery is evaluated after each month, and is not part of the trip operation optimization. After a single trip is executed in a month t, the voltage loss in the PEMFC and capacity loss in the Li-ion battery are calculated for the entire month. The next step is to update the cumulative voltage loss(equation 39) in the PEMFC ($dV_{cumulative}$) and the cumulative capacity loss of the battery (Q_{loss}) upto the current month. The State of health of both the PEMFC (SOH_{PEMFC}) and battery (SOH_{batt}) are evaluated and if either of them drop below 80% the optimization loop stops (equations 41 and 42).

If neither of the SOH's are below 80% the loop continues onto the next month. Here the reduction in battery capacity is updated, and the total voltage loss of the PEMFC is updated. The voltage loss of the PEMFC is compensated by increasing the output current density of the cell. This is achieved using the equation 40, which updates the coefficient of current density (k_{1p}) in equation 3, which in turn leads increase in hydrogen consumption to deliver the same amount of power (equation 2).

Updating the losses of PEMFC and battery

$$dV_{cumulative} += \left[\sum_{t \in T} dV_{1,t}\right] \cdot 5 \tag{39}$$

$$k_{1p} = k_{1deg} \cdot dV_{cumulative} + k_{2deg} \tag{40}$$

$$SOH_{PEMFC} = \frac{V_{ref,fc} - dV_{cumulative}}{V_{ref,fc}} \tag{41}$$

$$SOH_{batt} = \frac{E_{battos} - Q_{loss}}{E_{battos}} \tag{42}$$

3.3 Input Optimization Parameters

Table 2: Input optimization parameters

Parameter	Unit	Value	Reference
PEMFC Parameters			
C_{FC}	\$/kW	635	[33]
V_{FC}	m^3/kW	0.00396	[26]
Δ_{PFC}	%	10	[28], [23]
k_{1p}, k_{2p}	$kW cm^2$/A, kW	0.1245, 8.83	[26], [30], [28]
k_{1f}, k_{2f}	$kg \cdot cm^2/A$, kg	0.0074, 0.3236	[26], [30], [28], [34]
I_{fcmin}	A/cm^2	0	[30], [34], [28]
I_{fcmax}	A/cm^2	1500	[30], [34], [28]
k_{fcmin}	%	10	[23]
k_{fcmax}	%	90	[23]
P_{fcmax}	kW	150	[26]
F^{FC}_{max}	kg/hr	8.82	[26]
F_{start}	%	10	[23]
Δ_{load}	$\mu V/\Delta kW$	0.0441	[22], [35], [36]
Δ_{stup}	$\mu V/cycle$	23.91	[22], [35], [36]
$V_{ref,fc}$	V	0.979	[23], [28], [34], [30]
k_{1dv}, k_{2dv}	$\mu V cm^2/A$, μV	0.0018, 9.4166	[22], [35], [36]
k_{1deg}, k_{2deg}	$kW cm^2/A \mu V$, $kW cm^2/A$	0.09866, 0.1245	[30], [22], [35], [36], [28]
Hydrogen Parameters			
H_2 grade	-	PEM, ALK, SMR, SMR+CCS, ATR+CCS	[37]

C_{H2}	\$/kg	8.4, 7.19, 2, 3.82, 3.77	[37]
$CO_{2eq}H_2$	$kgCO_{2eq}/kgH_2$	0, 0, 12.34, 2.5, 3	[38], [39]
C^S_{LH2}	\$/kg	200	[40]
C_{liqH2}	\$/kg	1	[41]
Battery Parameters			
C_{batt}	\$/kWh	150	[42]
η_{batt}	%	95	[43], [44], [45]
V_{batt}	m^3/kWh	0.01515	[25]
SOC_{min}	%	10	[25], [46]
SOC_{max}	%	90	[25], [46]
E_{module}	kWh	3.1	[25]
$C_{ratemax}$	C	1	[25], [43]
Diesel Generator Parameters			
C_{DG}	\$/kW	300	[47], [12]
k_{ENGmin}	%	11	[27]
k_{ENGmax}	%	100	[27]
η_{DG}	%	95	[27]
P_{ENGmax}	kW	800	[27]
V_{DG}	m^3/kW	0.0296	[27]
k_{1dg}, k_{3dg}, k_{5dg}	kg/kW	0.00292, 0.0031875, 0.003375	[27]
k_{2dg}, k_{4dg}, k_{6dg}	kg	0.238, 0.0775, -0.05	[27]
Δ_{DG}	%	33	[27]
Marine Gas Oil (MGO) Parameters			
C_{MGO}	\$/kg	0.844	[48]
C^S_{MGO}	\$/kg	1.3	[49]
CO^{MGO}_{2eq}	$kgCO_{2eq}/kg$	4.211	[50]
Other Parameters			
CO_{2tax}	$\$/kgCO_{2eq}$	0.0963	[51]
V_{ENG}	m^3	135	-
Δt	time	1 min	-
C_{ov}	-	0.2	[28], [23]
C_{elec}	\$/kWH	0.095	[52]
$Load_t$	kW	from dataset	-
M	-	100000	-

4 Results and Discussion

In this section, the results of both the stages of the optimization are discussed.

4.1 Stage 1: Design Optimization and emission analysis across various grades of hydrogen

In this section the design optimization of the two hybrid energy systems, i.e. (i) PEMFC/LIB hybrid system, and (ii) DG/PEMFC/LIB hybrid system across the various grades of hydrogen has been presented. First the results of PEMFC/LIB hybrid energy system are presented, and in the next subsection the results of the DG/PEMFC/LIB hybrid energy system are presented.

4.1.1 Stage 1: PEMFC/LIB

Irrespective of the costs and emission intensities of the various grades of hydrogen the optimal system configuration of the PEMFC/LIB hybrid energy system remains the same across all the grades. The system configuration is as follows.

Table 3
PEMFC/LIB solution

Component	Variable	Value	Total Capacity
150kW PEMFC stacks	n_{FC}	7	1050 kW
3.1 kWh LFP modules	n_{batt}	29	89.90 kWh

The installed battery charge/discharge power vs SOC is shown in figure 6. The power schedule of the different installed components is shown in the figure 7. As seen from the figure 7, majority of the power is supplied by the PEMFC stacks. The reason for this is due to limited transient loading needed to be handled by the battery. The load profile has been linearly interpolated from 5 minutes to 1 minute, meaning that the load change between time steps is smaller compared to the 5 minute profile, and this can be handled by the fuel cells alone resulting in a smaller battery capacity. Further checks are needed with the exact profile to verify that the current configuration can handle the different load transients.

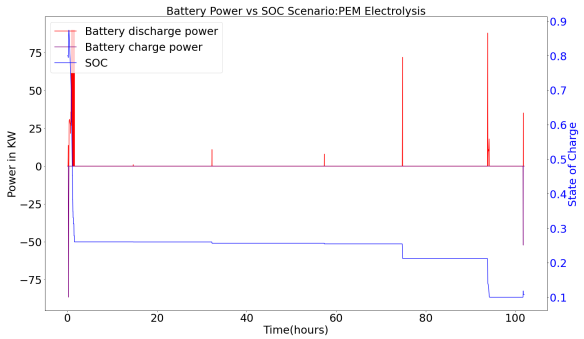

Fig. 6. Battery charge/discharge power vs SOC in the PEMFC/LIB hybrid system

The CAPEX, OPEX and total emissions for a single trip of the hybrid energy system across the various grades of hydrogen are shown in the figure 8. The quantity of hydrogen consumed across all the different hydrogen grades is 4784.14 kg for the entire trip.

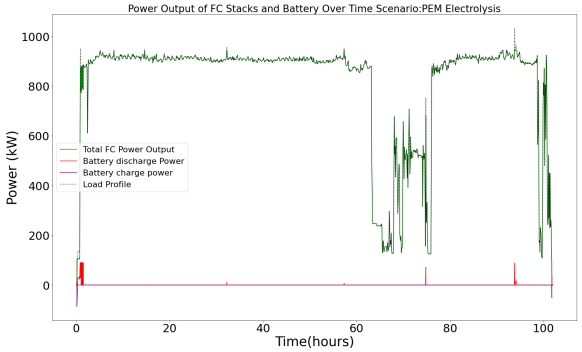

Fig. 7. Power schedule of the installed components in the PEMFC/LIB solution

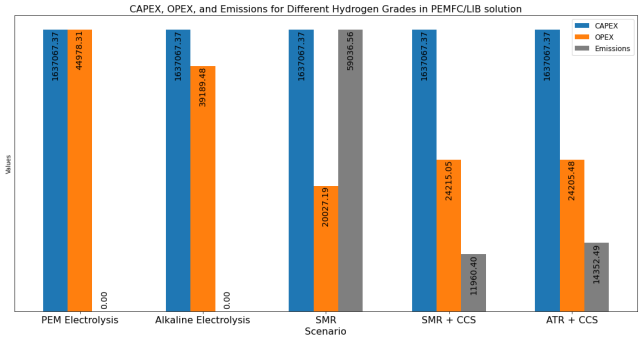

Fig. 8. CAPEX (in $), OPEX (in $) and CO_{2eq}(in kg) emissions of the PEMFC/LIB hybrid energy system for various grades of hydrogen

The MGO consumed across the entire trip with respect to the original power train configuration consisting of 1.8MW ICE is 19.7 tons, leading to total emissions of 82.95 tons of CO_{2eq}. A total emission reduction of 100% is possible with the use of electrolytic hydrogen. But this leads to an OPEX increase from $ 18,923.91 (using MGO) to $ 44,978.8 using PEM hydrogen and $ 39,189.30 using ALK hydrogen, which is a 137% increase and 107% increase in OPEX respectively.

The highest emitting PEMFC/LIB solution is the usage of hydrogen produced using SMR. This leads to a total emissions of 59.03 tons, which is a reduction of 28% total emissions. The OPEX of this solution is $ 20,027.09 which is a minor increase of 5.8%. The solutions using hydrogen produced using carbon capture provide a good trade-off between emission reduction and costs. The SMR+CCS hydrogen leads to an increase in costs of 27%, but a reduction in emissions of almost 85%, while the ATR+CCS hydrogen leads to an increase in costs of 27% and reduction in emissions of 83%.

4.1.2 Stage 1: DG/PEMFC/LIB

Similar to the PEMFC/LIB solution, irrespective of the costs and emission intensities of the various grades of hydrogen the optimal system configuration of the DG/PEMFC/LIB hybrid energy system remains the same across all the grades. The system configuration is shown in table 4.

Table 4
DG/PEMFC/LIB solution

Component	Variable	Value	Total Capacity
800kW DG sets	n_{DG}	1	800 kW
150kW PEMFC stacks	n_{FC}	2	300 kW
3.1 kWh LFP modules	n_{batt}	47	145.70 kWh

The battery charge/discharge power vs SOC and the power schedule of the different installed components is shown in figures 9 and 10. The battery is being utilized at the start of the trip for the DG and PEMFC stacks to reach the optimal power based on the transient constraints set, and once they reach the optimal power, the battery is being discharged across the length of the trip until around the time step 3700 to reduce the H_2 consumption. There are no rules set in place on how the battery needs to be discharged if there are no excessive demands that the PEMFC stacks and DG can't handle. The DG in this part of the trip is being operated at it's maximum rated power due to the high costs of the hydrogen storage. Around the time step 4000, the PEMFC stacks are switched-off and the DG set is being operated at higher % of it's rated power(better efficiency) to charge the battery back up to the maximum SOC limit. Further on, after the power demands are back to normal, the DG set operates at it's maximum rated power, and the battery is discharged to reduce the H_2 consumption.

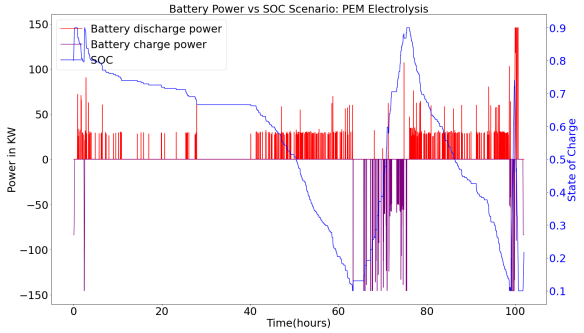

Fig. 9. Battery charge/discharge power vs SOC in DG/PEMFC/LIB solution

The CAPEX, OPEX and total emissions for a single trip of the hybrid energy system across the various grades of hydrogen are shown in figure 11. The quantity of hydrogen consumed across all the different hydrogen grades is 685.02 kg, and MGO consumed is 14,095.43 kg.

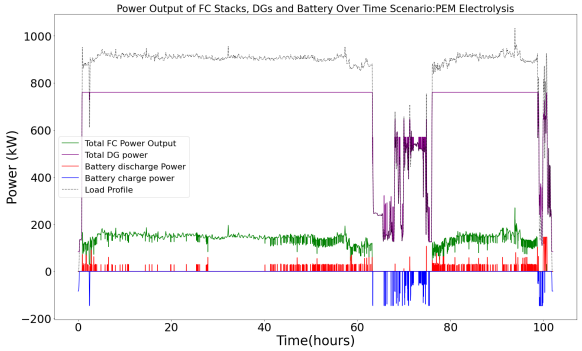

Fig. 10. Power output of the installed components in the DG/PEMFC/LIB solution

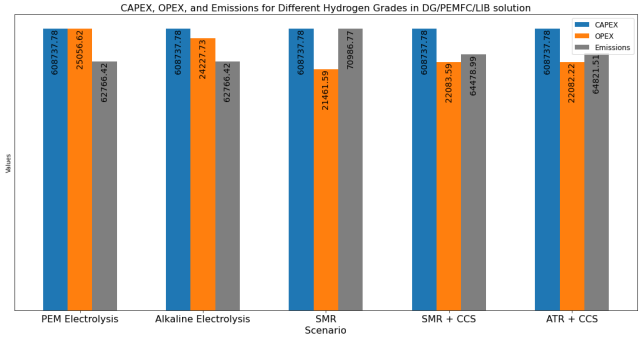

Fig. 11. CAPEX (in $), OPEX (in $) and CO_{2eq} (in kg) emissions of the DG/PEMFC/LIB hybrid energy system for various grades of hydrogen

As can be seen from the figure 11, the CAPEX of this hybrid energy system is same across all the different grades of hydrogen, i.e. $ 608737.78, which is 62.8% less expensive than the PEMFC/LIB hybrid energy system.

Among the different grades of hydrogen, due to high cost of the electrolytic hydrogen, the OPEX is higher if PEM and ALK hydrogen are used. The OPEX if PEM hydrogen is used is $ 25,056.62, and if ALK hydrogen is used is $ 24,227.75 which is a 32% and 28% increase respectively. The emissions for the entire trip are reduced from 82.5 tons to 62.76 tons which is a ≈ 24% reduction in emissions.

Among the fossil sources of hydrogen, the SMR leads to the highest amount of emissions of 70.98 tons, which is a 13.6% reduction in emissions from the original configuration. The OPEX is the lowest for this solution at $ 21,461.65 which is an increase of 13.43%. The better trade-off between emissions and costs can be achieved by using Fossil hydrogen using CCS. The SMR+CCS solution leads to a ≈17% increase in OPEX while reducing the emissions by 21.85%. The ATR+CCS solution also gives similar results, a 16.68% increase in OPEX and 21.42% reduction in emissions.˚

4.2 Stage 2: Lifetime Estimation of components

In this subsection, the estimated lifetime of the installed PEMFC and LFP battery components has been elaborated on for both the (i) PEMFC/LIB hybrid energy system and (ii) DG/PEMFC/LIB hybrid energy system. The methodology used for the lifetime estimation has been described in the section 3.2.

Before the start of the analysis, to ensure that the installed battery retains the necessary capacity for operation till end of life the battery capacity is increased according to equation 34 for both the solutions. The modified system configurations are as below:

Table 5
Modified PEMFC/LIB configuration

Component	Variable	Value	Total Capacity
150kW PEMFC stacks	n_{FC}	7	1050 kW
3.1 kWh LFP modules	n_{batt}	37	114.70 kWh

Table 6
Modified DG/PEMFC/LIB configuration

Component	Variable	Value	Total Capacity
800kW DG sets	n_{DG}	1	800 kW
150kW PEMFC stacks	n_{FC}	2	300 kW
3.1 kWh LFP modules	n_{batt}	59	182.90 kWh

4.2.1 Lifetime of components in the PEMFC/LIB solution

In this subsection, the voltage loss of the PEMFC stacks and the number of cycles that the battery undergoes in a single trip are evaluated. Further along, the lifetime of the components and the increase in hydrogen consumption has been observed.

The power schedule of the components of both the single objective OPEX optimization and the multi-objective hierarchical optimization with the voltage loss of a single cell representative of the entire stack as the 2^{nd} objective is shown in the figures 12 and 13. Similarly the charge/discharge power vs SOC of the battery is shown in the figure 14, 15

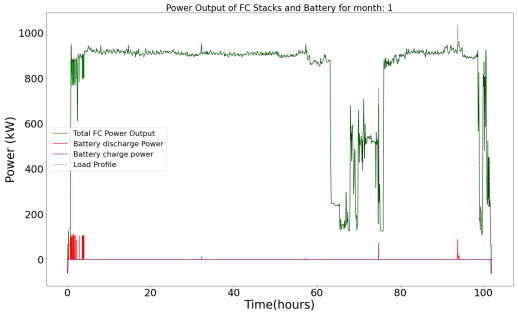

Fig. 12. Power schedule of the installed PEMFC/LIB components in the single objective OPEX optimization

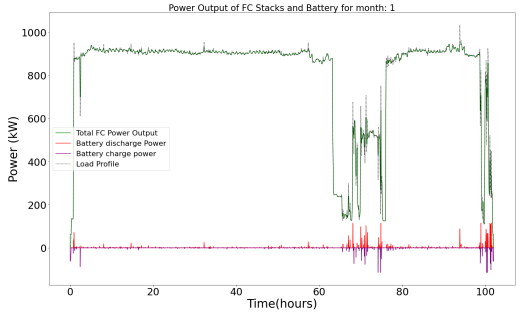

Fig. 13. Power schedule of the installed PEMFC/LIB components in the multi objective OPEX and PEMFC degradation optimization

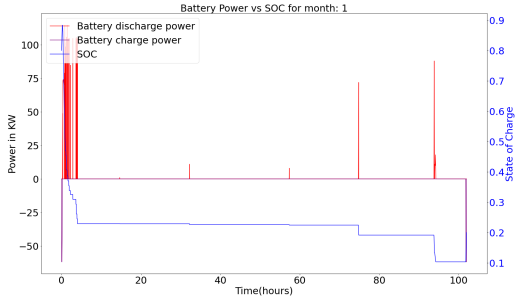

Fig. 14. Battery power vs SOC: single objective OPEX optimization

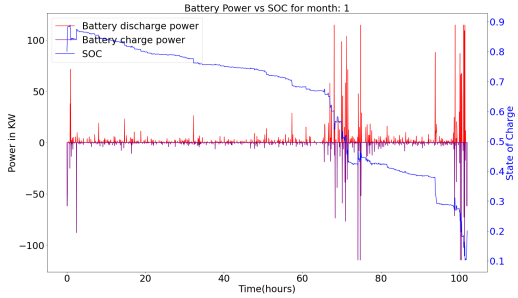

Fig. 15. Battery power vs SOC in the multi objective OPEX and PEMFC degradation optimization

Table 7
Voltage loss comparison of single objective vs multi-objective optimization in the PEMFC/LIB solution

Voltage Loss in μV	**Single Objective**	**Multi Objective**	**% reduction**
start-up	23.91	23.91	0
transient loading	153.81	79.12	48.55
operating power	1118.52	1118.54	0
total voltage loss	1297.24	1221.57	5.83

From the table 7, it is observed that the major contribution to the voltage loss of the PEMFC stack is due to operating power of the PEMFC stack which is similar for both the methods. Since the fuel cell stacks undergo only a single start-stop cycle across the entire trip, it is also the same for both the methods. The voltage loss due to transient loading has been reduced significantly, which is a 48.55% reduction from the single objective to the multi objective method. The overall voltage loss is reduced from 1297.24 μV to 1221.57 μV.

The number of battery cycles have been counted based on the SOC history of the battery after the trip according to the algorithm proposed by Gundogdu and Gladwin [31], and have increased from 0.88 cycles for the entire trip in the single objective optimization to 1.56 in the multi-objective optimization. This is due to the transient loading on the fuel cell being limited by the battery system.

The OPEX of the trip also didn't increase as expected of hierarchical multi-objective optimization where the lower priority objective (PEMFC voltage loss) does not degrade the optimal value of the higher priority objective (OPEX). It is $ 44,975.25 for the multi-objective optimization and $ 44,973.05 for the single objective optimization.

The operation optimization of the vessel has been performed for 1 trip representative of each month to reduce the computational burden and the voltage loss of the PEMFC stack and the battery cycles are calculated. The calendar aging of the battery is evaluated for each month according to the equation 35 and the fitting parameters in [32]. The battery is assumed to be stored at 25°C for 5 days in a month, at the SOC obtained after the end of the trip (SOC_{end}).

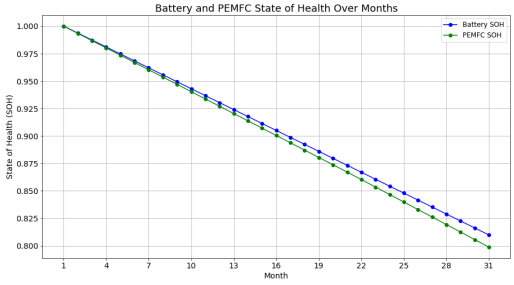

Fig. 16. PEMFC and Battery SOH for single objective optimization in PEMFC/LIB solution

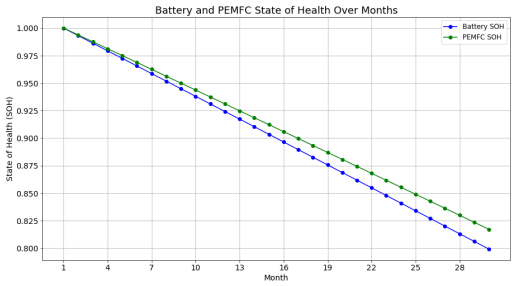

Fig. 17. PEMFC and Battery SOH for multi-objective optimization in the PEMFC/LIB solution

The resulting PEMFC and battery lifetime are shown

in the above figures. For the single objective optimization the PEMFC reaches 80% SOH at the 31^{st} month, whereas at the same time, the battery still is at 81% SOH, and it can last for an additional 1-2 months (figure 16). For the multi-objective optimization the battery reaches its end of life at the 29^{th} month where the SOH is at 80% and the PEMFC is still at a SOH of 82%, meaning that the PEMFC stack can last for an additional 3-4 months (figure 17).

The voltage loss of the PEMFC stack, leads to an increase in the current density to deliver the same power, which in turn leads to an increase in hydrogen consumption.

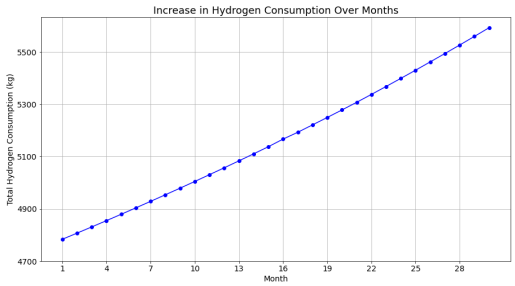

Fig. 18. Increase in H_2 consumption for single objective optimization-PEMFC/LIB solution

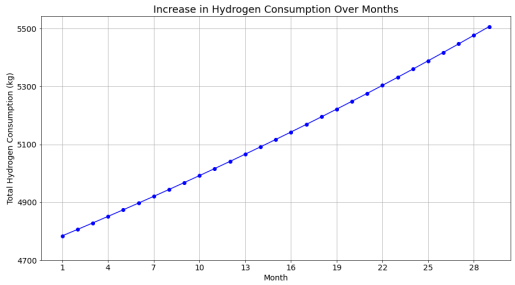

Fig. 19. Increase in H_2 consumption for multi-objective optimization-PEMFC/LIB solution

There is a significant increase in H_2 consumption due to the degradation of the PEMFC stack as can be seen in the figures 18 and 19. At the start of the plant lifetime the H_2 consumed for the entire trip is 4783.39 kg, where as towards the end of life of the stack, this has increased to 5592.96 kg in the single objective optimization which is a 16.92%(809.57kg) increase in hydrogen consumption. In-case of the multi-objective optimization this has increased to 5505.33kg.

This increase in H_2 consumption needs to be accounted for by the vessel owner at the new build stage due to the high costs of liquefied hydrogen storage. There is a $161,914 increase in the hydrogen storage costs due to the PEMFC voltage loss.

4.3 Lifetime of components in the DG/PEMFC/LIB solution

Similar to the above subsection 4.2.1, first the voltage loss of the PEMFC stacks and the number of cycles that the battery undergoes in a single trip are evaluated. Further along, the lifetime of the components and the increase in hydrogen consumption has been observed.

The power schedule of the components of both the single objective OPEX optimization and the multi-objective optimization with the voltage loss of the single cell representative of the entire stack as the 2^{nd} objective is shown in figures 20 and 21. Similarly the charge/discharge power vs SOC of the battery is shown in the figures 22 and 23.

From the table 8, it can be seen that the major contributor to the voltage loss is the operation of the PEMFC stack which is the same for both the single objective and multi-objective optimization methods at 876.60 μV. In both the methods the fuel cell stack is switched on/off twice as can be seen from the figures 20 and 21, due to which the voltage loss is 47.82 μV. The major reduction in the voltage loss is due to the reduction in transient loading of the PEMFC stack in the multi objective optimization. It has reduced significantly from 556.67 μV to 26.09 μV which is a 95% reduction. The total voltage loss for a single trip has reduced from 1479.08 μV to 950 μV.

Comparing the figures 22 vs 23, it can be seen that the battery is discharging strategically to limit the transient loading on the PEMFC stack. The number of battery cycles has increased from 2.37 in the single objective optimization to 2.62 in the multi-objective optimization. The total OPEX of the entire trip has remained the same for both the methods at $25,035.50.

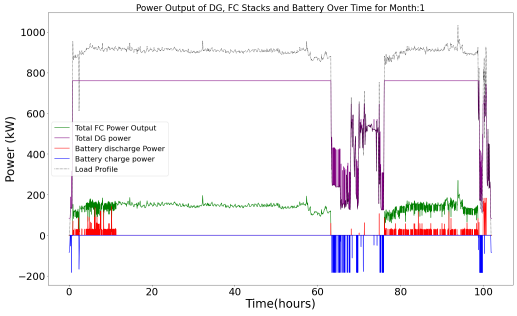

Fig. 20. Power schedule of the installed components in the single objective OPEX optimization-DG/PEMFC/LIB solution

The procedure to evaluate the lifetime of the PEMFC and battery are similar to the above subsection. The resulting plant lifetime is shown in the figures 24 and 25. For a single objective optimization, the PEMFC stack reaches it's end-of-life at the 27^{th} month and the battery is at a SOH of 80% and can last for an additional 1 month. In case of the multi-objective method, the bat-

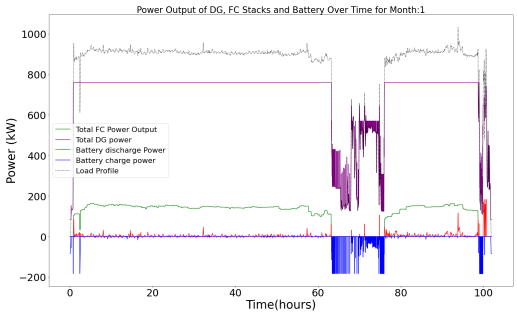

Fig. 21. Power schedule of the installed components in the multi objective OPEX and PEMFC degradation optimization-DG/PEMFC/LIB solution

Table 8
Voltage loss comparison of single objective vs multi-objective operation optimization in the DG/PEMFC/LIB solution

Voltage Loss in μV	**Single Objective**	**Multi Objective**	**% reduction**
start-up	47.82	47.82	0
transient loading	554.67	26.09	95.29
operating power	876.60	876.63	0
Total voltage loss	1479.08	950.54	35.73

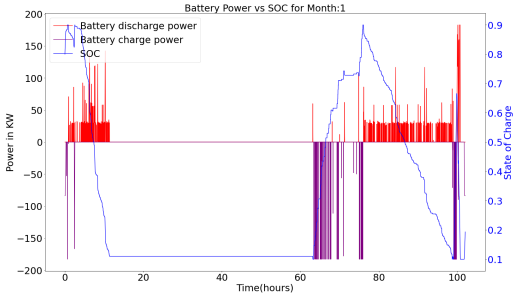

Fig. 22. Battery charge/discharge power vs SOC: single objective OPEX optimization-DG/PEMFC/LIB solution

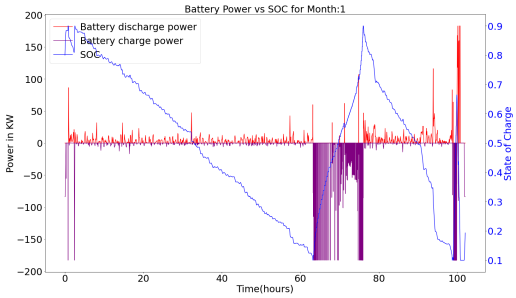

Fig. 23. Battery charge/discharge power vs SOC in the multi objective OPEX and PEMFC degradation optimization-DG/PEMFC/LIB solution

tery reaches it's end of life at the 26^{th} month, and the PEMFC is still at a SOH of 87%. To evaluate the exact time at which the PEMFC stack reaches it's end of life, the battery is replaced at the end of the 26^{th} month. The resulting plant lifetime evaluation is shown in figure 26.

It can be clearly seen that the PEMFC stacks would last for 42 months after which they need to be replaced.

The resulting increase in H_2 due to the degradation of the PEMFC stack and battery is shown in figure 27 & 28. The H_2 consumption per trip increases from 681.74kg in the first month to 799.84kg in the single objective method, and 750.98kg in the hierarchical method at the end of life. This increase in hydrogen consumption of 70kg(multi-objective method) can easily be accounted for in the design stage by the vessel owner compared to the PEMFC/LIB solution.

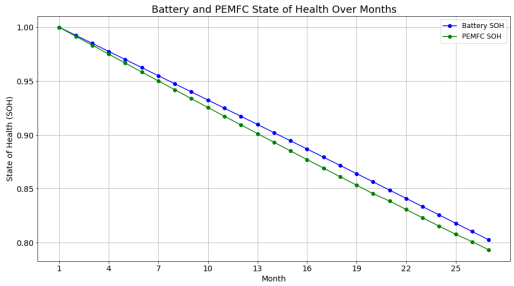

Fig. 24. PEMFC and Battery SOH for single objective OPEX optimization in the DG/PEMFC/LIB solution

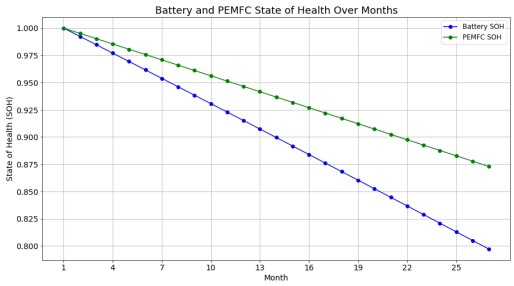

Fig. 25. PEMFC and Battery SOH for multi-objective optimization in the DG/PEMFC/LIB solution

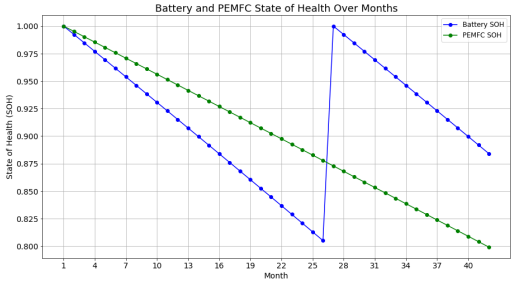

Fig. 26. PEMFC and Battery SOH for multi-objective optimization in the DG/PEMFC/LIB solution with battery replaced at it's end of life

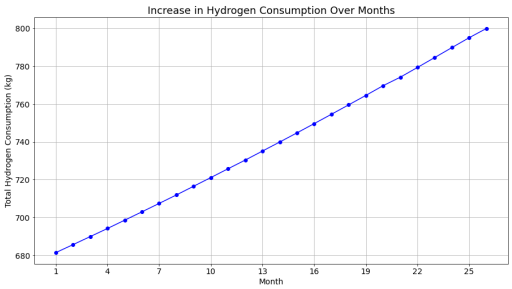

Fig. 27. H_2 consumption increase for single objective optimization-DG/PEMFC/LIB solution

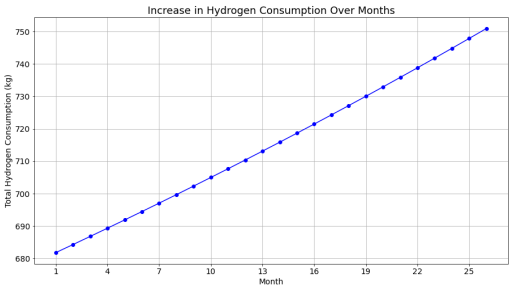

Fig. 28. H_2 consumption increase for multi-objective optimization-DG/PEMFC/LIB solution

5 Conclusions

This study suggests a methodology for the D&O optimization of (i)PEMFC/LIB, and (ii)DG/PEMFC/LIB hybrid energy systems for a general cargo vessel. A MILP modelling approach has been taken to describe the conversion and energy storage units. To analyse the trade-off between costs and emissions across different grades of hydrogen a single objective CAPEX and OPEX optimization has been performed for both hybrid systems. The configurations of both hybrid systems do not vary across all the grades of hydrogen and the DG/PEMFC/LIB hybrid system is 62.8% less expensive than the PEMFC/LIB configuration. In the PEMFC/LIB system the use of electrolytic hydrogen leads to a OPEX increase of 137%. SMR+CCS leads to an emission reduction of 85% with an OPEX increase of 27%. The maximum emission reduction possible for the DG/PEMFC/LIB system is 24% using electrolytic hydrogen with an OPEX increase of 30%.

For the lifetime estimation of the PEMFC and battery components in both the hybrid systems, a hierarchical multi-objective method has been used with the OPEX and PEMFC degradation as the objectives. The PEMFC degradation was modelled using a stack voltage degradation method. The SOC data of the trip is used in calculating the cycling aging of the battery, and also the calendar aging effects of the battery were modelled. In the DG/PEMFC/LIB system the degradation of the PEMFC was reduced by 35% across an entire trip and the lifetime of the PEMFC was 42 months with the Li-ion battery lasting 26 months. The hierarchical method was only able to extend the PEMFC lifetime by 3 months in the PEMFC/LIB solution with a 16.92% increase in H_2 consumption observed at end of life.

In the design of the hybrid systems, the weight constraints of the engine room are to be added along with on-board restrictions of liquefied hydrogen storage. The impact of uncertainties due to fuel and power component costs on the optimization results need to be studies in detail. The component sizes chosen can also be experimented with further. In addition, uncertainties of different power profiles on the optimization need to be studied. The accuracy of the results can also be improved further by reducing the size of the time step.

References

[1] L. Van Biert, K. Mrozewski, and P. Hart, "Public final report: Inventory of the application of fuel cells in the maritime sector (fcmar)," *Maritime Knowledge Centre (MKC): London, UK*, 2021.

[2] E. (EMSA), *Study on the use of fuel cells in shipping*, Jan. 2017. [Online]. Available: `https://www.emsa.europa.eu/publications/item/2921-emsa-study-on-the-use-of-fuel-cells-in-shipping.html`.

[3] W. Vielstich, A. Lamm, and H. Gasteiger, "Handbook of fuel cells. fundamentals, technology, applications," 2003.

[4] P. Thounthong, V. Chunkag, P. Sethakul, B. Davat, and M. Hinaje, "Comparative study of fuel-cell vehicle hybridization with battery or supercapacitor storage device," *IEEE transactions on vehicular technology*, vol. 58, no. 8, pp. 3892–3904, 2009.

[5] R. Geertsma, R. Negenborn, K. Visser, and J. Hopman, "Design and control of hybrid power and propulsion systems for smart ships: A review of developments," *Applied Energy*, vol. 194, pp. 30–54, 2017.

[6] O. B. Inal, J.-F. Charpentier, and C. Deniz, "Hybrid power and propulsion systems for ships: Current status and future challenges," *Renewable and Sustainable Energy Reviews*, vol. 156, p. 111 965, 2022.

[7] B. De Jager, T. Van Keulen, and J. Kessels, *Optimal control of hybrid vehicles*. Springer, 2013.

[8] *Hydrogen as a marine fuel - an introduction*. London, England: Society for Gas as a Marine Fuel, Feb. 2023, ISBN: 9781739870379.

[9] H. K. Fathy, J. A. Reyer, P. Y. Papalambros, and A. Ulsov, "On the coupling between the plant and controller optimization problems," in *Proceedings of the 2001 American Control Conference.(Cat. No. 01CH37148)*, IEEE, vol. 3, 2001, pp. 1864–1869.

[10] E. Silvas, T. Hofman, N. Murgovski, L. P. Etman, and M. Steinbuch, "Review of optimization strategies for system-level design in hybrid electric vehicles," *IEEE Transactions on Vehicular Technology*, vol. 66, no. 1, pp. 57–70, 2016.

[11] A. Panday and H. O. Bansal, "A review of optimal energy management strategies for hybrid electric vehicle," *International Journal of Vehicular Technology*, vol. 2014, 2014.

[12] F. Baldi, S. Brynolf, and F. Maréchal, "The cost of innovative and sustainable future ship energy systems," *ECOS*, 2019.

[13] O. Balland, S. O. Erikstad, and K. Fagerholt, "Concurrent design of vessel machinery system and air emission controls to meet future air emissions regulations," *Ocean Engineering*, vol. 84, pp. 283–292, 2014.

[14] J. Zhu, L. Chen, B. Wang, and L. Xia, "Optimal design of a hybrid electric propulsive system for an anchor handling tug supply vessel," *Applied energy*, vol. 226, pp. 423–436, 2018.

[15] K. Deb, A. Pratap, S. Agarwal, and T. Meyarivan, "A fast and elitist multiobjective genetic algorithm: Nsga-ii," *IEEE transactions on evolutionary computation*, vol. 6, no. 2, pp. 182–197, 2002.

[16] C. C. Coello and M. S. Lechuga, "Mopso: A proposal for multiple objective particle swarm optimization," in *Proceedings of the 2002 Congress on Evolutionary Computation. CEC'02 (Cat. No. 02TH8600)*, IEEE, vol. 2, 2002, pp. 1051–1056.

[17] A. Dolatabadi and B. Mohammadi-Ivatloo, "Stochastic risk-constrained optimal sizing for hybrid power system of merchant marine vessels," *IEEE Transactions on Industrial Informatics*, vol. 14, no. 12, pp. 5509–5517, 2018.

[18] Z. Wang, L. Chen, F. Guo, and B. Wang, "Optimal design of hybrid electric propulsive system for a mini polar cruise," in *The 31st International Ocean and Polar Engineering Conference*, OnePetro, 2021.

[19] X. Bao, X. Xu, Y. Zhang, Y. Xiong, and C. Shang, "Optimal sizing of battery energy storage system in a shipboard power system with considering energy management optimization," *Discrete Dynamics in Nature and Society*, vol. 2021, pp. 1–12, 2021.

[20] X. Wang, U. Shipurkar, A. Haseltalab, H. Polinder, F. Claeys, and R. R. Negenborn, "Sizing and control of a hybrid ship propulsion system using multi-objective double-layer optimization," *Ieee Access*, vol. 9, pp. 72 587–72 601, 2021.

[21] S. Karagiorgis, S. Nasiri, and H. Polinder, "Implementation of ship hybridisation: Sizing a hybrid crew transfer vessel considering uncertainties," in *Proceedings of the International Naval Engineering Conference*, vol. 16, 2022, p. 49.

[22] P. Wu and R. Bucknall, "Hybrid fuel cell and battery propulsion system modelling and multi-objective optimisation for a coastal ferry," *International journal of hydrogen energy*, vol. 45, no. 4, pp. 3193–3208, 2020.

[23] D. Pivetta, C. Dall'Armi, and R. Taccani, "Multi-objective optimization of hybrid pemfc/li-ion battery propulsion systems for small and medium size ferries," *International Journal of Hydrogen Energy*, vol. 46, no. 72, pp. 35 949–35 960, 2021.

[24] S. Xie, X. Hu, Q. Zhang, X. Lin, B. Mu, and H. Ji, "Aging-aware co-optimization of battery size, depth of discharge, and energy management for plug-in hybrid electric vehicles," *Journal of power sources*, vol. 450, p. 227 638, 2020.

[25] EAS, *Easy marine 80ah lfp battery module*. [Online]. Available: `https://eas-batteries.com/system/files/attachments/Data%20sheet%20EASy%20Marine%20rev.3.2_2.pdf`.

[26] ZEPP.SOLUTIONS, *Zepp.x150: Ultra high power density fuel cell system (150kw)*, Oct. 2022. [On-

line]. Available: https://zepp.solutions/en/x150/.

[27] Wartsila, *Wärtsilä 20 product guide*. [Online]. Available: https://www.wartsila.com/marine/products/engines-and-generating-sets/diesel-engines/wartsila-20.

[28] C. Dall'Armi, D. Pivetta, and R. Taccani, "Health-conscious optimization of long-term operation for hybrid pemfc ship propulsion systems," *Energies*, vol. 14, no. 13, p. 3813, 2021.

[29] C. Dall'Armi, "Energy modelling and optimization of PEM fuel cells power plants in view of shipping decarbonization," 2023.

[30] Nedstack, *PRODUCT DATA SHEET FCS 3-XXL Gen 2.9*, Jul. 2022. [Online]. Available: https://nedstack.com/sites/default/files/2022-07/nedstack-fcs-13-xxl-gen-2.9-datasheet-rev01.pdf.

[31] B. Gundogdu and D. T. Gladwin, "A fast battery cycle counting method for grid-tied battery energy storage system subjected to microcycles," in *2018 International Electrical Engineering Congress (iEECON)*, IEEE, 2018, pp. 1–4.

[32] H. Ali, H. Beltran, N. J. Lindsey, and M. Pecht, "Assessment of the calendar aging of lithium-ion batteries for a long-term—space missions," *Frontiers in Energy Research*, vol. 11, p. 1 108 269, 2023.

[33] A. Kampker, H. Heimes, M. Kehrer, S. Hagedorn, P. Reims, and O. Kaul, "Fuel cell system production cost modeling and analysis," *Energy Reports*, vol. 9, pp. 248–255, 2023.

[34] J. Zhang, *PEM fuel cell electrocatalysts and catalyst layers: fundamentals and applications*. Springer Science & Business Media, 2008.

[35] L. Balestra and I. Schjølberg, "Modelling and simulation of a zero-emission hybrid power plant for a domestic ferry," *International Journal of Hydrogen Energy*, vol. 46, no. 18, pp. 10 924–10 938, 2021.

[36] T. Fletcher, R. Thring, and M. Watkinson, "An energy management strategy to concurrently optimise fuel consumption & pem fuel cell lifetime in a hybrid vehicle," *international journal of hydrogen energy*, vol. 41, no. 46, pp. 21 503–21 515, 2016.

[37] S&PGlobal, *Platts hydrogen price wall*. [Online]. Available: https://www.spglobal.com/commodityinsights/PlattsContent/_assets/_files/en/specialreports/energy-transition/platts-hydrogen-price-wall/index.html.

[38] D. McFarlane, D. Rodriguez, and E. Abramson, *The carbon intensity of hydrogen production*, Oct. 2022. [Online]. Available: https://www.carbonsolutionsllc.com/hydrogen-lca/.

[39] D. McFarlane, D. Rodriguez, and E. Abramson, *Hydrogen a climate solution*, Oct. 2022. [Online]. Available: https://www.carbonsolutionsllc.com/hydrogen-a-climate-solution/.

[40] H. K. Shin and S. K. Ha, "A review on the cost analysis of hydrogen gas storage tanks for fuel cell vehicles," *Energies*, vol. 16, no. 13, p. 5233, 2023.

[41] S. Z. Al Ghafri, S. Munro, U. Cardella, *et al.*, "Hydrogen liquefaction: A review of the fundamental physics, engineering practice and future opportunities," *Energy & environmental science*, vol. 15, no. 7, pp. 2690–2731, 2022.

[42] IEA, *Global EV Outlook 2023-catching up with climate ambitions*. Apr. 2023. [Online]. Available: https://www.iea.org/reports/global-ev-outlook-2023.

[43] E. (EMSA), *Study on electrical energy storage for ships*, May 2020. [Online]. Available: https://www.emsa.europa.eu/publications/item/3895-study-on-electrical-energy-storage-for-ships.html.

[44] T. S. Schmidt, M. Beuse, X. Zhang, *et al.*, "Additional emissions and cost from storing electricity in stationary battery systems," *Environmental science & technology*, vol. 53, no. 7, pp. 3379–3390, 2019.

[45] T. Terlouw, T. AlSkaif, C. Bauer, and W. Van Sark, "Multi-objective optimization of energy arbitrage in community energy storage systems using different battery technologies," *Applied energy*, vol. 239, pp. 356–372, 2019.

[46] J. Groot, *State-of-health estimation of Li-ion batteries: Ageing models*. Chalmers Tekniska Hogskola (Sweden), 2014.

[47] A. Ritari, J. Huotari, and K. Tammi, "Marine vessel powertrain design optimization: Multiperiod modeling considering retrofits and alternative fuels," *Proceedings of the Institution of Mechanical Engineers, Part M: Journal of Engineering for the Maritime Environment*, p. 14 750 902 221 145 747, 2023.

[48] Ship and Bunker, *Rotterdam bunker prices*. [Online]. Available: https://shipandbunker.com/prices/emea/nwe/nl-rtm-rotterdam#MGO.

[49] TNO, *Tno power-2-fuel cost analysis - smartport*, Sep. 2020. [Online]. Available: https://smartport.nl/wp-content/uploads/2020/09/Cost-Analysis-Power-2-Fuel_def_2020.pdf.

[50] B. Comer and L. Osipova, *Update: Accounting for well-to-wake carbon dioxide equivalent emissions in maritime transportation climate policies*, Aug. 2021. [Online]. Available: https://theicct.org/wp-content/uploads/2021/08/update-well-to-wake-co2-aug21-1.pdf.

[51] A. Mengden, *Carbon taxes in europe*, Oct. 2023. [Online]. Available: https://taxfoundation.org/data/all/eu/carbon-taxes-in-europe-2023/#timeline.

[52] *Ember. (January 4, 2024). Average monthly electricity wholesale price in the Netherlands from January 2019 to December 2023 (in euros per megawatt-hour) [Graph]. In Statista*, en, Accessed: 2023-01-15. [Online]. Available: https://www-statista-com.tudelft.idm.oclc.org/statistics/1314549/netherlands-monthly-wholesale-electricity-price/.

B
Appendix B

B.1. Fuel Cells for Shipping

Invented already in 1838, fuel cells can hardly be referred to as a novel technology. However, the interest in fuel cells has gained renewed interest in the past decades for their role in renewable energy systems [3]. The electrochemical cells can be used to convert electricity to hydrogen, referred to as electrolysis, and convert it back to electricity. Electrochemical conversion of electricity to fuels and back is regarded as a key technology for storage, transport and use of renewable electricity [4].

Fuel cells are well-known from their application in hydrogen-powered cars, where they are used to convert hydrogen to electricity with high efficiency and no emissions other than water vapor. However, fuel cells can in principle electrochemically oxidize any fuel, including hydrocarbons, alcohols and ammonia [5]. In contrast to conventional power generation systems fuel cells do not rely on a thermodynamic heat cycle. Therefore, the fuel is not combusted first to produced heat. Although both can achieve the same efficiency in theory, fuel cells have lower heat and conversion losses, while the formation of pollutants is avoided [6].

B.1.1. Working principle of Fuel Cells

Fuel cells consist of at least three functional layers: an ion conducting membrane and electronically conducting electrodes for fuel and air. This is commonly referred to as the membrane electrode assembly (MEA) or positive electrode-membrane-negative electrode (PEN) structure. The membrane is a dense, gas-tight and electronically isolating layer which conducts mobile ions. The electrodes are usually porous structures which allow reactants, products and electrons to diffuse to and from the reaction sites, which are in close vicinity to the membrane. These reaction sites are typically located at the interface of the gas, an electronic conductor and an ionic conductor, more commonly referred to as the triple phase boundary. In addition, a catalyst is usually incorporated in the electrodes to facilitate the electrochemical reaction and, therefore, achieve a sufficiently high reaction rates [7].

Fig. B.1 shows a simplified schematic of a fuel cell with a proton conducting electrolyte when fueled with hydrogen. The fuel and oxidant compartment are separated by a membrane with electrodes on either side. Hydrogen is supplied at the fuel electrode, the anode, while air is supplied at the oxygen electrode, the cathode. The membrane is a gas-tight and an electric isolating material, but mobile ions, protons in this case, can migrate from the anode through it to react with oxygen at the cathode, producing water. The flux of protons is driven by the chemical potential over the membrane, which results in an electric potential known as the electromotive force. The electrons released during hydrogen oxidation at the anode travel through an external circuit to be recombined in the oxidation reaction at the cathode. This yields an electric current and enables the fuel cell to provide useful work [7].

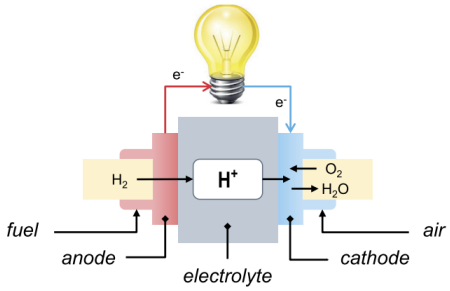

Figure B.1: Simplified Schematic of the working principle of a fuel cell with a proton conducting electrolyte [7]

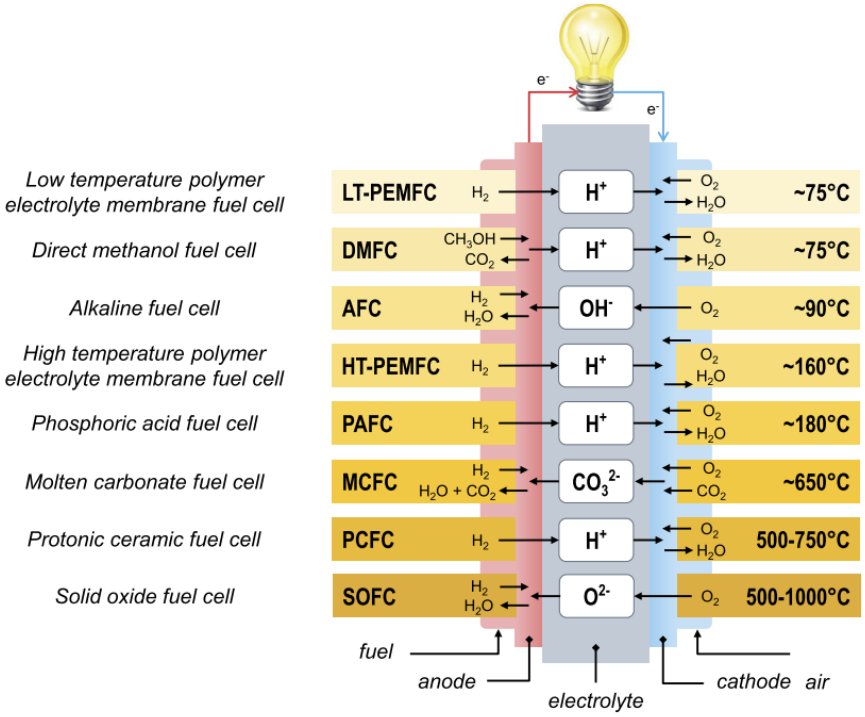

Figure B.2: An overview of commonly applied fuel cell types, including an indication of their typical operating temperature and the mobile ion in the electrolyte [7].

Fuel cells are classified primarily by the type of electrolyte material that separates the fuel and air electrode. These materials also determine the mobile ion, electro-chemical reactions and the temperature ranges at which these occur. In addition, it dictates the nature of the catalyst as well as the type and required purity of the fuel. Each fuel cell type comes with its own set of characteristics and specific needs in terms of process control, which in turn determine the degree of complexity of its Balance-of-Plant (BoP), i.e. the auxiliary components in the system. All of the above factors influence heavily the applicability of each type of fuel cells in maritime applications. In recently conducted studies, the technologies identified as the most promising are LT- and HT-PEMFC and SOFC, for which reason they will be introduced in more detail.

B.1.2. Low temperature Polymer Electrolyte Membrane Fuel Cells (LT-PEMFC)

The LT-PEMFC is currently the most widely used fuel cell technology and has been used successfully both in marine and other heavy duty applications. They employ solid polymer-acid membranes (mostly based on Perfluorosulfonic acid (PFSA)) as electrolyte and porous carbon electrodes that also act as support for a platinum-based catalysts. This specific type of polymer electrolyte membrane has to

stay hydrated for the membrane to conduct mobile protons, resulting in operating temperatures below 100°C. The redox reaction within PEMFCs transforms the energy stored in hydrogen into electricity, heat and water using an oxidizing agent, most commonly ambient air. Electrons liberated during the reaction cannot travel through the electrolyte and are redirected via an external load, thus producing an electric current for useful work. This process is schematically shown on the top of figure B.2. This energy conversion process occurs at relatively low temperatures, ranging from roughly 65 to 85°C, reaching peak efficiencies of around 50-60%. Maintaining this temperature range is mandatory, given that liquid water contained in the membrane acts as the hydrogen H^+ ion transporting medium [8].

Advantages of LT-PEMFC

LT-PEMFCs offer a wide range of attractive characteristics. Low temperature operation induces less stringent material requirements and offers flexible operation, that is tolerance for load cycling, resulting in good transient performance and load following capabilities. The use of a solid yet flexible electrolyte that offers chemical, thermal and mechanical stability up to 100°C, means that electrolyte management problems are significantly reduced compared to the liquid electrolytes used in some of the other fuel cell types (AFC, PAFC, MCFC). Low-temperature operation also allows for a short warm-up time, allowing cold starts in seconds. Moreover, degradation processes are slowed down in comparison to high temperature fuel cells, inducing less wear on system components leading to longer operational lifetimes. High achievable current densities and small physical size also result in high power-to-weight ratios, making LT-PEMFCs a suitable technology for weight- and volume sensitive applications such as transport [8].

Disadvantages of LT-PEMFC

Given the low temperature of operation, main safety aspects are related to the use and storage of hydrogen on a vessel. One of the main disadvantages of operating at low temperature is the relatively slow rate at which the chemical reactions occur, which induces the need for a catalyst from the noble metal family (typically platinum) and, subsequently, adds to system cost. Furthermore, at this range of operating temperatures, the platinum catalyst is extremely sensitive to fuel impurities, in particular carbon monoxide (CO). CO has a strong surface adsorption, which deactivates the catalyst and blocks hydrogen access. For this reason, very high purity hydrogen ($> 99.99\%$) is required to maintain satisfactory performance [8].

The second significant drawback is water management. On one hand, the polymer membranes needs high liquid water content to achieve low resistance to the flow of H+ ions, but at the same time, the pores of the electrodes have to remain dry to allow for a rapid diffusion of reactant gases. Because the delicate balance between water generated, transported and removed inside the fuel cell, LT-PEMFCs have typically a complex water management system. This drawback is set to be rapidly alleviated as state-of-the-art fuel cell solutions contain advanced gas diffusion layers that facilitate the extraction of liquid water from reaction sites (e.g. the Toyota fuel cell system used in the Mirai [140]) . This allows to simplify system management and its structure by removing the external humidifier. Finally, the low operating temperature and the resulting low quality heat produced mean that heat recovery is considered to provide very limited benefits [8].

Even though perfectly capable of load following, the carbon support and platinum catalyst inside LT-PEMFCs have been proven to degrade at a much faster rate under load cycling conditions. Because of this, it is highly recommended to operate at steady-state as much as possible and delegate rapidly varying load demands to fast-response energy storage devices such as batteries or super-capacitors [8].

B.1.3. High temperature polymer electrolyte membrane fuel cells (HT-PEMFC)

In response to some of the technological limitations of LT-PEMFCs, a variant capable of working at higher temperatures has been developed. In HT-PEMFCs, the water-based PFSA membrane is replaced by another proton transport assisting solvent that possesses a higher boiling point. One of the most popular electrolytes currently in use is a polybenzimidazole (PBI) polymer matrix doped with phosphoric acid (H_3PO_4). This technology offers good protonic conductivity and catalytic activity in the range of 140-180°C, while demonstrating mechanical, chemical and thermal stabilities beyond the 200°C thresh-

old [8].

Advantages of HT-PEMFC

The advantages of working at elevated temperatures are numerous, including higher achievable performance due to increased reaction kinetics and lower diffusion losses (as water vapour exists only in its gaseous state) and increased tolerance to impurities, like CO or sulphur compounds. Since the adsorption of CO is reduced at higher temperatures, the tolerance to it is raised to $\sim 3\%$ of content in the fuel stream, allowing the use of lower purity hydrogen originating from, for instance, the steam reforming process. There are, for example, HT-PEMFC systems available on the market with integrated fuel reformers for natural gas and methanol. This does, however, imply that some of the fuel need to be bled and the fuel utilisation is limited to <100% and consequently the efficiency of such systems is typically lower than for pure hydrogen [8].

Alongside the fuel cell itself, higher operating temperatures can have a positive impact on the BoP components. The increased temperature gradient between the system and the ambient air allows for a smaller cooling system, while enabling the recovery of excess high quality heat for further use. This can improve the overall efficiency of the system, leading to applications like Combined Heat and Power (CHP) units. Moreover, the absence of liquid water in the fuel cell eliminates the need for a water management system [8].

Disadvantages of HT-PEMFC

Unfortunately, working at this temperature range also comes at a cost as the heating and cooling management systems start to play a crucial role. HT-PEMFCs need to be pre-heated by external means to (typically) at least 120°C before power can be generated. This is mainly due to the fact that the proton-carrying H_3PO_4 is extremely hydrophilic and binds effortlessly with liquid water molecules. This can result in rapid removal of the electrolyte from the PBI polymer matrix, substantially decreasing fuel cell performance and lifetime. For this reason, the introduction of liquid water should be avoided at all costs and as a consequence, cold start is impossible. Start-up and shut-down sequences become longer and more complex when compared to LT-PEMFCs [8].

Long term operation at high temperatures and dry conditions accelerate membrane degradation. Also, during transient operation, changing operating conditions (load, temperature) may lead to increased formation of water, increased thermal and mechanical stresses and voltage cycling that accelerates carbon support and catalyst degradation [8].

B.1.4. Solid Oxide Fuel Cell-SOFC

Solid oxide fuel cells (SOFC's) rely on a ceramic membrane material that allows diffusion of oxide ions (O^{2-}) at relatively high temperatures. Functional temperatures vary from 500 to 1000°C, depending on the cell design and the electrolyte material of choice. Designs vary from thick electrolyte supported cells to functional layers supported on a porous electrode or metal support [8].

Advantages of SOFC

The high operating temperature enables the use of non-noble catalysts in the electrodes, such as nickel. In addition, SOFCs have higher tolerance for fuel impurities, and carbon monoxide is effectively a fuel. Therefore, SOFCs can be fuelled with (reformed) hydrocarbons as well. Light hydrocarbons, such as methane, can even be reformed internally on the SOFC anode. Likewise, ammonia can be cracked internally and, therefore, directly used as a fuel. SOFCs are, for example, used for (micro-)CHP generation from natural gas, taking advantage of the high temperature waste heat produced. Products with peak electrical efficiencies up to 60% have been on the market for several years in Japan and more recently in Europe. Today, SOFC are applied in distributed power generation as well, most notably to provide power at businesses and data-centres in remote locations or locations with no access to a reliable electricity grid. These systems are designed to use natural gas and have a peak net electric efficiencies up to 65% [8].

SOFC technology can also be applied in a combined cycle configuration with a heat cycle, for which

net electrical efficiencies of 70% are projected [8]. The emissions and fuel consumption associated with an SOFC are also relatively very low compared to a Dual-fuel engine, supplying the same amount of power with LNG as the fuel. In the below table the emission factors are listed between a dual-fuel engine and an SOFC [141].

Emissions	**DF Engine**	**SOFC**
SOx (mg/kWh)	32±17	Negligible
NOx(mg/kWh)	7000±2100	4.8±0.2
CO (mg/kWh)	15,000±4230	2.1±0.1
PM (mg/kWh)	175±108	Negligible
CO_2 (g/kWh)	725±234	343±37

Table B.1: Estimation of a dual-fuel engine (DF) and SOFC system emission factors. [141]

Disadvantages of SOFC

Compared to other fuel cell systems, SOFCs typically have a large amount of auxiliary components, like heat exchangers, fuel reformers and combustors. In addition, a substantial amount of insulating material is used to minimise heat loss to the environment and maintain the high operating temperature of the stack. Although the power density can be high at cell level, relatively thick repeating units and the large balance of plant typically results in lower power densities than LT-PEMFC systems. In addition, the thermal mass of the system calls for adequate thermal management, resulting in time consuming cold starts and sluggish load following [8].

B.1.5. Other Types of Fuel Cells

The viability of using a specific fuel cell technology in maritime applications depends largely on its operational characteristics and ease of implementation. Because of the broad spectrum of interesting attributes offered by LT- and HT-PEMFCs and SOFCs, these types are considered a viable choice for maritime use. For completions, this section describes other fuel cell types which are less likely to be applied in ships, either due to severe intolerance to impurities, high cost, low power density, low system efficiencies, liquid electrolyte management and resulting high system complexity and maintenance requirements [8].

Alkaline Fuel Cell(AFC)

AFCs consist of an alkaline solution electrolyte, typically potassium hydroxide (KOH), where hydroxyl OH^- ions are transported from the silver-based cathode to the nickel-based anode. AFCs have a moderate efficiency of around 50-60%, employ low-cost catalysts and readily available electrolytes, which renders them a relatively low-cost system.

The fuel cell uses hydrogen and oxygen as reactant gases and operates between ambient temperature and 90°C, which ensures that the requirements for the material used are less stringent and reduce cost. The biggest drawback of AFCs is their high intolerance to CO_2. For this reason, pure oxygen and pure hydrogen gases need to be delivered for it to function in an optimal range over a prolonged period of time, or potassium carbonate has to be removed and the electrolyte replenished. This implies that AFC systems typically use a scrubber to remove CO_2 from the cathode air. However, the AFC membrane has a high tolerance for ammonia, which is an advantage compared to the acidic proton conducting membranes employed in some fuel cell types if ammonia is considered as a fuel [8].

Phosphoric Acid Fuel Cell (PAFC)

PAFC have an electrolyte consisting of silicon carbide matrix saturated with liquid phosphoric acid and carbon electrodes that support a platinum catalyst. This is the precursor technology that lead to the development of HT-PEMFC, for which reason they share many of the same benefits and shortcomings.

The higher operating temperature from 140 to 200°C reduces the required platinum loading and increases CO tolerance, but also offers to use the excess high quality heat, increasing the overall efficiency of the fuel cell from around 40% up to 80%. Reachable current densities are relatively low which translates into low power densities and result in large and heavy systems. Higher temperature operation results in slower start up times and accelerated component ageing [8].

Direct Methanol Fuel Cell(DMFC)

DCFCs employ a polymer membrane electrolyte, similarly to PEMFCs, but to generate electricity they use a 3% methanol (CH_3OH) in water solution, without prior reforming to hydrogen. The ability to do so is granted by electrodes containing a platinum-ruthenium catalyst. The DMFC normally operates between 50-120°C. Increasing operating temperature and pressure can improve cell efficiency, but will also cause higher overall losses, leading to losing the benefit [8].

DMFCs are good for delivering small power outputs, typically of up to 5 kW, over prolonged periods of time. The methanol is as fuel with high energy density, that is easy to handle and store compared with hydrogen but its use during the oxidation at the anode leads to CO_2 production. The efficiency of a DMFC is low, around 20% with a major challenge being methanol crossover from the anode to the cathode where it reacts directly with oxygen. This can lead to severe reductions of cell efficiency [8].

Molten Carbonate Fuel Cells (MCFC)

MCFC use a mixture of molten alkali metal carbonates as electrolyte, where the carbonate ions (CO_3^{2-}) move from the cathode to the anode. MCFC currently reach electrical efficiencies of upto 50%, but theri high operating temperature (600-700°C) makes them suitable also for cogeneration plants, where they can achieve an overll efficiency of upto 85%. MCFC have a good tolerance to impurities, and can be fed by multiple fuels (e.g. NG, H_2). Nonetheless, major drawbacks such as slow start-up timing and low power density makes them less attractive than other FC technologies for maritime applications [8].

B.1.6. Summary of promising FC technology characteristics

As seen in the table B.2, the most developed fuel cell solution is LT-PEM. The main drawback of utilizing LT-PEMFC is the need for high purity hydrogen. HT-PEMFC on the other hand also uses hydrogen, but can cope with lesser quality hydrogen. SOFC's can be fuelled with different types of hydrocarbon fuels, ammonia and also hydrogen. In-terms of power density, LTPEM fuel cells are the most competitive and are also competitive with gas fuelled engines. The lifetime of LT-PEM fuel cells is competitive and have demonstrated close to 65,000 hours in the field. The system lifetime of all the fuel cell types in the field is greater that 10 years, which includes the fuel cell stack (fuel cell stack is the primary electrochemical component in the fuel cell electrolysis system).

Table B.2: Summary of SOFC, LT-PEMFC and HT-PEMFC [8]

	LT-PEMFC	**HT-PEMFC**	**SOFC**
Operating Temperature (^{o}C)	65-85	140-180	500-1000
Electrical Efficiency(%LHV)	40-60	40-50	50-65, up to 90 (CHP)
Fuel Requirements	99.99% H_2	CO <3%	S <20ppm
Gravimetric power density (W/kg)	125-750	25-150	8-80
Volumetric power density (W/L)	50-400	10-100	4-32
Stack lifetime (kh)	5-35	5-20	20-90
System lifetime	$\geq$ 10 years with stack replacement		
Cold start-up time	<10 s	10-60 minutes	>30 minutes
Load transients (0 to 100%)	seconds	<5 minutes	<15 minutes

Current Capital cost ($/kW)	1000-2500	3000-5000	3500-15000
Future capital cost ($/kW)	60-600	150-1500	500-2000
Maritime TRL(2020)	6-7	5-6	4-5
Cooling medium	Liquid	Liquid	Air

The figure B.3 shows the typical operating characteristics of fuel cells which differ from traditional internal combustion engines. Fuel cells typically have a high efficiency at relatively low load, where the electrochemical losses in the stack are limited, while internal combustion engines are usually most efficient close to their operating point [9].

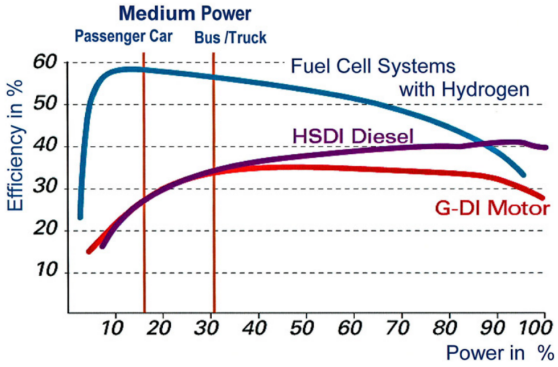

Figure B.3: Comparison of efficiencies of Fuel cells and Internal combustion engines [9]

C
Appendix C

C.1. Verification tests-PEMFC/LIB hybrid system

To verify whether the above model is working as intended, certain verification tests were conducted as follows:

C.1.1. Checking the power balance constraint

To verify that the power balance constraint 4.23 is not violated, the difference in load and power supply from components has been plotted as shown in figure C.1. The fluctuations in the graph are due to rounding errors.

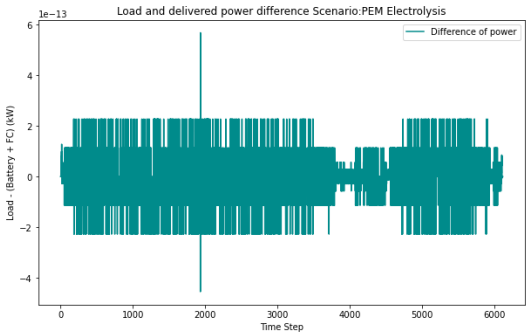

Figure C.1: Difference in power supply and demand-PEMFC/LIB

As seen in the above figure, the difference in the load and supplied power has not been violated across the entire length of the trip.

C.1.2. Reducing the number of PEMFC stacks

In this test, the number of available PEMFC stacks has been reduced from 8 to 6. To compensate, it is expected that the installed battery capacity needs to be increased.

This resulted in a infeasible solution due to the limited available battery capacity of 300kWH. To check how much additional battery capacity needs to be installed, the upper limit of the battery capacity has been removed. This resulted in the following results as shown in figure C.2.

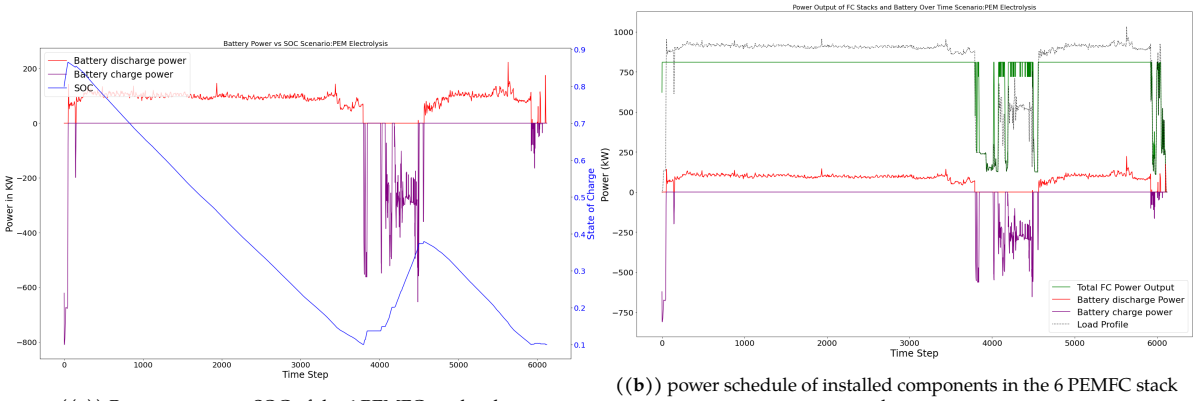

((**a**)) Battery power vs SOC of the 6 PEMFC stack solution

((**b**)) power schedule of installed components in the 6 PEMFC stack solution

Figure C.2: Verification test-Power schedule of components and SOC for 6 PEMFC stack solution

This resulted in a massive increase in the required battery capacity. The battery capacity has increased from 89.90kWH to 8128.20kWH. The CAPEX increased significantly from $1637062.97 to $2734751.74. The hydrogen consumed across the entire length of the trip is 4505.12kg, which is a reduction of 279.02kg. The intended changes were observed.

C.1.3. Reducing the battery capacity

In this test, the available battery capacity was reduced from 300kWH to 62kWH (20 modules). Due to the limited available battery capacity, the number of selected stacks need to increase.

The above change has resulted in all 8 PEMFC stacks being selected and a battery capacity of 58.90kWH. The resulting CAPEX increases from $1637062.97 to $1768636.29. The battery SOC and power schedule of components has been shown in figure C.3.

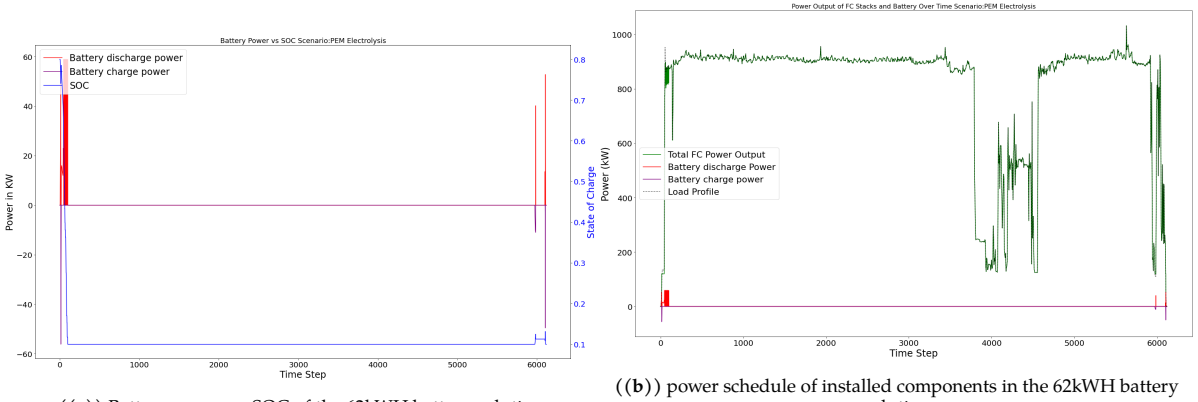

((**a**)) Battery power vs SOC of the 62kWH battery solution

((**b**)) power schedule of installed components in the 62kWH battery solution

Figure C.3: Verification test-Power schedule of components and SOC for 62kWH battery limit

C.2. Verification tests-DG/PEMFC/LIB hybrid system

To verify if the above model is working as intended, certain verification tests were conducted as follows:

C.2.1. checking the power balance constraint

To verify that the power balance constraint in equation 4.32 has not been violated, the difference in load and power supply of components has been plotted in figure C.4

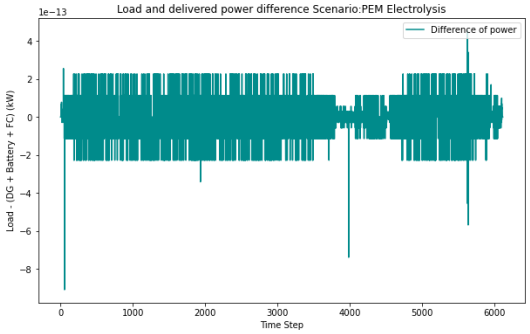

Figure C.4: Power difference between load and supply-DG/PEMFC/LIB

C.2.2. Reducing the number of PEMFC stacks

In this test, the number of available PEMFC stacks has been reduced from 7 to 1. An increase in the number of DG's or battery capacity is expected.

The solution was infeasible despite 2 DG sets being available. The reason behind is due to the transient loading limits of the diesel generator and the battery SOC at the start. The increase in load in a single time step on the diesel generator are the limited to 33% of the ICE rated power, and the battery is shore charged to 80% SOC at the start.

To check the validity of the above reasons the start SOC of the battery is set to 0.1. Due to this modification, the model again becomes feasible, and the DG's rapidly charge the batteries at the start to reach their operating power output required. The single PEMFC stack available has not been selected and both the DG's along with a battery capacity of 167.40kWH needs to be installed. A reduction in CAPEX was observed from $608735.62 to $528800.59, which is much cheaper

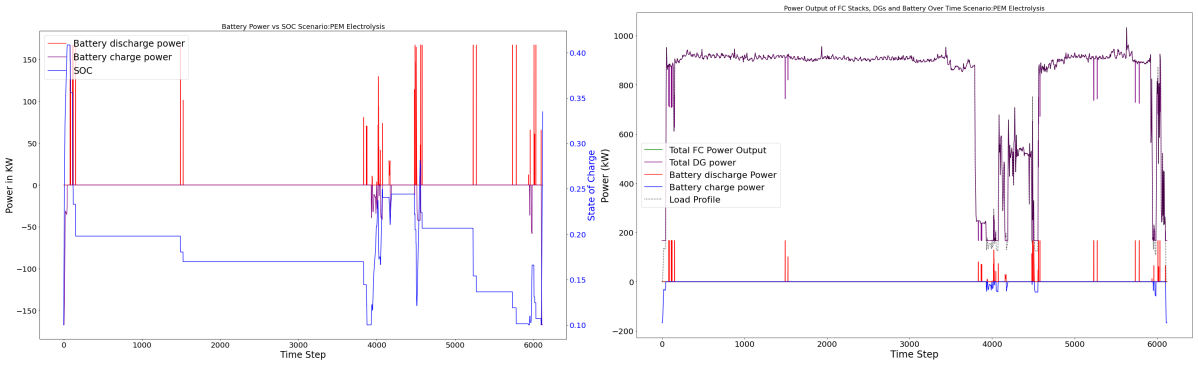

((**a**)) Battery power vs SOC for 1 PEMFC stack limit

((**b**)) power schedule of installed components for 1 PEMFC stack limit

Figure C.5: Verification test-Power schedule of components and SOC for 1 PEMFC stack limit

C.2.3. Reducing the number of DG's

Reducing the number of DG's to 0 results in the same hybrid configuration of the PEMFC/LIB solution.

C.2.4. Reducing the battery capacity

Reducing the battery capacity to 100kWH results in the same solution as the PEMFC/LIB solution of 7 stacks and 89.90kWH battery.